Thermal Bioswitches for Non-Invasive Control of Cellular Therapies

Thesis by

Mohamad Abedi

In Partial Fulfillment of the Requirements for

the Degree of

Bioengineering

CALIFORNIA INSTITUTE OF TECHNOLOGY

Pasadena, California

2021

(Defended February 5, 2021)

Mohamad Abedi
ORCID: 0000-0001-9717-6288

ACKNOWLEDGEMENTS

It's challenging to decide where I should start this section. Do I begin by thanking the immigration officer that approved my family's green card application? Or should I start by acknowledging the neighbor that drove me to community college when I didn't have a car? The task is difficult, and my memory is far from perfect, but one thing is certain: I would not be writing this section and receiving this degree if not for the support of others, some that I know of and some that I will never know, who dedicated their time, energy, and resources to support me. The world is not an equal place, certainly academia is not. It is on us to create a supportive community and ensure that everyone gets a fair shot. I was lucky to have people that fought for my shot whom I will do my best to acknowledge here. But more importantly, I will do my best to repay them by always striving to be a source of support for people that need it the most.

When I first arrived in this country, I didn't know what a scientist was. My goal, my family's goal, was to immigrate and earn US citizenship so we could finally cease to be Palestinian refugees. That was it, my dreams ended there. However, when I immigrated, I left many people behind with their own dreams and goals. I didn't know how, but I knew that I wanted to use the opportunity I was given to help them. It was in the laboratory of Professor Elliot Hui at UC Irvine that I first got a glance into how I could help. During my undergraduate studies, Elliot took me into his laboratory where I discovered the wonders and powers of science. In that laboratory, I met Siavash Ahrar, Kamran Ali, and David Li. These brilliant graduate students ignited in me a passion for science. In the evenings, we spent hours chatting and getting lost in the possibilities of science, and when the daytime came, they taught me how to translate these dreams into tractable experiments. I would also like to acknowledge Professor Chang Liu, for his constant support and encouragement. Chang has been an influential role model that shaped my scientific career. Thank you, Chang, for believing in me and investing in my success.

It is true that my passion for science started at UC Irvine, but it was only here at Caltech that I learned what it truly meant to be a scientist. However, I wouldn't have had this opportunity if not for the support of generous graduate fellowships. When I applied to Caltech, I was placed on the waiting list with slim hopes of making it out. If not for three reviewers that read my NSF graduate student fellowship application, believed in the potential of a stranger, and decided to give me a shot, I wouldn't have made it off that list. I would also like to thank the Paul and Daisy Soros family for believing and investing in me. While their fellowship supported my studies financially, that wasn't their biggest impact on my education. The Soros family gave me the opportunity to join a wonderful family composed of the most brilliant and inspiring leaders in the country. A family of fellows that is united by the common goal of making the United States a better home for everyone.

Amongst the many brilliant Soros fellows, one person stands out: my graduate advisor, Mikhail Shapiro. Mikhail's formal role was to be my graduate advisor and that he excelled at. However, I'm lucky and honored to say that Mikhail for the past six years has been more than that, he has been my friend. He was there for me whenever I needed his financial, emotional, or scientific support. I'm grateful that he chose to give me the chance of being a part of his scientific family. It was there that I met friends that will stay with me for the rest of my life. Dan Piraner and Pradeep Ramesh were my family at Caltech and frankly the main reason why I would come to work on most days. Despite being in a different office, Di Wu and I managed to find each other and build a lifelong friendship while exploring the LA food scene. Thank you to everyone in the lab, especially Anupama Lakshmanan, Avinoam Bar-Zion, Zhiyang Jin, Rob Hurt, Michael Yao, and Audrey Lee-Gosselin. I've learned a lot from each of you. I would also like to acknowledge Arnab Mukherjee for being both an amazing postdoc and a dedicated mentor who shaped me as a scientist. Arnab is a brilliant scientist, a great friend, and a selfless mentor. You have been there for me every time I reached out for help, and even when I didn't. I hope that one day I will get to repay the generosity and the care you've shown.

In my last years at Caltech, I got to meet Abdullah Farooq and Shirin Shivaei, two people that unexpectedly changed my life forever. Shirin is one of the smartest and most driven people I've met at Caltech. I'm grateful that I got to meet her, learn from her, and share many beautiful memories together. Abdullah Farooq is also one of the brightest people I met at Caltech, but more importantly one of the kindest hearts. Despite circulating rumors, we are not cousins, but we are definitely life-long friends. In my last year, I also had the pleasure to live and quarantine with Linlin Chen. Thank you for being a wonderful roommate, cook, and a great friend. Finally, I am also indebted to my committee members, Profs. David Baltimore, Ellen Rothenberg, and Richard Murray. David, you have always made yourself available to discuss my research, career goals, and occasionally crazy ideas. I've learned so much from you, and I have no doubt that I will keep coming back to seek your advice. Ellen, thank you for being my biggest cheerleader. Thank you for helping me build the confidence to pursue bold directions and showing me how to excel not only as a scientist but also as a person. I would also like to also thank Richard for taking the time to support and advocate for me.

I cannot end my acknowledgments without recognizing some of the most important people in my life, my family. To my parents, Hassan Abde and Wafaa Farran. Thank you for dedicating your life to your children. Your goal was to help us escape the life of a refugee. Your dream was for us to be educated and successful. I think it's fair to say that with your strong will and dedication you have succeeded at both. Thank you for instilling in me the belief that anyone, no matter their background, can be successful with hard work and determination. To my brother Ali, you have been the rock that supported me throughout all of this. I will never forget the day when it looked like I would have to drop out of college because I couldn't afford it. It was scary until you stepped up and told me that no matter what happens you would help me finish my degree. To my sister, thank you for your love and great company. And again, I would like to thank Shirin Shivaei, who is not only a brilliant scientist but also a wonderful life companion who is constantly teaching me new things beyond science. I'm thrilled to have the chance to explore the world together, once the pandemic ends of course. Finally, I would like to end by thanking my childhood friends Sameh Emghaoech, Antoni Yousef, Roger Debaneh, Ahmad Abdulrazak, and Bashar

Hanna. We had a beautiful childhood together, and when I had to leave to become a stranger in a new land, you kept me company on WhatsApp. Thank you.

ABSTRACT

Temperature is a unique input signal that could be used by engineered therapeutic cells to sense and respond to host conditions or spatially targeted external triggers such as focused ultrasound. To enable these possibilities, I present here a new class of thermal bioswitches that enables thermal control over bacterial and mammalian cells. For bacterial applications, we developed two new families of tunable, orthogonal, temperature-dependent transcriptional repressors providing switch-like control of bacterial gene expression at thresholds spanning the biomedically relevant range of 32–46 °C. We integrated these molecular bioswitches into thermal logic circuits and demonstrated their utility in three in vivo microbial therapy scenarios, including spatially precise activation using focused ultrasound, modulation of activity in response to a host fever, and self-destruction after fecal elimination to prevent environmental escape. This technology provides a critical capability for coupling endogenous or applied thermal signals to cellular function in basic research, biomedical and industrial applications.

To apply this technology in a relevant clinical scenario, we sought to engineer microbial immunotherapies that can be thermally controlled with focused ultrasound. This technology was enabled by rapid advances in synthetic biology that are driving the development of genetically modified microbes as therapeutic agents for a multitude of human diseases, including cancer. In particular, the reduced immune surveillance within the core of some solid tumors creates an ideal environment for microbes to engraft and release therapeutic payloads. However, these therapeutic payloads could be harmful if released in healthy tissues where microbes tend to also engraft in smaller numbers. As described in Chapter 2, my colleagues and I introduced a temperature-actuated state switch that enables tight spatiotemporal control over the activity of therapeutic microbes when combined with focused ultrasound hyperthermia. Through a combination of rational design and high throughput screening, we optimized the behavior of this switch to minimize leakage and maximize inducibility. When tested in a clinically relevant in *vivo* model, engineered microbes, successfully switched states, and induced a marked suppression of tumor growth

upon focal activation. This bioswitch provides a critical tool to attain selective and sustained activity of therapeutic microbes in *vivo*.

Encouraged by the successful development of thermally actuated circuits in microbes, we aimed to establish equivalent technologies for thermal control of human T cells. Genetically engineered T cells are actively being developed to perform a variety of therapeutic functions with great clinical promise. However, no robust mechanisms exist to externally control the activity of T cells at specific locations within the body. Such spatiotemporal control could help mitigate potential off-target toxicity due to incomplete molecular specificity in applications such as T-cell immunotherapy against solid tumors. In Chapter 4, my colleagues and I tested the ability of heat shock promoters to mediate thermal actuation of genetic circuits in primary human T cells in the well-tolerated temperature range of 37−42 °C, and we introduced genetic architectures enabling the tuning of the amplitude and duration of thermal activation. We demonstrated the use of these circuits to control the expression of chimeric antigen receptors and cytokines, and the killing of target tumor cells. Overall, the technologies developed here provide critical tools to direct control therapeutic cells after they have been deployed deep inside the body.

PUBLISHED CONTENT AND CONTRIBUTIONS

Piraner, D. I.*, **Abedi, M. H.***, et al. (2017). "Tunable thermal bioswitches for in vivo control of microbial therapeutics". In: *Nature chemical biology 13*, pp. 75-80. Doi: 10.1038/nchembio.2233

M.A. participated in the conception of the project, constructed and tested genetic circuits in vitro and in vivo, prepared the data, and participated in the writing of the manuscript.

Maresca, D., Lakshmanan, A., **Abedi, M. H.**, et al. (2018). "Biomolecular ultrasound and sonogenetics". In: *Annual review of chemical and biomolecular engineering 9*. pp. 229-252. Doi: 10.1146/annurev-chembioeng-060817-084034.

M.A. participated in the writing of the manuscript.

Bar-Zion, A., Nourmahnad, A., Mittelstein, D. R., Yoo, S., Malounda, D., **Abedi, M. H.**, et al. (2019). "Acoustically detonated biomolecules for genetically encodable inertial cavitation". In: *bioRxiv.* Doi: 10.1101/620567

M.A. helped design genetic circuits and participated in the writing of the manuscript.

Abedi, M. H., et al. (2020). "Thermal Control of Engineered T-cells". In: *ACS Synthetic Biology 9*, pp. 1941-1950. Doi: 10.1021/acssynbio.0c00238

M.A. conceived, planned, and conducted experiments, analyzed the resulting data, and prepared the manuscript.

Abedi, M. H.*, Yao M. S.* et al. (2021). "Acoustic Remote Control of Microbial Immunotherapies". In preparation

M.A. conceived, planned, and conducted experiments, analyzed the resulting data, and prepared the manuscript.

TABLE OF CONTENTS

LIST OF ILLUSTRATIONS AND/OR TABLES

C h a p t e r 1

ULTRASOUND ACTUATED BIOSWITCHES IN CELL THERAPY

This chapter is in large part a reformatted version of the manuscript entitled "Biomolecular Ultrasound and Sonogenetics" published by Maresca, D., Lakshmanan, A., Abedi, M., Bar-Zion, A., Farhadi, A., Lu, G. J., ... & Shapiro, M. G, in *Annual Review of Chemical and Biomolecular Engineering*

.

1.1 Introduction

Studying biological function within the context of living organisms and the development of biomolecular and cellular therapy requires methods to image and control the function of specific molecules and cells in vivo. However, most popular methods for achieving spatiotemporally precise interactions with biological substances, such as fluorescent imaging and optogenetics, have limited utility in deep tissues owing to the strong scattering of visible light. Unlike photons, which are scattered within approximately one millimeter of tissue, ultrasound waves easily penetrate several centimeters deep while retaining spatial and temporal coherence. This capability has made ultrasound one of the world's leading modalities for medical imaging of anatomy, physiology, and noninvasive therapy. However, historically ultrasound has played a relatively small role in molecular and cell biology owing to a lack of effective methods to couple sound waves to specific processes such as gene expression and cellular signaling.

Recent advances are changing this picture by enabling ultrasound to image and control the function of specific biomolecules and cells and drive biomolecular transport across cellular and tissue barriers. These emerging capabilities for biomolecular ultrasound are the focus of this chaper. We start with a brief primer on ultrasound physics and technology. We then

describe proteins and genetic circuits allowing focused ultrasound (FUS) to remotely control gene expression and other aspects of cellular signaling through sonogenetic strategies analogous to optogenetics and chemogenetics. Finally, we discuss the prospects for ultrasound in enhancing cell therapies. We aim to convey both the exhilarating recent developments underlying the emergence of biomolecular ultrasound and the exciting opportunities this nascent field holds for creative biomolecular and ultrasound engineers.

1.2 Wave Behavior and Tissue Interactions

Ultrasound is defined by sound wave frequencies above those audible to humans (>20,000 Hz). Generated by transducers coupled to a transmission medium such as biological tissue, ultrasound waves travel through the medium and interact with its components to form images or provide momentum and energy for perturbation. In biological tissues, as in liquids, compression waves are dominant and are used for most modes of imaging and control. In tissue, sound waves travel at ~1,540 m/s and are reflected and scattered wherever they experience a change in acoustic impedance, which is a function of the local density and compressibility (1). The relative homogeneity of the speed of sound in soft tissues results in sound waves remaining coherent as they traverse the tissue, enabling simple image reconstruction without major aberrations (2). By comparison, visible light is strongly scattered in tissues, making it challenging for it to retain a ballistic path at depths greater than a few hundred microns.

Ultrasound reflection at tissue interfaces is highly directional and reveals anatomical contours. Soft tissues have similar acoustic impedance values, resulting in relatively low contrast between them; air and bones have much lower and higher acoustic impedances, respectively, resulting in strong reflections (2). When the ultrasound wave encounters a target smaller than approximately one-tenth of the wavelength, it is scattered omnidirectionally (3). Biological tissues include a wide range of such scatterers in the form of fibers, cells, and organelles. The echo from a single scatterer is usually very weak. When several very close

scatterers are imaged, the result is a dominant spatially coherent interference pattern called speckle (2). The amplitude of the ultrasound wave decreases exponentially as a function of depth. Part of the energy of the ultrasonic wave is absorbed in the tissue and dissipated as heat. Attenuation refers to both absorption and any reduction in wave amplitude owing to reflection or scattering. Each tissue is characterized by a different attenuation coefficient value, which increases nonlinearly with frequency (2). As they pass through a medium, ultrasound waves also deposit momentum into that medium, resulting in mechanical forces known as acoustic radiation forces (ARF). Appreciable at higher ultrasound intensities and pulse durations, these forces, as well as localized heating, can be used to perturb and manipulate tissues and other materials.

1.3 Focused Ultrasound Actuation

Thanks to the low attenuation of soft tissues, energy can be deposited at a specific location deep within the body using FUS. Ultrasound can be applied based on known anatomical targeting or used under real-time guidance from magnetic resonance imaging (4), allowing accurate localization of the target site and monitoring effects on the tissue. Ultrasound can be focused using either a curved single-element transducer or electronically focused multielement phased arrays, which, in addition to steering the beam, can correct for wave-front aberrations caused by acoustically mismatched tissues, such as the human skull (5).

There are three basic modes of ultrasound energy delivery (**Figure 1-1**): heat generation, exertion of ARF, and acoustic cavitation (6). Heating occurs owing to viscous dissipation as molecules move back and forth at the ultrasound focus, increasing with greater acoustic frequency and intensity. Reaching substantial temperature elevations typically requires pulse durations on the order of seconds. ARF in traveling ultrasound waves arises from the loss of momentum as sound waves become attenuated or reflected; by conservation, this momentum is transferred to particles in the medium. This effect scales with attenuation and usually requires pulses on the order of milliseconds for target tissues to reach their maximal elastic

response to ARF. In addition to traveling waves, ARF can also arise in standing ultrasound waves owing to the presence of pressure nodes and antinodes, attracting or repelling particles based on their material properties (7). Finally, cavitation arises through the interaction of ultrasound with bubbles, which may arise spontaneously in the medium or become nucleated at material interfaces or are introduced as external cavitation agents (8). Cavitation can be stable, with gas bubbles periodically oscillating around their initial radius at the frequency of the acoustic wave, or inertial, in which rapid growth of the bubble followed by violent collapse releases large forces and fluid jets into surrounding media. Stable cavitation occurs preferentially at the resonance frequency of each bubble, with inertial cavitation becoming more likely with increases in the ratio between the peak negative pressure and the square root of the frequency—a ratio termed the mechanical index, with units of MPa MHz−1 /2 (1).

Each of these modes has been exploited for therapeutic purposes, such as thermal tissue ablation (9–12), local drug delivery (13–15), and thrombolysis (16), and has the potential to interact with biomolecules. Not covered in this review, unfocused ultrasound in the 20–100-kHz range is also widely used in laboratory and industrial processes to disrupt material structures, accelerate chemical processes, and clean surfaces. Most of these effects are thought to be mediated by cavitation (17).

1.4 Sonogentic Actuation of Cellular Signaling

FUS has a long history of use as a therapeutic modality, with current applications primarily focused on localized ablation of deep tissue targets (9–12). However, ultrasound's ability to be focused and deliver energy to a site of interest with millimeter precision could also be used to provide an input signal for biomolecular and cellular signaling. For example, ultrasound's ability to controllably elevate temperature by several degrees Celsius under image guidance could provide a safe, rapid, reversible signal for biomolecular actuation. In addition, its ability to apply mechanical forces to tissues and scattering objects could be harnessed to control mechanical signaling. Coupled to appropriate genetically encoded

molecular constructs, this would provide sonogenetic control of cellular function, analogous to optogenetic and chemogenetic techniques, which use optical and chemical inputs. Specific examples would be the excitability of specific neurons, the proliferation of microbes in the gut, or the release of cell-expressing therapeutic payloads.

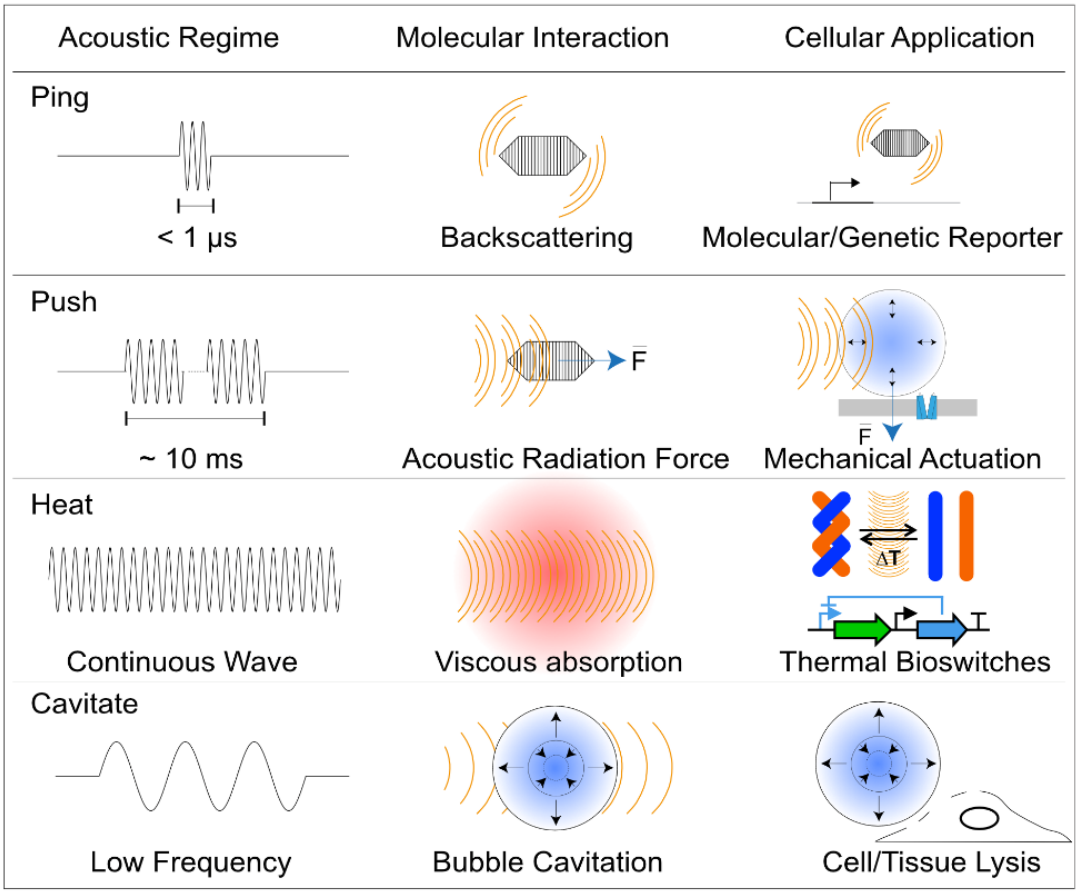

Figure *1-1* – Regimes of biomolecular ultrasound. (Top) Short ultrasound pulse basckattering is used to image acoustic biomolecules in vivo. (Upper middle) Extended ultrasound pulses induce an acoustic radiation force that can actuate ultrasound sensitive particules. (Lower middle) Continous ultrasound waves lead to local heating and can be used to turn on thermal bioswitches. (Bottom) Low frequency ultrasound can be used to cavitate microbubbles that can induce cell or vascular barrier disruption.

1.5 Thermally Mediated Ultrasonic Control

A wide array of thermal bioswitches have the potential to translate elevations in temperature into biochemical reactions that control cellular signaling and/or the expression of specific genes. These switches include heat shock promoters (18), temperature-sensitive ion channels (19), riboswitches (20), and heat-responsive transcription repressors (21, 22).

Pioneering studies on temperature-mediated responses to ultrasound have focused on the mammalian heat shock promoter HSP70, whose induction upon FUS has been linked to several genetic outputs, including the expression of reporter genes (23), suicide genes (24), and cytokines (25). HSP70 is a good starting point for thermal control because it is tightly repressed in the off state and rapidly inducible after only a few minutes of stimulation at 43◦C, with the potential to reach several thousand-fold induction levels (26, 27). However, HSP70 can also respond to other stress stimuli, such as hypoxia, glucose starvation, and viral infection (28), which renders controlling gene expression solely via changes in temperature more challenging. Moreover, thermal induction of HSPs is transient and varies among cell types; therefore, it is ineffective in some cell types, such as neurons (29, 30). Finally, in bacteria, heat shock promoters have a fairly modest dynamic range and also respond pleiotropically (31, 32).

Recently, a new class of tunable, orthogonal temperature-dependent transcriptional repressors was engineered to enable the next generation of sonogenetic thermal bioswitches (33). These switches use engineered versions of the orthogonal bacterial transcriptional repressors TlpA and TcI, which have sharp transition temperatures (3–4◦C) and more than 300-fold induction. These switches were engineered using directed evolution to have tunable set-points within the biomedically relevant temperature range of 32–46◦C. They have been integrated into thermal logic circuits to perform complex functions, such as multiplexing and bandpass activation, and provide precise control over the spatiotemporal profile and dose of gene expression. Spatially precise activation of these circuits with FUS was demonstrated in

bacterial culture phantoms and inside mammalian hosts with a brief thermal pulse (33). Unlike other bioswitches, these proteins respond solely to temperature elevations, with a sharp transition that can be tuned for specific applications. Combining these molecular devices with synthetic biology circuits may advance the use of FUS beyond simple transient switches to more complex functions, such as sustained, multiplexed, and on-off switching.

Nontranscriptional responses to ultrasound based on temperature may also be possible. For example, magnetic and optical hyperthermia have been used in conjunction with temperature sensitive ion channels (34–38). Unfortunately, most temperature-sensitive channels also respond to other inputs and depend on cellular states such as membrane potential and pH. RNA thermometers could provide thermal responses at the translational level, but these switches typically suffer from a broad thermal transition, with relatively small fold changes and leaky expression at baseline (20).

1.6 Cell Therapies and Ultrasound

One of the most powerful applications of ultrasound actuated bioswitches lies in their ability to enable tight spatiotemporal control over the activity of cellular therapies deep inside the body. Cell therapies are rapidly emerging as an effective therapeutic approach to address a multitude of human diseases, including cancer. Recent advances in synthetic biology and immunology enabled the rapid development of technologies to harvest immune cells from patients, engineer them with targeted receptors against tumor cells, and safely inject them back into patients. These engineered cells have shown remarkable results with unprecedented remission rates. However, once they are deployed inside the body, clinicians lose control over their activity. The absence of a mechanism to regulate and direct the function of these therapies could be detrimental in patients where on-target off-tumor killing activity results in serious, sometimes fatal, side effects. Therefore, developing a technology that can locally target engineered cells within tumors and activate their therapeutic potential represents an urgent unmet need. Ultrasound actuated bioswitches provide an ideal technology that can fill this need to enable safer and more effective therapies. While immune cells are attractive

candidates for targeted cellular control in *vivo,* they only represent a small subset of the potential cell types with an unmet need for cellular control post-deployment into patients. Ultrasound actuated switches have the potential to enhance the safety and efficacy of many other cellular chassis communities used in therapies including stem cells and therapeutic microbes.

1.7 Outlook

In summary, ultrasound is a versatile modality for observing and perturbing biological function in living organisms, with intrinsic advantages owing to its fundamental physics and tissue interactions. The field of biomolecular ultrasound and sonogenetics seeks to connect these characteristics to the function of specific biomolecules and cells to enable precise imaging and control of cellular processes. This is accomplished by identifying and engineering biomolecular agents with the appropriate properties to interact with sound waves or their resultant thermal and mechanical effects. Although this field is in its infancy, the recent developments in temperature-sensitive biomolecules open the door to precise sonogenetic control, analogous to optogenetics and chemogenetics, and will create new opportunities to deploy advanced biomolecular tools in biological and clinical scenarios.

Much work remains to be done before these nascent technologies will have a major impact on biology or medicine. For example, current FUS heating technologies target both the engineered cells and bystander tissues. This off-target heating could be detrimental in healthy tissues and limits the scope of FUS heating to tumors where damage to the surrounding tissue can be seen as a beneficial side effect. To overcome this bottleneck, there is a need for technologies that exclusively localize heating to engineered cells. This could be done by expressing the genes necessary to form magnetic particles within engineered cells. These magnetic particles could then be used as receivers that locally respond to magnetic waves and elevate temperature within engineered cells. In parallel, there is a great need for purely thermal sensitive bioswitches that function within mammalian cells. While similar

technologies are feasible in microbes, a lot more work and engineering is needed before these switches become a reality in mammalian cells.

6. References

1. Szabo TL. 2004. *Diagnostic ultrasound imaging: inside out*: Academic Press
2. Azhari H. 2010. *Basics of biomedical ultrasound for engineers*: John Wiley & Sons
3. Cobbold RS. 2006. *Foundations of biomedical ultrasound*: Oxford University Press
4. Hynynen K, Darkazanli A, Unger E, Schenck JF. 1993. MRI-guided noninvasive ultrasound surgery. *Med Phys* 20: 107-15
5. Hynynen K, Clement GT, McDannold N, Vykhodtseva N, King R, et al. 2004. 500-element ultrasound phased array system for noninvasive focal surgery of the brain: a preliminary rabbit study with ex vivo human skulls. *Magn Reson Med* 52: 100-7
6. Nyborg WL, Miller DL. 1982. Biophysical Implications of Bubble Dynamics. *Applied Scientific Research* 38: 17-24
7. Petersson F, Nilsson A, Holm C, Jonsson H, Laurell T. 2004. Separation of lipids from blood utilizing ultrasonic standing waves in microfluidic channels. *Analyst* 129: 938-43
8. Postema M. 2011. *Fundamentals of medical ultrasonics*: CRC Press
9. Jolesz FA, Hynynen K, McDannold N, Tempany C. 2005. MR imaging-controlled focused ultrasound ablation: a noninvasive image-guided surgery. *Magn Reson Imaging Clin N Am* 13: 545-60
10. Hesley GK, Gorny KR, Woodrum DA. 2013. MR-guided focused ultrasound for the treatment of uterine fibroids. *Cardiovasc Intervent Radiol* 36: 5-13
11. Uchida T, Nakano M, Hongo S, Shoji S, Nagata Y, et al. 2012. High-intensity focused ultrasound therapy for prostate cancer. *Int J Urol* 19: 187-201
12. Illing RO, Kennedy JE, Wu F, ter Haar GR, Protheroe AS, et al. 2005. The safety and feasibility of extracorporeal high-intensity focused ultrasound (HIFU) for the treatment of liver and kidney tumours in a Western population. *Br J Cancer* 93: 890-5
13. Carpentier A, Canney M, Vignot A, Reina V, Beccaria K, et al. 2016. Clinical trial of blood-brain barrier disruption by pulsed ultrasound. *Sci Transl Med* 8: 343re2
14. Hynynen K, McDannold N, Vykhodtseva N, Jolesz FA. 2001. Noninvasive MR imaging-guided focal opening of the blood-brain barrier in rabbits. *Radiology* 220: 640-6
15. Machet L, Boucaud A. 2002. Phonophoresis: efficiency, mechanisms and skin tolerance. *Int J Pharm* 243: 1-15
16. Chaussy C, Brendel W, Schmiedt E. 1980. Extracorporeally induced destruction of kidney stones by shock waves. *Lancet* 2: 1265-8
17. Mason T, Lorimer J. 2002. Applied Sonochemistry. *Applied Sonochemistry*
18. Leung TK, Rajendran MY, Monfries C, Hall C, Lim L. 1990. The human heat-shock protein family. Expression of a novel heat-inducible HSP70 (HSP70B') and isolation of its cDNA and genomic DNA. *Biochem J* 267: 125-32
19. McKemy DD, Neuhausser WM, Julius D. 2002. Identification of a cold receptor reveals a general role for TRP channels in thermosensation. *Nature* 416: 52-8
20. Hoynes-O'Connor A, Hinman K, Kirchner L, Moon TS. 2015. De novo design of heat-repressible RNA thermosensors in E. coli. *Nucleic Acids Res* 43: 6166-79
21. Valdez-Cruz NA, Caspeta L, Perez NO, Ramirez OT, Trujillo-Roldan MA. 2010. Production of recombinant proteins in E. coli by the heat inducible expression system based on the phage lambda pL and/or pR promoters. *Microb Cell Fact* 9: 18
22. Hurme R, Berndt KD, Normark SJ, Rhen M. 1997. A proteinaceous gene regulatory thermometer in Salmonella. *Cell* 90: 55-64

23. Madio DP, van Gelderen P, DesPres D, Olson AW, de Zwart JA, et al. 1998. On the feasibility of MRI-guided focused ultrasound for local induction of gene expression. *J Magn Reson Imaging* 8: 101-4
24. Braiden V, Ohtsuru A, Kawashita Y, Miki F, Sawada T, et al. 2000. Eradication of breast cancer xenografts by hyperthermic suicide gene therapy under the control of the heat shock protein promoter. *Hum Gene Ther* 11: 2453-63
25. Xiong X, Sun Y, Sattiraju A, Jung Y, Mintz A, et al. 2015. Remote spatiotemporally controlled and biologically selective permeabilization of blood-brain barrier. *J Control Release* 217: 113-20
26. Deckers R, Quesson B, Arsaut J, Eimer S, Couillaud F, Moonen CT. 2009. Image-guided, noninvasive, spatiotemporal control of gene expression. *Proc Natl Acad Sci U S A* 106: 1175-80
27. Guilhon E, Voisin P, de Zwart JA, Quesson B, Salomir R, et al. 2003. Spatial and temporal control of transgene expression in vivo using a heat-sensitive promoter and MRI-guided focused ultrasound. *J Gene Med* 5: 333-42
28. Giaccia AJ, Auger EA, Koong A, Terris DJ, Minchinton AI, et al. 1992. Activation of the heat shock transcription factor by hypoxia in normal and tumor cell lines in vivo and in vitro. *Int J Radiat Oncol Biol Phys* 23: 891-7
29. Batulan Z, Shinder GA, Minotti S, He BP, Doroudchi MM, et al. 2003. High threshold for induction of the stress response in motor neurons is associated with failure to activate HSF1. *J Neurosci* 23: 5789-98
30. Oehler R, Pusch E, Zellner M, Dungel P, Hergovics N, et al. 2001. Cell type-specific variations in the induction of hsp70 in human leukocytes by feverlike whole body hyperthermia. *Cell Stress Chaperones* 6: 306-15
31. de Marco A, Vigh L, Diamant S, Goloubinoff P. 2005. Native folding of aggregation-prone recombinant proteins in Escherichia coli by osmolytes, plasmid- or benzyl alcohol–overexpressed molecular chaperones. *Cell Stress & Chaperones* 10: 329-39
32. Zhao K, Liu M, Burgess RR. 2005. The Global Transcriptional Response of Escherichia coli to Induced σ32 Protein Involves σ32 Regulon Activation Followed by Inactivation and Degradation of σ32 in Vivo. *Journal of Biological Chemistry* 280: 17758-68
33. Piraner DI, Abedi MH, Moser BA, Lee-Gosselin A, Shapiro MG. 2017. Tunable thermal bioswitches for in vivo control of microbial therapeutics. *Nat Chem Biol* 13: 75-80
34. Stanley SA, Sauer J, Kane RS, Dordick JS, Friedman JM. 2015. Remote regulation of glucose homeostasis in mice using genetically encoded nanoparticles. *Nat Med* 21: 92-98
35. Huang H, Delikanli S, Zeng H, Ferkey DM, Pralle A. 2010. Remote control of ion channels and neurons through magnetic-field heating of nanoparticles. *Nat Nano* 5: 602-06
36. Chen R, Romero G, Christiansen MG, Mohr A, Anikeeva P. 2015. Wireless magnetothermal deep brain stimulation. *Science*
37. Yoo S, Kim R, Park J-H, Nam Y. 2016. Electro-optical Neural Platform Integrated with Nanoplasmonic Inhibition Interface. *ACS Nano* 10: 4274-81
38. Carvalho-de-Souza JL, Treger JS, Dang B, Kent SBH, Pepperberg DR, Bezanilla F. 2015. Photosensitivity of neurons enabled by cell-targeted gold nanoparticles. *Neuron* 86: 207-17

C h a p t e r 2

TUNABLE THERMAL BIOSWITCHES FOR IN VIVO CONTROL OF MICROBIAL THERAPEUTICS

Piraner, D. I., Abedi, M. H., Moser, B. A., Lee-Gosselin, A., & Shapiro, M. G. (2017). Tunable thermal bioswitches for in vivo control of microbial therapeutics. *Nature Chemical Biology*, *13*(1), 75–80. https://doi.org/10.1038/nchembio.2233

2.1 Introduction

Rapid advances in synthetic biology[1, 2] are driving the development of genetically engineered microbes as therapeutic[3-6] and diagnostic[7-10] agents for a multitude of human diseases. A critical capability for many envisioned applications is the ability to control the function of engineered microbes *in situ* to enable spatially and temporally specific activation at anatomical and disease sites such as the gastrointestinal tract or tumors[2]. However, among existing control methods, systemic chemical administration typically lacks the spatial precision needed to modulate activity at specific anatomical locations, while optical approaches suffer from poor light penetration into tissues[11]. On the other hand, temperature can be controlled both globally and locally--at depth--using technologies such as focused ultrasound[12], infrared light[13] and magnetic particle hyperthermia[14]. In addition, body temperature can serve as an indicator of microbial entry and exit from the host organism and of the host's condition (*e.g.*, fever).

Given this potential, remarkably few high-performance thermal bioswitches are available to control gene expression in engineered microbes. The ideal bioswitch should have a sharp thermal transition resulting in a large change in activity (> 100-fold over a few degrees), and its switching temperature should be tunable to enable a broad range of applications. In

addition, the bioswitch should be orthogonal to endogenous cellular machinery and compatible with other thermo-responsive components to allow multiplexed thermal logic. Existing temperature-dependent regulators of gene expression--including microbial heat shock factors, membrane-associated proteins, RNA thermometers, and transcriptional repressors--fail to fulfill these criteria. Microbial heat shock promoters undergo a relatively low level of thermal induction (~10-fold)[15], have crosstalk with other stimuli such as chemical stress[16], and may be difficult to tune without deleterious effects on the cell. Likewise, the switching temperature of membrane-associated proteins depends on bilayer composition and occupies second messenger pathways[17]. Meanwhile, RNA thermometers, while orthogonal to the host and amenable to tuning, generally have small dynamic ranges (< 10-fold) and broad transitions (> 10 °C)[18-25]. Of the available molecular machinery, several natural and mutant transcriptional repressors have the most robust thermal switching and potential for orthogonality[26-32]. However, their relative performance has not been characterized, they have not been systematically engineered to operate at specific transition temperatures, and their potential utility for *in vivo* microbial therapy applications has not been demonstrated.

To address the need for robust, tunable, orthogonal thermal control of engineered microbial systems, we systematically screened candidate transcriptional regulators, developed two orthogonal families of high-performance thermal bioswitches with tunable thresholds within the biomedically relevant range of 32ºC to 46ºC, and demonstrated the potential utility of these devices in three distinct *in vivo* scenarios relevant to mammalian microbial therapy. These scenarios include spatially selective activation within a mammalian host using focused ultrasound, sensing and response to a fever, and self-destruction at ambient temperatures to prevent environmental contamination after leaving the intended host.

2.2: Results

2.2a: High-Performance Thermal Bioswitches

In order to engineer new families of robust, tunable, orthogonal thermal bioswitches, we began by characterizing the performance of six temperature-dependent transcriptional repressors and six endogenous heat shock promoters. Our panel included TlpA, a transcriptional autorepressor from the virulence plasmid of *Salmonella typhimurium*. This protein contains an approximately 300 residue C-terminal coiled-coil domain that undergoes sharp, temperature-dependent uncoiling between 37ºC and 45ºC , and an N-terminal DNA binding domain that, in its low-temperature dimeric state, blocks transcription from the 52 bp TlpA operator/promoter[26, 32]. In addition, we tested a well-known temperature-sensitive variant of the bacteriophage λ repressor cI (mutant cI^{857}, here referred to as TcI) acting on a tandem pR/pL operator/promoter[27]. In most previous applications, TcI repression has been modulated via large changes in temperature (e.g., steps from 30°C to 42°C)[27]. However, its original description as a virulence factor suggested that much sharper switching may be possible[28]. Alongside TlpA and TcI, we tested four reported temperature-sensitive mutants of the *E. coli* repressors TetR (A89D and I193N)[29] and LacI (A241T and G265D)[30, 31], together with a panel of endogenous heat shock promoters, including GrpE, HtpG, Lon, RpoH, Clp and DnaK (**Fig. 2-1a**).

The performance of these constructs is summarized in **Figure 2-1b**. TlpA and TcI had by far the largest dynamic ranges (355 ± 45 and >1,432, respectively), reflecting a combination of tighter repression at sub-threshold temperatures and stronger promoter activity above threshold. Both of these repressors show sharp thermal transitions, with greater than 30-fold induction over ranges of 5ºC and 3ºC centered at 43.5°C and 39.5ºC for TlpA and TcI, respectively (**Fig. 2-1c**). Furthermore, both systems are capable of rapid induction, with greater than 10-fold changes in expression observed after a 1 hour thermal stimulus (**Fig. 2-1d**). Complete time-temperature induction profiles for TlpA and TcI are shown in **Figure 2-1, e–f**. In addition to their high performance, TlpA and TcI are expected to be more orthogonal to cellular machinery than both the native heat shock promoters and the engineered TetR and LacI repressors, the latter of which is utilized in multiple endogenous

and engineered gene circuits[33-35]. A homology search[36] showed that TlpA and TcI repressors are present in far fewer bacterial species than either TetR or LacI (**Supplementary Fig. 2-S1**). Based on these factors, we chose TlpA and TcI as our starting points for further bioswitch engineering.

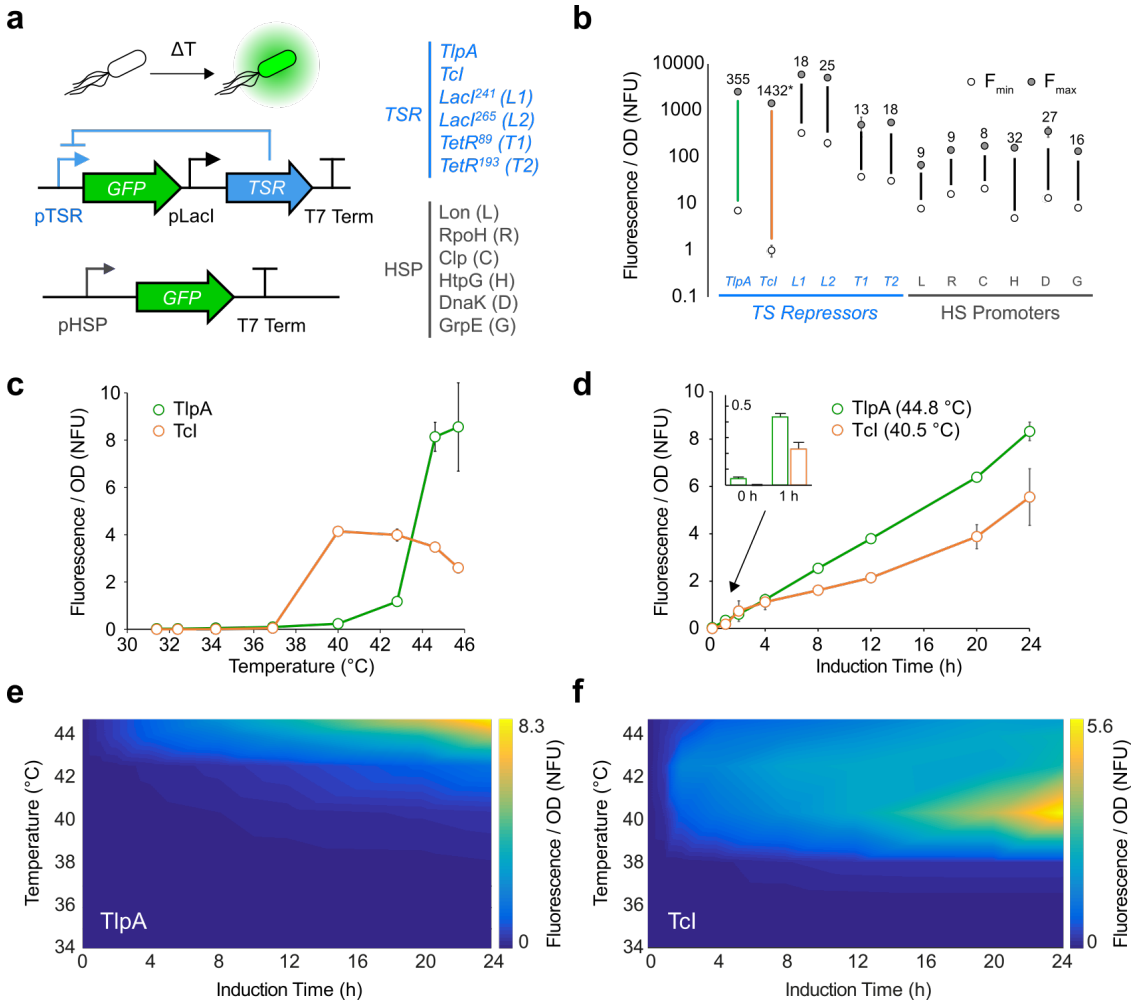

Figure 2-1: High-performance thermal bioswitches. (**a**) Constructs used to assay the performance of temperature-sensitive repressors (TSr, top) and heat shock promoters (HSP, bottom). The specific repressors and promoters assayed are listed in blue and gray, respectively. (**b**) Optical density (oD)-normalized fluorescence after 12 h of thermal induction for the constructs shown in **a**. nFu, normalized fluorescence units. Fmin represents expression at 31.4 °C; Fmax is the maximum

fluorescence intensity measured for each construct, measured up to 45.7 °C. The fold changes between Fmin and Fmax are listed above each sample. Where not seen, error bars are smaller than the symbol. N = 4 for TSrs and N = 3 for HSPs. The Fmin for TcI (indicated by *) is reported from measurement at 34.2 °C because expression at lower temperatures was below the detection limit of the assay. (**c**) oD-normalized fluorescence from the Tlpa- and TcI-regulated constructs as a function of induction temperature for a fixed duration of 12 h. N = 4. (**d**) oD-normalized fluorescence as a function of thermal induction duration at the maximal induction temperature for the Tlpa and TcI constructs. N = 4. (**e**,**f**) oD-normalized fluorescence landscapes for Tlpa- and TcI-gated constructs, respectively, as a function of both incubation temperature and duration. Data shown interpolated from an 8 × 8 sampling matrix. All samples in d–f were maintained at 30 °C after the indicated period of thermal induction for a total experimental duration of 24 h before measurement. Error bars represent ± s.e.m.

Since the TlpA operator/promoter has not been studied in *E. coli*, we characterized its molecular mechanisms to inform its utilization in genetic circuits. As shown in **Supplementary Figure 2-S2**, the TlpA operator is a strong promoter (88-fold stronger than $LacI^{Q}$) driven by the transcription factor σ^{70}. Interestingly, this promoter has bidirectional activity with identical thermal regulation in both orientations, but approximately 200-fold lower maximal expression in the reverse direction (**Supplementary Fig. 2-S2, c–d**). This property will enable convenient adjustment of TlpA-regulated expression according to circuit requirements.

2.2b: Tuning Bioswitch Activation Temperatures

Applications in microbial therapy require thermal bioswitches that activate at different transition temperatures. For example, a host colonization sensor should be activated at 37ºC, while a fever detector may work best with a thermal threshold of 39ºC, and a focused ultrasound-activated switch may require a transition point of 41ºC to avoid nonspecific actuation. Synthetic biology applications outside biomedicine may likewise have a variety of thermal requirements. It is thus highly desirable to be able to tune thermal bioswitches to

activate at new temperatures while retaining sharp, robust switching performance. To enable such tuning of TlpA and TcI, we devised a simple and effective high-throughput assay based on colony fluorescence. We grew *E. coli* expressing GFP under the control of mutant repressors (generated by error-prone PCR) on solid media and replica-plated the colonies onto separate plates for simultaneous incubation at desired "off" and "on" temperatures (**Supplementary Fig. 2-S3a**). We then imaged the plates with wide-field fluorescence, as shown in **Figure 2-2a**. As expected, many colonies show constitutive expression (ostensibly due to loss of repressor function) while others fail to de-repress (most likely retaining their original high transition point). However, several colonies show thermal induction in the desired regime. Within each screen, we selected several such colonies to undergo liquid phase characterization of induction temperature, switching sharpness, and expression levels (**Fig. 2-2b**). From these variants, we selected mutants that retained the desirable performance characteristics of the wild type repressor, but with shifted transition temperatures.

Screening of TlpA mutants at off-on temperatures of 30–37ºC and 37–40ºC produced high-performance bioswitches centered at 36 °C and 39 °C, respectively, which we named $TlpA_{36}$ and $TlpA_{39}$ (**Fig. 2-2c**). For TcI, we selected both downshifted (TcI_{38}, T_m = 38°C) and upshifted (TcI_{42}, T_m = 42 °C) variants relative to the original protein (**Fig. 2-2d**). Together, the engineered TlpA and TcI repressor families cover the biomedically relevant range of 32ºC to 46ºC (**Supplementary Fig. 2-S3b**) while demonstrating a dynamic range similar to that of the wild type protein (**Supplementary Table 2-T1**). The amino acid substitutions identified in these bioswitch variants are shown in **Supplementary Figure 2-S4**. The observed decrease in fluorescence at the highest temperatures tested may be due to thermal instability of the cell's transcriptional and translational machinery. Remarkably, a single round of mutagenesis was sufficient in all cases to obtain at least one variant with the desired switching behavior, suggesting that both TlpA and TcI are highly tunable for a broad range of applications.

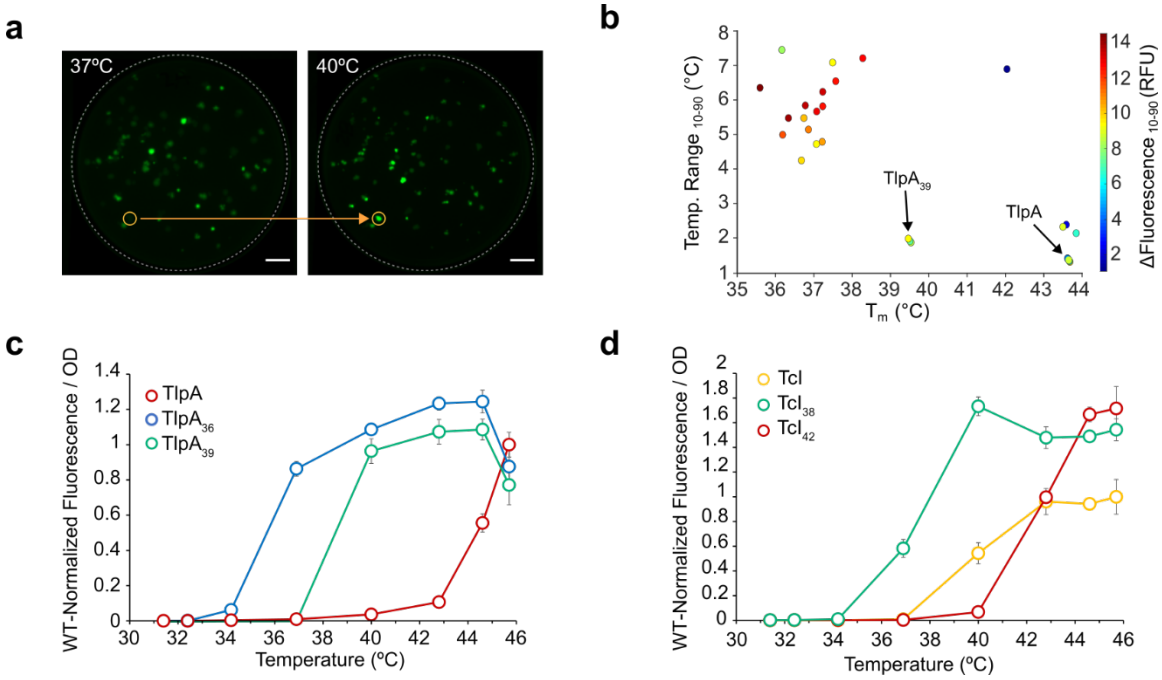

Figure 2-2: Tuning the transition temperature of thermal bioswitches. (**a**) Fluorescence image of replica plates used to screen for TlpA variants turning on between 37 °C and 40 °C. One colony selected for further assay is indicated by the orange circle. Scale bars, 1 cm. (**b**) TlpA variants plotted by their measured midpoint transition temperatures (T50) and 10–90% transition range (T10–90), estimated by linear interpolation. The color of each data point maps to the change in fluorescence over the T10–90 span. (**c**) oD-normalized fluorescence of the novel Tlpa variants normalized to wild type (WT). (**d**) oD-normalized fluorescence of the novel TcI variants normalized to wild type. N = 4 for c and d. RFR, relative fluorescence units. Error bars represent ± s.e.m.

3.2c: Thermal Logic Circuits Using Orthogonal Bioswitches

To enable microbial therapy applications, it is useful to develop thermal logic circuits capable of controlling multiple functions at different temperatures or confining activity to within a narrow thermal range. This would enable cells to, for example, initiate one therapeutic function upon host colonization and switch to a different function during a host fever

response or local activation with focused ultrasound. We hypothesized that since TlpA and TcI act on orthogonal target sequences, we could combine them in circuits designed for multiplexed thermal control or band-pass activation of microbial function. To assess the first possibility (**Fig. 2-3a**), we made a construct encoding a GFP modulated by $TlpA_{36}$ and an RFP regulated by TcI (**Fig. 2-3b**). As predicted, upon exposure to a range of temperatures, the two reporter genes were activated independently at their expected thresholds, with no apparent crosstalk in their induction (**Fig. 2-3c**). Independent thermal control of the co-expressed circuits is illustrated by spatially patterned bacterial variants incubated at 37ºC and 42ºC (**Fig. 2-3d**). Next, to develop a thermal band-pass filter (**Fig. 2-3e**), we engineered a circuit placing the expression of RFP under the control of the lambda operator, gated by both TcI (turning on above 36ºC) and the temperature-independent wild type cI repressor, which was itself placed under the control of TlpA (activating above 43ºC) as shown in **Figure 2-3f**. The cI open reading frame was preceded by a T7 terminator and a weak ribosome binding site to reduce buildup of this repressor at 40–43 °C due to leakage of the upstream TlpA operon. This resulted in RFP expression confined between 36 and 44ºC, while simultaneously turning on GFP above RFP's turn-off temperature (**Fig. 2-3, g–h**).

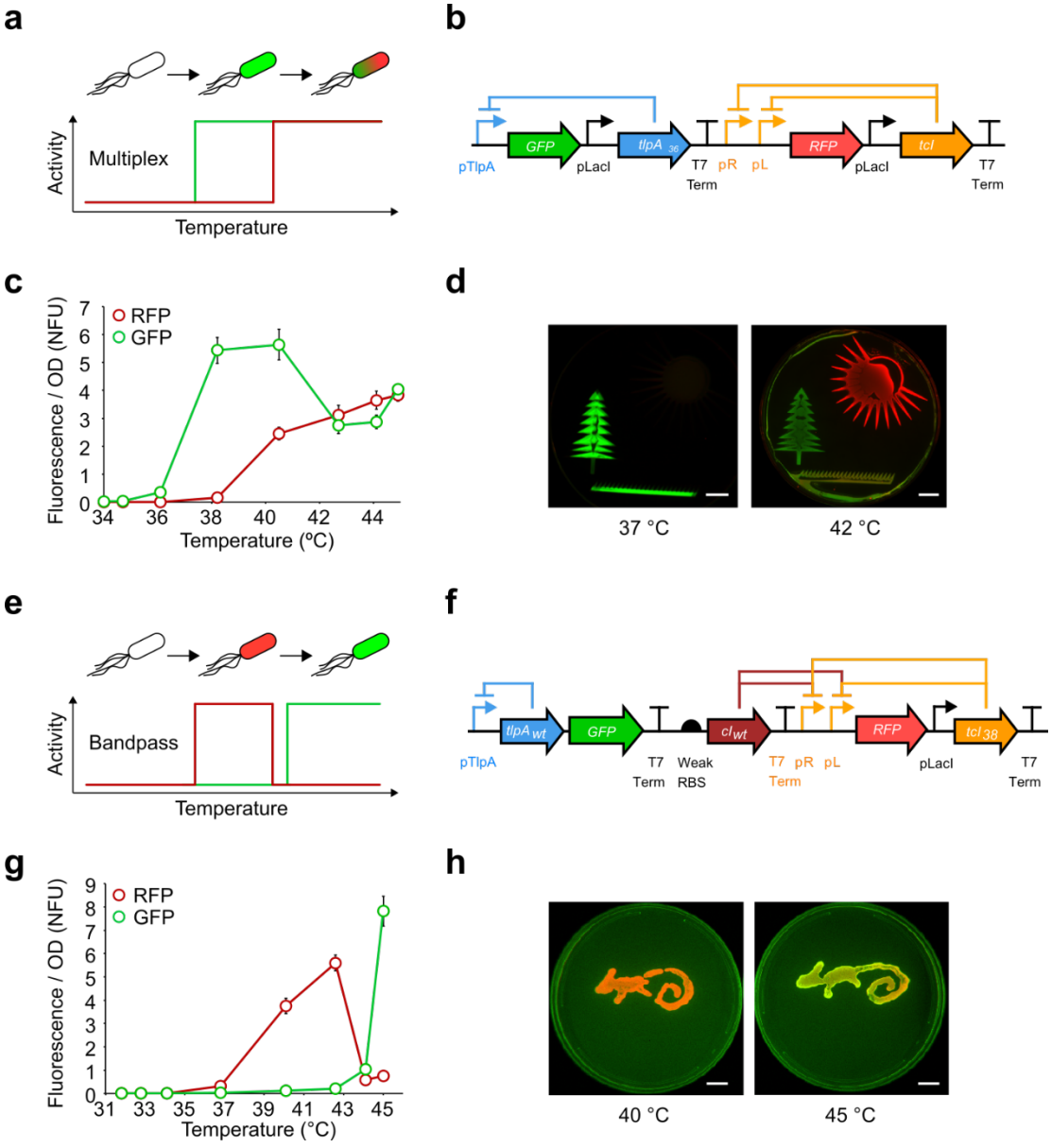

Figure 2-3: Thermal logic circuits. (**a**) Diagram illustrating multiplexed thermal activation. (**b**) Circuit diagram of the pCali2 plasmid, which contains GFP gated by $TlpA_{36}$ and RFP gated by TcI. (**c**) Expression of GFP and RFP from pCali2-containing *E. coli* over the indicated range of temperatures (12-h incubation). (**d**) Plate images of overlaid GFP and RFP fluorescence from the pCali2 plasmid (grass) and plasmids expressing only the green (tree) and red (sun) components. Note that at 42 °C the grass shows both green and red fluorescence. (**e**) Diagram illustrating a thermal

bandpass filter. (**f**) Circuit diagram of the pThermeleon plasmid, in which RFP is gated by TcI_{38} and also by the wild-type cI repressor. GFP is gated by $TlpA_{wt}$ on the same plasmid, which also weakly drives the expression of cI_{wt} through a T7 terminator and weak ribosome-binding site. (**g**) Thermal expression profile of RFP and GFP from pThermeleon-containing *E. coli* (12 h incubation). (**h**) Overlaid GFP and RFP fluorescence images of plated bacteria containing pThermeleon cultured at 40 °C and 45 °C. Scale bars, 1 cm. N = 4 for **c** and **g**. Error bars represent ± s.e.m.

2.2d: Spatially Targeted Control Using Focused Ultrasound

After developing TlpA and TcI-based thermal bioswitches, we demonstrated their utility in three prototypical microbial therapy scenarios. First, we tested the ability of thermal bioswitches to mediate spatially-selective control of microbial therapies using focused ultrasound, a modality that is well established in its ability to elevate temperatures in deep tissues with millimeter spatial precision [12] and utilized clinically to treat diseases such as cancer[37] and essential tremor[38]. Focused ultrasound has been used to activate gene expression in mammalian cells[39], but has not, to our knowledge, been employed to control the activity of microbes *in vivo*. Such control could be highly advantageous in applications where the activity of a systemically administered microbial therapy needs to be localized to a specific anatomical site, such as a deep-seated tumor or section of the gastrointestinal tract, which would be difficult to reach with optogenetic triggers. To test this concept, we first activated gene expression using focused ultrasound in tissue-mimicking phantoms under the guidance of magnetic resonance imaging (MRI)[40] (**Fig. 2-4a**). This guidance enabled precise spatial targeting of the ultrasound focus and real-time monitoring and adjustment of local temperature. We first applied this technique to a flat lawn of *E. coli* containing the multiplexed expression circuit shown in **Figure 2-3b**. This specimen was assembled with a tissue-mimicking tofu phantom, and steady-state focal heating over 45 min resulted in a radial thermal gradient with an average focal temperature of 42ºC, as observed by real-time MRI thermometry (**Fig. 2-4b**). A corresponding pattern of spatially localized fluorescence is seen in **Figure 2-4c**.

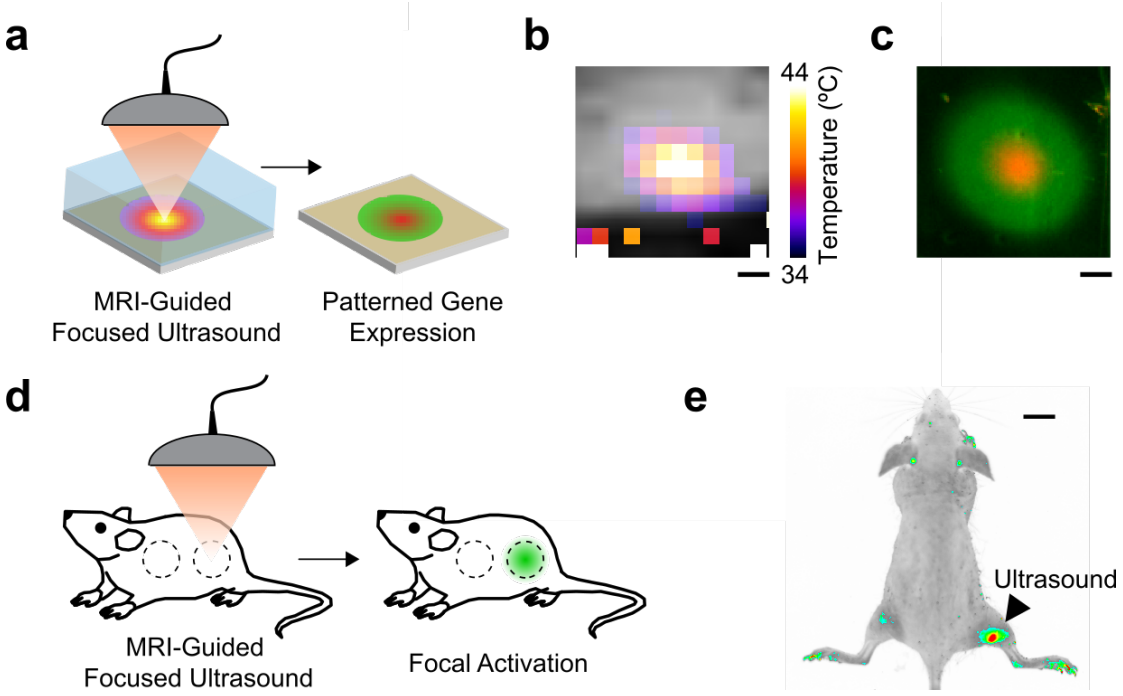

Figure 2-4: Remote control of bacterial agents using focused ultrasound. (**a**) Illustration of the *in vitro* focused ultrasound experiment: focused ultrasound is used to heat a target area of a bacterial culture lawn through a tofu phantom (depicted as translucent) under MRI guidance, followed by fluorescence imaging. (**b**) MRI-based temperature map of the bacterial specimen during steady-state ultrasound application, overlaid on a raw grayscale MRI image of the phantom. (**c**) Fluorescence image of the region targeted by ultrasound, showing activation consistent with a bacterial construct expressing GFP under the control of $TlpA_{36}$ and RFP regulated by TcI. (**d**) Illustration of the *in vivo* experiment, in which focused ultrasound is used to activate subcutaneously injected bacterial agents at a specific anatomical site. (**e**) Representative thresholded fluorescence map of a mouse injected subcutaneously in both left and right hindlimbs with *E. coli* expressing GFP under the control of $TlpA_{36}$, following ultrasound activation directed at only the right hindlimb. Scale bars, 2 mm (**b**,**c**) and 1 cm (**e**).

To establish the feasibility of this approach *in vivo*, we injected *E. coli* expressing GFP under the control of $TlpA_{36}$ subcutaneously into both hindlimbs of a nude mouse and applied MRI-

guided focused ultrasound to one location (**Fig. 2-4d**) to produce a local steady-state temperature of 41ºC for 45 min to 1 hour. This thermal dose is below the damage thresholds for mammalian tissues such as muscle and brain[41, 42]. *In vivo* fluorescence imaging four hours after ultrasound treatment showed robust expression of GFP specifically at the ultrasound-targeted anatomical site (**Fig. 2-4e**). Two additional animals undergoing the same procedure are shown in **Supplementary Figure 2-S5**. $TlpA_{36}$ was selected as the thermal bioswitch for these experiments because its activation threshold is approximately 4ºC above the typical murine cutaneous temperature[43], a sufficient difference for site-specific ultrasound activation.

2.2e: Programmed Responses to Mammalian Host Temperature

Next, we sought to develop autonomous thermosensitive microbes responsive to endogenous changes in host temperature. First, we investigated whether bacteria can be engineered to sense and respond to a host fever (**Fig. 5a**). We subcutaneously injected one flank of a nude mouse with *E. coli* expressing GFP under the control of $TlpA_{36}$, and the other flank with *E. coli* expressing GFP controlled by wild type TlpA as a high-threshold control for non-specific activation. The mouse was then housed at 41ºC for two hours in an established fever model paradigm[44]. *In vivo* fluorescent imaging four hours after fever induction shows robust expression of GFP in the flank injected with $TlpA_{36}$–regulated bacteria (**Fig. 5b**). No significant activation is seen in the opposite flank or in a mouse housed at room temperature (**Fig. 5c**). Two additional replicates are shown in **Supplementary Figure 6**.

Second, we tested whether a thermal bioswitch operating at 37ºC could be used to confine the activity of genetically engineered microbes to the *in vivo* environment of a mammalian host and thereby limit the potential for environmental contamination. Towards this end, we designed a genetic circuit in which $TlpA_{36}$ controls the expression of CcdA, a bacterial antitoxin, while constitutively expressing the toxin CcdB, thereby restricting growth to temperatures above 37ºC (**Fig. 5d**). A degradation tag was fused to CcdA to accelerate cell

death at non-permissive temperatures. Bacteria carrying this plasmid grew normally above this permissive temperature, while bacteria incubated at 25ºC had significantly reduced survival as demonstrated by their CFU counts in **Figure 5e**. We administered these bacteria to mice by oral gavage and collected fecal pellets after five hours to allow transit through the gastrointestinal tract. The pellets were kept for 24 hours at either 25ºC, corresponding to excretion into the ambient environment, or at 37ºC, equivalent to persistent residence in the gut, and subsequently assayed for colony formation. The survival of cells excreted into ambient temperature was reduced by ten thousand-fold compared to cells maintained under host conditions (**Fig. 5f**).

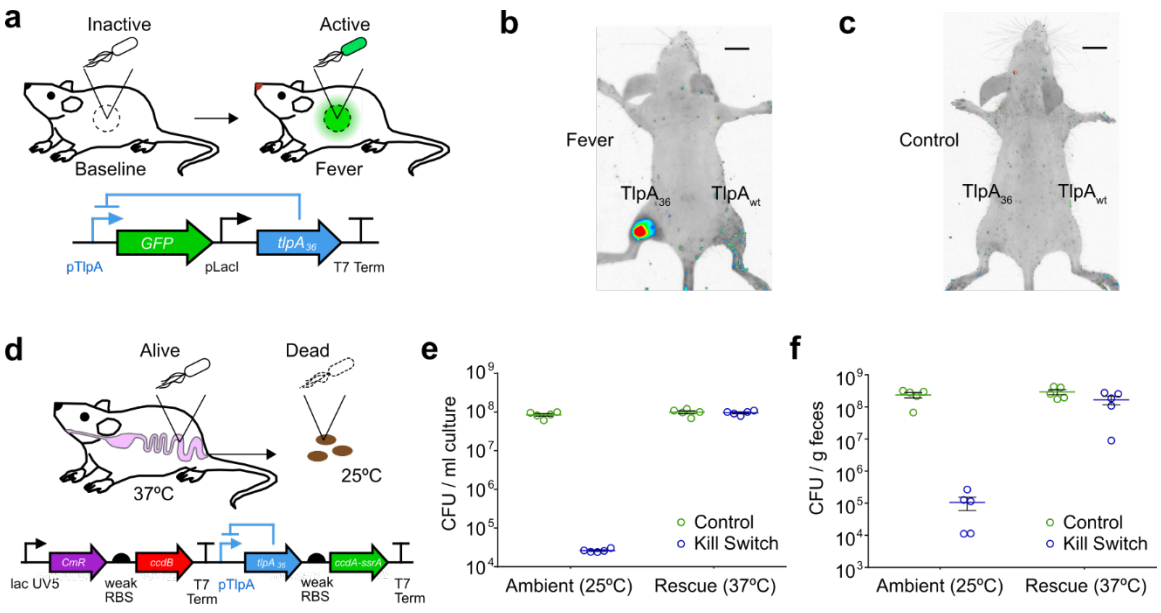

Figure 2-5: Programmed responses to mammalian host temperature. (**a**) Illustration of the fever-induced activation experiment and circuit diagram of the corresponding *E. coli* construct. (**b**) Representative thresholded fluorescence map of a mouse that underwent fever induction after being injected subcutaneously with plasmids expressing TlpaA$_{36}$- and TlpA-regulated GFP into the left and right hindlimbs, respectively. (**c**) Representative thresholded fluorescence map of a mouse that was prepared identically to the animal in **b** but maintained at room temperature. (**d**) Illustration of the

temperature-based host confinement strategy, and circuit diagram of the thermal kill switch permitting bacterial survival only at temperatures above 36 °C, at which antitoxin expression is derepressed by $TlpA_{36}$. (**e**) Colony counts from liquid cultures of kill-switch-containing cells and controls (containing no toxin system) after 24 h of incubation at the indicated temperature. P = 0.0002 for kill switch versus control cells at 25 °C and P < 0.0001 for kill switch at 25 °C versus 37 °C. N = 5. (**f**) Colony counts in fecal samples freshly collected from N = 5 mice 5 h after oral gavage of kill-switch-containing *E. coli* or controls. The feces were incubated at a temperature representative of post-defecation conditions (25 °C) or were rescued at 37 °C. P = 0.0067 for kill switch versus control cells at 25 °C and P = 0.0275 for kill switch at 25 °C versus 37 °C. N = 5. Error bars represent ± s.e.m. Scale bars, 1 cm.

2.3: Discussion

Our results establish two new families of high-performance, orthogonal thermal bioswitches with tunable activation thresholds to enable a variety of biotechnology applications. Both TlpA- and TcI-based switches respond to temperature with hundreds-fold changes in gene expression. If needed, this response could be further boosted using well-established strategies such as tandem operators and positive feedback amplification[45, 46]. In addition, the temporal response of thermal bioswitch circuits could be made either more transient, by manipulating the lifetime of the resulting transcripts and proteins, or longer-lasting using genetic toggle switches or recombinase-based architectures[30, 47]. This may enable persistent functions to be controlled with thermal stimuli shorter than those used in this study.

Our strategy for tuning the thermal response of TlpA and TcI is rapid and simple to implement. The fact that we could identify high-performance variants with new transition temperatures by screening several hundred mutants suggests that many different sequences could satisfy a given thermal requirement. Here, we focused on bioswitches operating between 32 and 46ºC, in keeping with potential therapeutic applications and the thermal tolerance of our bacterial chassis. We expect that a similar selection strategy using thermophilic or cryophilic bacteria could be used to tune TlpA and TcI over a yet broader

temperature range for industrial applications such as biofuel production. The thermal stability of the regulated gene product will need to be taken into account in these scenarios. Within the temperature range tested in this study, GFP, RFP and CcdA were functional.

The presented bioswitches have sequences orthogonal to bacterial host machinery and to each other, enabling multiplexed thermal actuation. If desired, additional multiplexing could be accomplished by replacing the DNA-binding domains of TlpA or TcI with those of other dimeric repressors. Additional engineering may be needed to adapt this technology to other host organisms. Certain species of therapeutic microbes, such as *Lactobacillus spp.*, are able to use some promoters transferred directly from *E. coli*[48]. Others may require incorporation of the relevant operator sequences into promoters native to the host[49]. Alternatively, fusions of TlpA and TcI with DNA binding domains from other microbes or eukaryotes could adapt TlpA and TcI for use in these species.

The three *in vivo* scenarios demonstrated in this work will inform the use of thermal bioswitches in future microbial therapy applications. For example, the ability to detect a host's fever provides a potential safety mechanism with which to curtail effector activity in response to runaway inflammation, a major and sometimes lethal side-effect of antitumor cell therapy[50]. In addition, temperature-dependent kill switches can be used to restrict the survival of enterically-administered microbes to host body temperature and thereby mitigate the risk of patients shedding genetically modified, pharmaceutically active organisms into the surrounding environment. Such kill switches can be incorporated into recently developed multilayered and multi-input containment circuits for greater efficiency in preventing mutational escape[51, 52]. Furthermore, the ability to activate microbial function at specific anatomical sites using focused ultrasound opens new therapeutic avenues by potentially allowing a physician to locally target therapeutic effects that would be intolerable via systemic administration. Additionally, the ability to trigger gene expression *in vivo* can be

combined with genetically encoded genomic or proteomic tools[53-55] to enable the study of cellular signaling within the context of mammalian hosts.

2.4: Methods

Plasmid Construction and Molecular Biology

All constructs were made via restriction cloning, KLD mutagenesis, or Gibson Assembly using enzymes from New England Biolabs. All plasmids and their sources of genetic material are described in **Supplementary Table 2-T2**. All constructs were cloned in Mach1 *E. coli* (Thermo Fisher) and the sequence-validated plasmids were assayed in NEB10β *E. coli* (NEB). Fluorescent reporters referred to in the text as GFP and RFP are mWasabi and mCherry, respectively[56, 57].

Thermal Regulation Assay

2 mL cultures of 2xYT media with 100 μg/mL ampicillin were inoculated with a single colony per culture and grown at 30 °C, 250 rpm for 20 hours. After dilution to OD_{600} = 0.1 in LB (Sigma) with 100 μg/mL ampicillin, the cells were propagated at 30 °C, 250 rpm for 1.5 hours, after which OD_{600} was measured using a Nanodrop 2000c (Thermo Scientific) in cuvette mode every 10 minutes. At OD_{600} = 0.25, the cultures were dispensed in 25 μL aliquots into 8 well PCR strips with optically transparent caps (Bio-Rad) using a multichannel pipette and placed into a spatial temperature gradient formed by a Bio-Rad C1000 Touch thermocycler with the lid set to 50 °C. The temperature in each thermocycler well was verified using a TEF-30-T thermocouple (J-KEM Scientific) immersed in 25 μL of pure water within a PCR tube. After the prescribed thermal stimulus, PCR strips were removed, vortexed, spun down on a tabletop centrifuge and the fluorescence was measured using a Stratagene MX3005p qPCR (Agilent). Immediately after measurement, the cultures were diluted with 75 μL LB/Amp and mixed, after which 90 μL of culture was transferred into 96 well plates (Costar black / clear bottom) for measurement of OD_{600} using a SpectraMax M5 plate reader (Molecular Devices). For studies of gene expression as a

function of thermal induction time (**Fig. 1, d–f**), samples were returned to incubation at 30 °C after their indicated thermal induction periods such that the total experimental duration was 24 hours. Fluorescence measurements were made at the end of this period. Gene expression (*E*) was determined according to Equation 1:

$$E = \frac{F_{sample} - F_{blank}}{OD_{sample} - OD_{blank}} - \frac{F_{background} - F_{blank}}{OD_{background} - OD_{blank}} \qquad (1)$$

Here, *F* is the raw fluorescence of the given sample and *OD* is the OD of the given sample at 600 nm. Raw OD measurements for all experiments are provided in **Supplementary Figure 2-S7**. As expected, bacterial growth is highest in the physiological range of 35 ºC to 39 ºC. The value of blank fluorescence was determined as the average of all 96 wells in a qPCR plate filled with 25 µL LB. Blank OD was taken as the y-intercept of a standard curve of 90 µL non-fluorescent *E. coli* cultures whose OD_{600} values were determined by cuvette measurements in a Nanodrop 2000c spectrophotometer (96 samples total). Background fluorescence was measured from a non-fluorescent construct derived by mutating the chromophore of mWasabi [58] in the pTlpA-Wasabi plasmid (pTlpA-Wasabi-NF). Fluorescence measurements for the thermal expression landscapes of TlpA and TcI were performed using the plate reader due to signal saturation of the qPCR at the 24 hour time point (Sample N = 3; Background N = 2 for each time point and temperature). Errors from background measurements were propagated by addition in quadrature. Errors from blank measurements were negligible relative to sample-to-sample variation (relative standard deviation < 2%) and were omitted from the calculation.

Colony Screening for TlpA Tuning

Error-prone PCR was performed on pTlpA-Wasabi (Stratagene GeneMorph II kit) and on pTcI-Wasabi (NEB Taq Polymerase/0.2 mM $MnCl_2$), and the PCR products were inserted into the parent constructs using Gibson Assembly. The resulting libraries were transformed into NEB10β *E. coli* and plated on LB Agar. Following overnight incubation at 30 °C and the appearance of colonies, a Replica-Plating Tool (VWR 25395-380) was used to replicate each seed plate into two receiver plates. One receiver plate was grown overnight at the

desired repressed temperature, and the other at the intended activation temperature. Upon the appearance of visible colonies, plates were imaged in a Bio-Rad ChemiDoc MP imager using blue epifluorescent illumination and the 530/28 nm emission filter. Images were examined manually for colonies that appeared dark or invisible on the "off plate" but showed bright fluorescence on the "on plate". Approximately 10^3 colonies were screened per library. These colonies were picked and subjected to the liquid culture thermal activation assay described above, whereupon their thermal induction profile was compared to that of their parent plasmid. Variants that demonstrated sharp switching and large dynamic range between the desired new transition temperatures were sequenced, re-transformed, and assayed using a higher number of replicates.

In Vitro *Toxin-Antitoxin Assays*

NEB10β cells were transformed with the thermally regulated toxin-antitoxin plasmid and allowed to grow at 37 °C overnight. Because reversion of plasmids carrying toxic genes such as CcdB is known to be a common phenomenon, we used a replica plate screen to isolate colonies that maintained a functional thermal kill switch after transformation. To this end, we replica-plated the original transformation into two new plates, one incubated at 25°C and the other maintained at 37 °C. Colonies that grew at the permissive temperature of 37 °C and not at 25°C were used in downstream *in vitro* or *in vivo* experiments. For *in vitro* experiments, the selected colonies were grown in 2xYT media with 100 μg/mL ampicillin at 37°C with shaking until OD_{600} of 0.6, whereupon they were diluted and plated onto LB agar plates. The plates were incubated overnight at either 25°C or 37°C, after which colony forming units (CFU) were counted.

Focused Ultrasound

MRI-guided focused ultrasound treatment was performed using a 16-channel ultrasound generator, motorized MRI-compatible transducer positioning system and an annular array transducer operating at 1.5 MHz (Image Guided Therapy, Pessac, France). Targeting and

real-time imaging was performed using a Bruker Biospec/Avance 7T MRI system with RF excitation delivered by a 7.2 cm diameter volume coil and detection via a 3 cm diameter surface coil. Temperature monitoring was performed using a continuously applied Fast Low Angle Shot sequence with a T_R of 75 ms and T_E of 2.5 ms, matrix size of 32 x 32, and varying FOVs as listed below. Phase images were processed in real time using ThermoGuide software (Image Guided Therapy) and temperature was calculated from the per-pixel phase accumulation due to a decrease in proton precession frequency of 0.01 ppm/°C.

For *in vitro* heating, 100 µL of a saturated NEB10β culture expressing the temperature-inducible reporter circuit was plated overnight at 30 °C and incubated for approximately 12 hours to form a lawn on a plate containing 0.24 %w/v LB (Sigma) and 0.32 %w/v Bacto Agar (BD). An approximately 3 cm x 3 cm square of agar was excised from the plate and placed, with the bacterial side facing up, onto a comparably sized pad of 1 cm thick extra firm tofu (O Organics) coated with SCAN ultrasound gel (Parker Laboratories) to exclude air at the interface. A 1 cm high plastic washer made by drilling through the lid of a VWR 35 mm plastic tissue culture dish was placed onto the bacteria and the assembly was inverted and placed onto the surface coil such that the bacterial lawn, facing down, was supported by the washer. The ultrasound transducer was positioned above the assembly, in contact with the tofu through another thin layer of ultrasound gel. To provide a reference to compensate for global phase drift during the experiment, a second piece of tofu was placed within the field of view but spatially separated by a 1 cm air gap from the object under insonation. A fiber optic thermometer (Neoptix T1) was inserted into the reference tofu, and the difference between the MRI-derived reference temperature and thermometer-reported temperature was accounted for at the site of insonation when calculating the true focal heating.

Ultrasound was applied with the focus aimed at the tofu immediately adjacent to the agar layer with manual control of power level and duty cycle so as to maintain a temperature of 41.5–43 °C for 45 minutes. Imaging was performed as described above with a matrix size of

5.39 x 5.05 cm and a slice thickness of 2 mm. The plate was subsequently returned to 30 °C for 5 hours and imaged using a Bio-Rad ChemiDoc MP imager with blue epi illumination and a 530/28 nm emission filter (mWasabi) and also green epi illumination and a 605/50 nm filter (mCherry).

Animal Procedures

All animal procedures were performed under a protocol approved by the California Institute of Technology Institutional Animal Care and Use Committee (IACUC). Nine-week old BALB/c female mice and 4-week old NU/J 2019 female mice were purchased from Jackson Laboratory (JAX); 4-week old SCID/SHC female mice were purchased from Charles River. For *in vivo* ultrasound actuation, *E. coli* expressing the pTlpA36-Wasabi plasmid were grown to OD 0.6, pelleted, and resuspended to OD 24. A 100 μL bolus was injected subcutaneously into both hindlimbs of a nude mouse (SCID or NU/J2019). Mice were anaesthetized using a 2% isoflurane-air mixture and placed on a dedicated animal bed with the surface coil positioned below the target limb of the mouse. Anesthesia was maintained over the course of the ultrasound procedure using 1–1.5% isoflurane. Respiration rate was maintained at 20–30 breaths per minute and temperature and respiration rate were continuously monitored using a pressure pad (Biopac Systems) and a fiber optic rectal thermometer (Neoptix). The target limb was thermally activated by elevating the temperature to 41°C and maintaining the elevated temperature for 45 min to 1 hour. Temperature monitoring and adjustment was performed as described above for *in vitro* experiments. Following ultrasound treatment, the mouse was returned to its cage for four hours, anaesthetized, and imaged using a Bio-Rad ChemiDoc MP imager with blue epi illumination and the 530/28 nm emission filter (mWasabi).

For host fever sensing experiments, SCID mice injected with bacteria as described above were housed in an incubator preset to 41°C for two hours and control mice were housed at room temperature. Following treatment, all mice were housed at room temperature for four

hours, anaesthetized, and imaged using a Bio-Rad ChemiDoc MP imager with blue epi illumination and the 530/28 nm emission filter (mWasabi).

Mouse images are representative of three independent *in vivo* experiments. Fever-induced and control mice were littermates randomly selected for each experimental condition. Investigators were not blinded to group allocation because no subjective evaluations were performed.

For host confinement experiments, BALB/c mice were given drinking water containing 0.5 mg/mL of ampicillin for 24 hours, and then starved for food overnight. *E.coli* were grown in 2xYT media containing ampicillin at 37°C with shaking until OD_{600} of 0.6. Cultures were pelleted and resuspended at 10^8 cells/mL in PBS containing 1.5% $NaHCO_3$. 200 μL of the suspension was administered orally using a gavage needle. Food was returned to the mice and the drinking water contained ampicillin throughout the entire experiment. Fresh fecal samples were collected from each mouse 5 hrs after gavage and incubated at 37°C or 25°C for 24 hours, then weighed, homogenized in PBS at 0.1 g/mL, diluted, and plated onto LB agar plates containing ampicillin. Plates were then incubated overnight at 25°C and 37°C. Bacterial colonies were counted as described above for *in vitro* toxin-antitoxin experiments. The sample size was N = 5 mice, which was chosen based on preliminary experiments indicating that it would be sufficient to detect significant differences in mean values.

Electrophoretic Mobility Shift Assay

Interaction between TlpA, σ^{70}-RNAp holoenzyme and DNA was demonstrated using a gel shift assay. For this, 50 pmoles of fluorescein-labeled double stranded DNA representing the TlpA operator with flanking padding sequences (70 base pairs in total) was incubated with either 50 pmoles of TlpA protein or 5 Units (8.5 pmoles) σ^{70}-RNAp holoenzyme (NEB M0551S) individually in 50 uL reaction buffer comprising 40 mM Tris-HCl, 150 mM KCl, 10mM MgCl2, .01% Triton-X-100, and 1 mM DTT at a pH of 7.5. As a negative control,

the wild type TlpA operator was replaced with a scrambled version. Following incubation at 37ºC for 30 minutes, 10 uL of the reaction mixture was supplemented with glycerol to a final concentration of 5 % and loaded in a nondenaturing 4 % polyacrylamide resolving gel. The gel was run at 65 V for 90 minutes in buffer comprising 45 mM Tris-borate and 1 mM EDTA at a pH of 8.3. DNA was visualized using Bio-Rad ChemiDoc MP imager using blue epifluorescent illumination and the 530/28 nm emission filter.

Statistics and Replicates

Data is plotted and reported in the text as the mean ± SEM. Sample size is N = 4 biological replicates in all *in vitro* experiments unless otherwise stated. This sample size was chosen based on preliminary experiments indicating that it would be sufficient to detect significant differences in mean values. P-values were calculated using a two-tailed unpaired heteroscedastic t-test.

2.5: References

1. Ford, T.J. & Silver, P.A. Synthetic biology expands chemical control of microorganisms. *Current opinion in chemical biology* **28**, 20-28 (2015).
2. Fischbach, M.A., Bluestone, J.A. & Lim, W.A. Cell-based therapeutics: the next pillar of medicine. *Science translational medicine* **5**, 179ps177-179ps177 (2013).
3. Steidler, L. et al. Treatment of murine colitis by Lactococcus lactis secreting interleukin-10. *Science* **289**, 1352-1355 (2000).
4. Daniel, C., Roussel, Y., Kleerebezem, M. & Pot, B. Recombinant lactic acid bacteria as mucosal biotherapeutic agents. *Trends in biotechnology* **29**, 499-508 (2011).
5. Claesen, J. & Fischbach, M.A. Synthetic microbes as drug delivery systems. *ACS synthetic biology* **4**, 358-364 (2014).
6. Wells, J.M. & Mercenier, A. Mucosal delivery of therapeutic and prophylactic molecules using lactic acid bacteria. *Nature Reviews Microbiology* **6**, 349-362 (2008).
7. Courbet, A., Endy, D., Renard, E., Molina, F. & Bonnet, J. Detection of pathological biomarkers in human clinical samples via amplifying genetic switches and logic gates. *Science translational medicine* **7**, 289ra283-289ra283 (2015).
8. Danino, T. et al. Programmable probiotics for detection of cancer in urine. *Science translational medicine* **7**, 289ra284-289ra284 (2015).
9. Kotula, J.W. et al. Programmable bacteria detect and record an environmental signal in the mammalian gut. *Proceedings of the National Academy of Sciences* **111**, 4838-4843 (2014).
10. Archer, E.J., Robinson, A.B. & Süel, G.r.M. Engineered E. coli that detect and respond to gut inflammation through nitric oxide sensing. *ACS synthetic biology* **1**, 451-457 (2012).
11. Ntziachristos, V. Going deeper than microscopy: the optical imaging frontier in biology. *Nature methods* **7**, 603-614 (2010).
12. Haar, G.T. & Coussios, C. High intensity focused ultrasound: physical principles and devices. *International journal of hyperthermia : the official journal of European Society for Hyperthermic Oncology, North American Hyperthermia Group* **23**, 89-104 (2007).
13. Huang, X., El-Sayed, I.H., Qian, W. & El-Sayed, M.A. Cancer cell imaging and photothermal therapy in the near-infrared region by using gold nanorods. *Journal of the American Chemical Society* **128**, 2115-2120 (2006).
14. Thiesen, B. & Jordan, A. Clinical applications of magnetic nanoparticles for hyperthermia. *International journal of hyperthermia* **24**, 467-474 (2008).
15. Zhao, K., Liu, M. & Burgess, R.R. The global transcriptional response of Escherichia coli to induced sigma 32 protein involves sigma 32 regulon activation followed by inactivation and degradation of sigma 32 in vivo. *The Journal of biological chemistry* **280**, 17758-17768 (2005).
16. de Marco, A., Vigh, L., Diamant, S. & Goloubinoff, P. Native folding of aggregation-prone recombinant proteins in Escherichia coli by osmolytes, plasmid- or benzyl alcohol-overexpressed molecular chaperones. *Cell stress & chaperones* **10**, 329-339 (2005).
17. Inda, M.E. et al. A lipid-mediated conformational switch modulates the thermosensing activity of DesK. *Proceedings of the National Academy of Sciences* **111**, 3579-3584 (2014).
18. Kortmann, J., Sczodrok, S., Rinnenthal, J., Schwalbe, H. & Narberhaus, F. Translation on demand by a simple RNA-based thermosensor. *Nucleic Acids Res* **39**, 2855-2868 (2011).

19. Neupert, J., Karcher, D. & Bock, R. Design of simple synthetic RNA thermometers for temperature-controlled gene expression in Escherichia coli. *Nucleic Acids Res* **36**, e124 (2008).
20. Waldminghaus, T., Kortmann, J., Gesing, S. & Narberhaus, F. Generation of synthetic RNA-based thermosensors. *Biological chemistry* **389**, 1319-1326 (2008).
21. Hoynes-O'Connor, A., Hinman, K., Kirchner, L. & Moon, T.S. De novo design of heat-repressible RNA thermosensors in E. coli. *Nucleic acids research* **43**, 6166-6179 (2015).
22. Satija, R., Sen, S., Siegal-Gaskins, D. & Murray, R.M. Design of a Toolbox of RNA Thermometers. *bioRxiv*, 017269 (2015).
23. Waldminghaus, T., Kortmann, J., Gesing, S. & Narberhaus, F. Generation of synthetic RNA-based thermosensors. *Biological chemistry* **389**, 1319-1326 (2008).
24. Neupert, J., Karcher, D. & Bock, R. Design of simple synthetic RNA thermometers for temperature-controlled gene expression in Escherichia coli. *Nucleic acids research* **36**, e124-e124 (2008).
25. Wieland, M. & Hartig, J.S. RNA quadruplex-based modulation of gene expression. *Chemistry & biology* **14**, 757-763 (2007).
26. Hurme, R., Berndt, K.D., Namork, E. & Rhen, M. DNA binding exerted by a bacterial gene regulator with an extensive coiled-coil domain. *The Journal of biological chemistry* **271**, 12626-12631 (1996).
27. Valdez-Cruz, N.A., Caspeta, L., Perez, N.O., Ramirez, O.T. & Trujillo-Roldan, M.A. Production of recombinant proteins in E. coli by the heat inducible expression system based on the phage lambda pL and/or pR promoters. *Microbial cell factories* **9**, 18 (2010).
28. Sussman, R. & Jacob, F. Sur un systeme de repression thermosensible chez le bacteriophage lambda d'Escherichia coli. *Comptes rendus hebdomadaires des séances de l'Académie des sciences*, 1517-1519 (1962).
29. Wissmann, A. et al. Selection for Tn10 tet repressor binding to tet operator in Escherichia coli: isolation of temperature-sensitive mutants and combinatorial mutagenesis in the DNA binding motif. *Genetics* **128**, 225-232 (1991).
30. Chao, Y.P., Chern, J.T., Wen, C.S. & Fu, H. Construction and characterization of thermo-inducible vectors derived from heat-sensitive lacI genes in combination with the T7 A1 promoter. *Biotechnology and bioengineering* **79**, 1-8 (2002).
31. McCabe, K.M., Lacherndo, E.J., Albino-Flores, I., Sheehan, E. & Hernandez, M. LacI(Ts)-regulated expression as an in situ intracellular biomolecular thermometer. *Applied and environmental microbiology* **77**, 2863-2868 (2011).
32. Hurme, R., Berndt, K.D., Normark, S.J. & Rhen, M. A proteinaceous gene regulatory thermometer in Salmonella. *Cell* **90**, 55-64 (1997).
33. Wilson, C.J., Zhan, H., Swint-Kruse, L. & Matthews, K.S. The lactose repressor system: paradigms for regulation, allosteric behavior and protein folding. *Cellular and molecular life sciences : CMLS* **64**, 3-16 (2007).
34. Bertram, R. & Hillen, W. The application of Tet repressor in prokaryotic gene regulation and expression. *Microbial biotechnology* **1**, 2-16 (2008).
35. Jensen, P.R., Westerhoff, H.V. & Michelsen, O. The use of lac-type promoters in control analysis. *European journal of biochemistry / FEBS* **211**, 181-191 (1993).
36. Altschul, S.F. et al. Gapped BLAST and PSI-BLAST: a new generation of protein database search programs. *Nucleic acids research* **25**, 3389-3402 (1997).

37. Al-Bataineh, O., Jenne, J. & Huber, P. Clinical and future applications of high intensity focused ultrasound in cancer. *Cancer treatment reviews* **38**, 346-353 (2012).
38. Elias, W.J. et al. A pilot study of focused ultrasound thalamotomy for essential tremor. *New England Journal of Medicine* **369**, 640-648 (2013).
39. Deckers, R. et al. Image-guided, noninvasive, spatiotemporal control of gene expression. *Proceedings of the National Academy of Sciences* **106**, 1175-1180 (2009).
40. Fite, B.Z. et al. Magnetic resonance thermometry at 7T for real-time monitoring and correction of ultrasound induced mild hyperthermia. *PloS one* **7**, e35509 (2012).
41. McDannold, N.J., King, R.L., Jolesz, F.A. & Hynynen, K.H. Usefulness of MR Imaging-Derived Thermometry and Dosimetry in Determining the Threshold for Tissue Damage Induced by Thermal Surgery in Rabbits 1. *Radiology* **216**, 517-523 (2000).
42. McDannold, N., Vykhodtseva, N., Jolesz, F.A. & Hynynen, K. MRI investigation of the threshold for thermally induced blood–brain barrier disruption and brain tissue damage in the rabbit brain. *Magnetic resonance in medicine* **51**, 913-923 (2004).
43. Rudaya, A.Y., Steiner, A.A., Robbins, J.R., Dragic, A.S. & Romanovsky, A.A. Thermoregulatory responses to lipopolysaccharide in the mouse: dependence on the dose and ambient temperature. *American journal of physiology. Regulatory, integrative and comparative physiology* **289**, R1244-1252 (2005).
44. Pritchard, M.T. et al. Protocols for simulating the thermal component of fever: preclinical and clinical experience. *Methods (San Diego, Calif.)* **32**, 54-62 (2004).
45. Illing, A.C., Shawki, A., Cunningham, C.L. & Mackenzie, B. Substrate profile and metal-ion selectivity of human divalent metal-ion transporter-1. *Journal of Biological Chemistry* **287**, 30485-30496 (2012).
46. Nistala, G.J., Wu, K., Rao, C.V. & Bhalerao, K.D. A modular positive feedback-based gene amplifier. *Journal of biological engineering* **4**, 4 (2010).
47. Andersen, J.B. et al. New unstable variants of green fluorescent protein for studies of transient gene expression in bacteria. *Applied and environmental microbiology* **64**, 2240-2246 (1998).
48. Natori, Y., Kano, Y. & Imamoto, F. Characterization and promoter selectivity of Lactobacillus acidophilus RNA polymerase. *Biochimie* **70**, 1765-1774 (1988).
49. Mimee, M., Tucker, A.C., Voigt, C.A. & Lu, T.K. Programming a human commensal bacterium, Bacteroides thetaiotaomicron, to sense and respond to stimuli in the murine gut microbiota. *Cell systems* **1**, 62-71 (2015).
50. Tey, S.-K. Adoptive T-cell therapy: adverse events and safety switches. *Clinical & translational immunology* **3**, e17 (2014).
51. Chan, C.T., Lee, J.W., Cameron, D.E., Bashor, C.J. & Collins, J.J. 'Deadman' and 'Passcode' microbial kill switches for bacterial containment. *Nat Chem Biol* **12**, 82-86 (2016).
52. Gallagher, R.R., Patel, J.R., Interiano, A.L., Rovner, A.J. & Isaacs, F.J. Multilayered genetic safeguards limit growth of microorganisms to defined environments. *Nucleic Acids Res* **43**, 1945-1954 (2015).
53. Lang, K. & Chin, J.W. Cellular incorporation of unnatural amino acids and bioorthogonal labeling of proteins. *Chemical reviews* **114**, 4764-4806 (2014).
54. Handley, A., Schauer, T., Ladurner, A.G. & Margulies, C.E. Designing cell-type-specific genome-wide experiments. *Molecular cell* **58**, 621-631 (2015).

55. Grammel, M. & Hang, H.C. Chemical reporters for biological discovery. *Nature chemical biology* **9**, 475-484 (2013).
56. Ai, H.W., Olenych, S.G., Wong, P., Davidson, M.W. & Campbell, R.E. Hue-shifted monomeric variants of Clavularia cyan fluorescent protein: identification of the molecular determinants of color and applications in fluorescence imaging. *BMC biology* **6**, 13 (2008).
57. Shaner, N.C. et al. Improved monomeric red, orange and yellow fluorescent proteins derived from Discosoma sp. red fluorescent protein. *Nature biotechnology* **22**, 1567-1572 (2004).
58. Wielgus-Kutrowska, B., Narczyk, M., Buszko, A., Bzowska, A. & Clark, P.L. Folding and unfolding of a non-fluorescent mutant of green fluorescent protein. *Journal of Physics: Condensed Matter* **19**, 285223 (2007).

2.6: Supplementary Results

Supplementary Table 2-T1 – Mutant and wild type bioswitch performance

Variant	Fold Change	SEM (±)	T_{off}	T_{max}
TlpA	355	45	31.4	44.6
$TlpA_{36}$	370	63	31.4	44.6
$TlpA_{39}$	1523	434	31.4	44.6
TcI	1432	404	34.2	40
TcI_{38}	1032	160	32.4	40
TcI_{42}	1692	444	32.4	45.7

***** The reported T_{off} for each variant is the lowest temperature at which fluorescence could be detected above noise. T_{max} is the temperature at which fluorescence was maximal.

Supplementary Table 2-T2 – Genetic constructs used in the study

All plasmids were constructed using the pETDuet-1 backbone (EMD Biosciences) with the relevant thermal biosensor elements replacing multiple cloning sites 1 and 2.

Plasmid	Transcriptional Regulator(s)	Output Gene Product(s)
pTlpA-Wasabi	TlpA	mWasabi
pTlpA-Wasabi-NF	TlpA	Nonfluorescent mWasabi (S71T, G73A)
pTcI-Wasabi	TcI (cI852 Repressor, cI A67T)	mWasabi
pLacI241-Wasabi	LacI A241T (mutation made in pETDuet-1 LacI)	mWasabi

pLacI265-Wasabi	LacI G265D (mutation made in pETDuet-1 LacI)	mWasabi
pTetR89-Wasabi	TetR A89D	mWasabi
pTetR193-Wasabi	TetR I193N	mWasabi
pLon-Wasasbi	Lon Promoter (GenBank CP009072)	mWasabi
pRpoH-Wasabi	RpoH Promoter (GenBank CP009072)	mWasabi
pClp-Wasabi	ClpP-ClpX Promoter (Genbank CP009072)	mWasabi
pHtpG-Wasabi	HtpG Promoter (Genbank CP009072)	mWasabi
pDnaK-Wasabi	DnaK Promoter (Genbank CP009072)	mWasabi
pGrpE-Wasabi	GrpE Promoter (Genbank CP009072)	mWasabi
pLacIq-Wasabi	LacIq Promoter	mWasabi
$pTlpA_{SP}$-Wasabi	TlpA Promoter with putative Pribnow box scrambled	mWasabi
$pTlpA_{Reverse}$-Wasabi	TlpA Promoter as reverse complement	mWasabi
$pTlpA_{36}$-Wasabi	$TlpA_{36}$	mWasabi
$pTlpA_{39}$-Wasabi	$TlpA_{39}$	mWasabi
$pTcI_{38}$-Wasabi	TcI_{38}	mWasabi
$pTcI_{42}$-Wasabi	TcI_{42}	mWasabi
pCali2	$TlpA_{36}$, TcI	mWasabi, mCherry
pThermeleon	TcI, TlpA, cI_{wt} (under control of TlpA)	mWasabi, mCherry
pKillswitch	$TlpA_{36}$	CcdA with SsrA degradation tag

Sources of genetic elements: TlpA: B. Finlay, Univ. British Columbia; mWasabi: F. Arnold, Caltech; mCherry: S. Qi, Stanford; CcdB: pLenti X1 Zeo DEST plasmid (Addgene #17299); TetR: pENTR1A plasmid (Addgene #22265); all other elements: Gblock synthesis (IDT).

Supplementary Table 2-T3 – List of mutations in selected variants of TlpA and TcI

Construct	Nonsynonymous Mutations	Synonymous Mutations
$TlpA_{36}$	P60L, D135V, K187R, K202I, L208Q	
$TlpA_{39}$	D135V, A217V, L236F	
TcI_{38}	M1V, L65S, K68R, F115L, D126G, D188G	A50 (GCT -> GCC), E128 (GAG -> GAA), R129 (AGA -> AGG), T152 (ACA -> ACC), L185 (CTT -> CTC)
TcI_{42}	K6N, S33T, Y61H, L119P, F122C	L51 (TTA -> CTA)

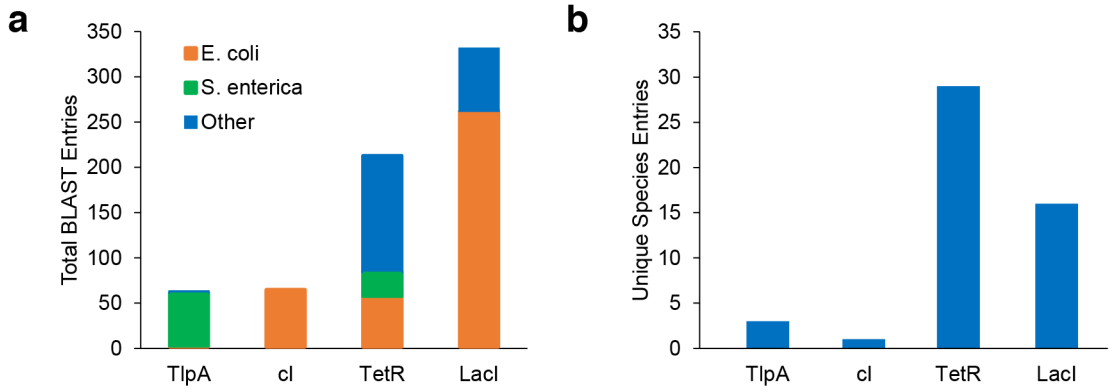

Supplementary Figure 2-S1 – Prevalence of repressor sequences in bacteria. (**a**) National Center for Biotechnology Information (NCBI) Basic Local Alignment Search Tool (BLAST) search results for the wild type TlpA, cI, TetR, and LacI genes showing the cumulative number of hits obtained. The NCBI nucleotide collection was searched with the source organism restricted to bacteria. Cloning vectors, synthetic constructs, and individual gene sequences were omitted; genomic and naturally occurring plasmid sequences were retained. Sequences with alignment lengths of less than 90% of the wild type protein sequence were not included. The LacI gene is distributed throughout many commonly utilized *E. coli* strains such as Nissle 1917 and BL21, whereas the cI gene is found in less widely used *E. coli* strains. (**b**) The number of bacterial species in which the selected repressors are found. Data were obtained as in (**a**) and substrains were binned together. TlpA is largely restricted to *S. enterica* and cI to *E. coli*; TetR and LacI can be found in a larger number of bacterial species.

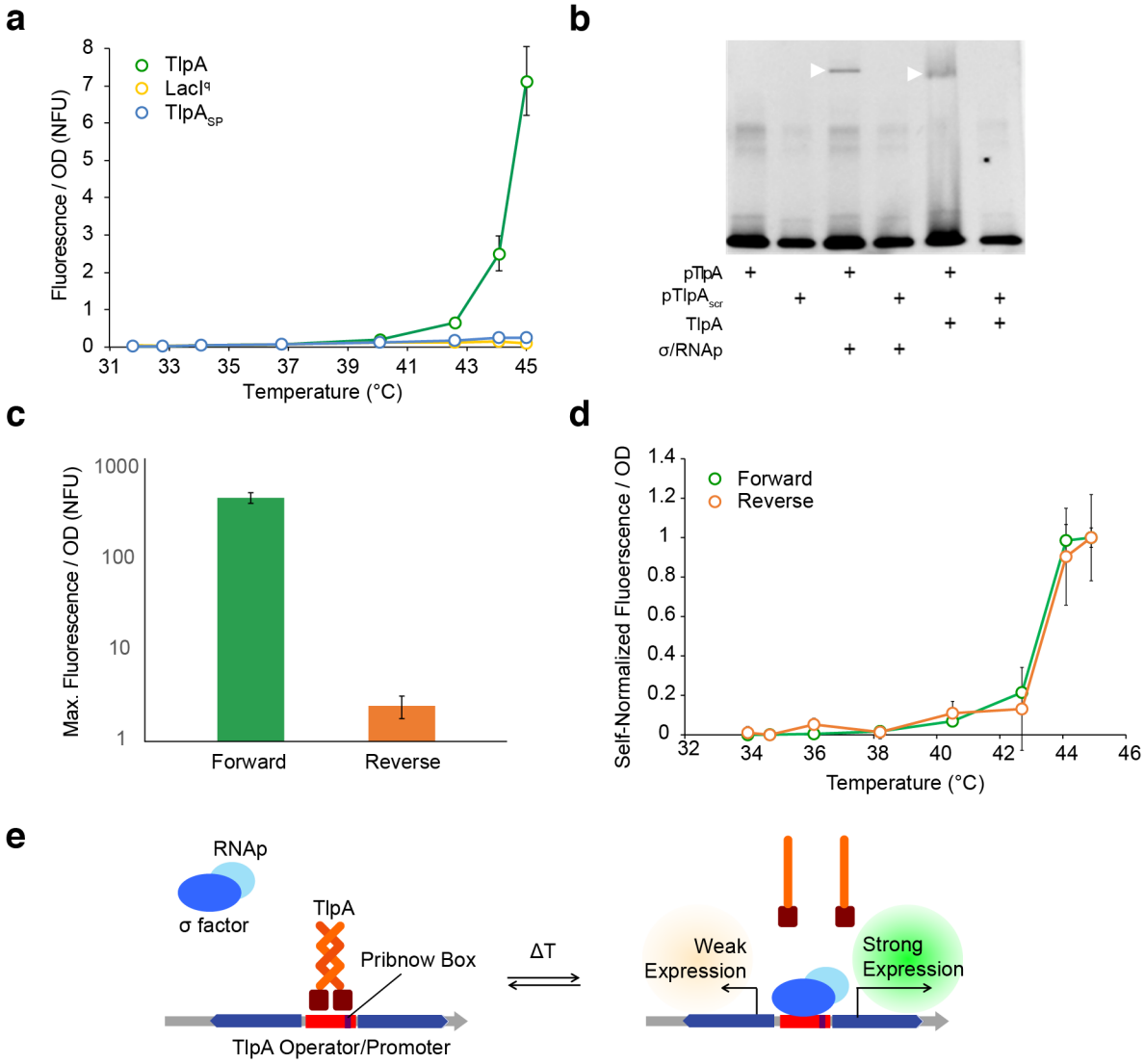

Supplementary Figure 2-S2 – Mechanisms and bidirectional activity of the TlpA operator. (**a**) OD-normalized expression of the GFP reporter gene under the control of TlpA, $LacI^q$, and $TlpA_{SP}$ (in which nucleotides within the Pribnow box of the operator are shuffled). (**b**) Electromobility shift assay using a FAM-labeled TlpA operator oligonucleotide, demonstrating association of the operator with both TlpA and the *E. coli* σ^{70}-RNAp holoenzyme. In contrast, scrambled TlpA operator fails to

associate with these proteins. The TlpA and σ^{70}-RNAp concentrations used in this experiment (1 μM and 0.18 μM, respectively) were similar to previous literature.[7,8] (**c**) GFP expression driven by the TlpA operator in the canonical and flipped orientations at 44.1ºC. (**d**) Thermal induction profiles for GFP expression under the control of forward and reverse-oriented TlpA operator. Each curve is self-normalized to its maximal fluorescence intensity. (**e**) Proposed mechanism of TlpA-based thermal transcriptional regulation.

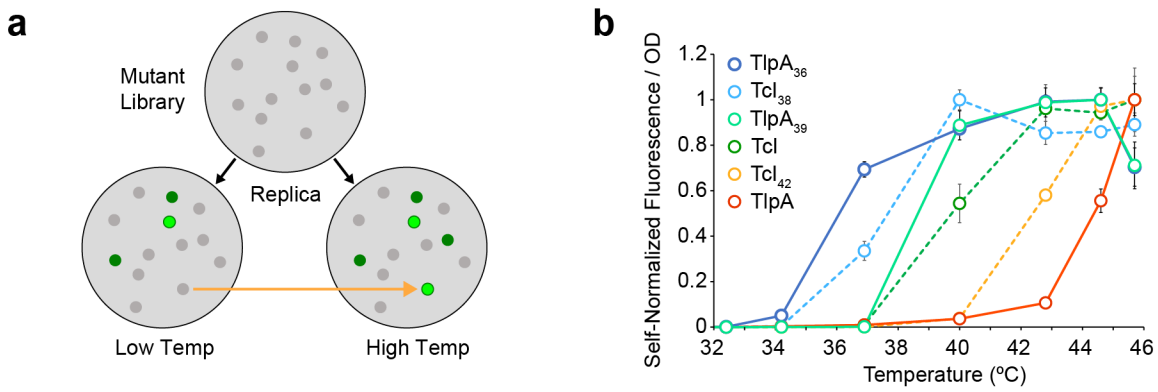

Supplementary Figure 2-S3 - Tuning the transition temperature of thermal bioswitches. (**a**) Illustration of the screening strategy used to identify temperature-shifted repressor variants. (**b**) Self-normalized fluorescence/OD profiles for the full set of TlpA (solid lines) and TcI (dashed lines) bioswitches, demonstrating the complete range of available transition temperatures.

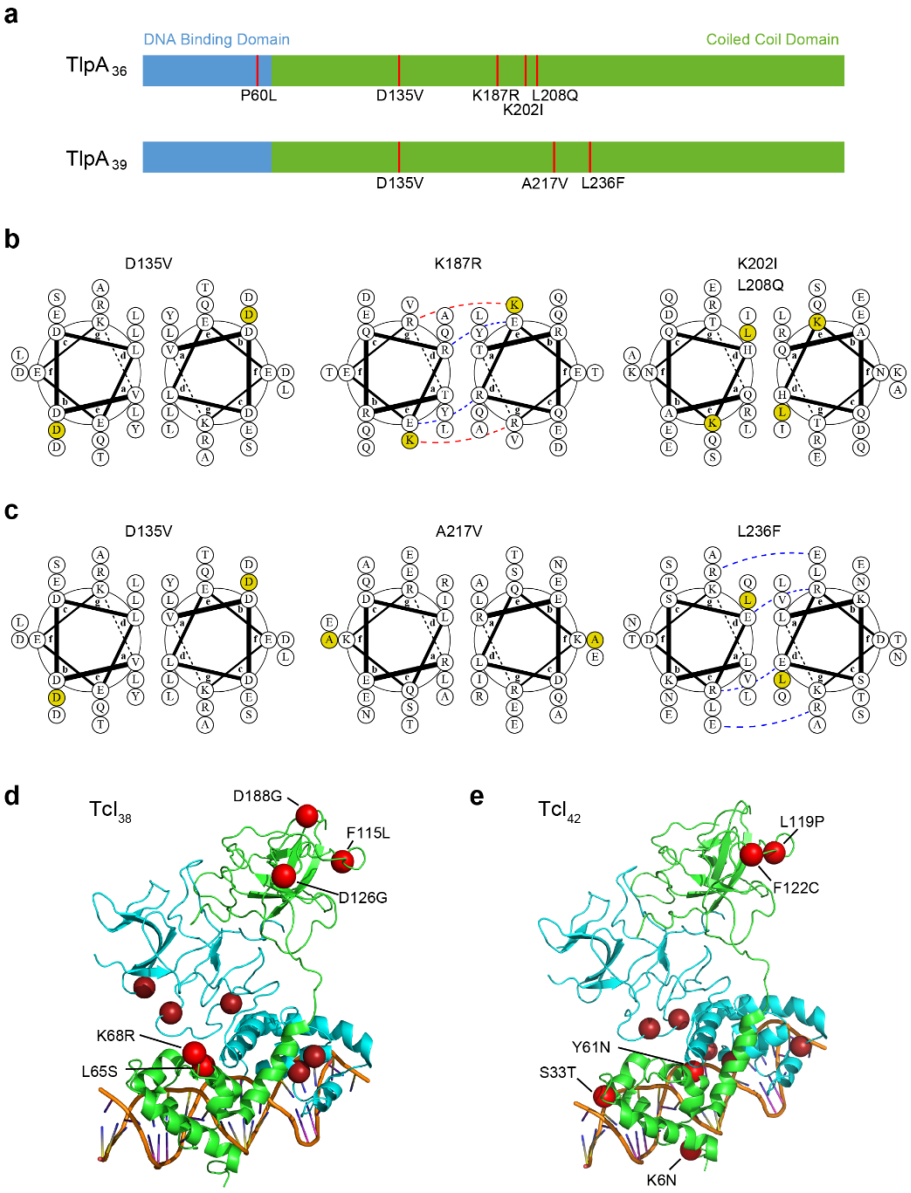

Supplementary Figure 2-S4 – Positions of mutations in selected variants of TlpA and TcI. (**a**) Schematic of mutation positions (red) within the predicted domain structure of $TlpA_{36}$ and $TlpA_{39}$. The DNA binding domain is depicted in blue and coiled-coil domain in green, as delineated by Koski et al[1]. The figure is drawn to the scale of the primary sequence. (**b**) Positions of mutations in $TlpA_{36}$ within the predicted structure of the coiled-coil interface as viewed down the long axis of the helix. Blue dashed lines represent predicted energetically favorable ionic interactions; red dashes indicate

predicted repulsive ionic interactions. The coil register was assigned based on consensus between previous literature[1] and the structure prediction servers COILS[2], Paircoil2[3], and LOGICOIL[4]. The images were produced using DrawCoil 1.0[5]. The P60L mutation is not shown because it falls outside of the predicted coiled-coil region. (**c**) Positions of mutations in $TlpA_{39}$. Register prediction and illustration were performed as in (b). (**d**) Mutation positions (red) for the lambda repressor variant TcI_{38}. The crystal structure of the wild type lambda repressor (PDB code 3BDN) was used as the homology model[6]. The original temperature-sensitizing mutation A67T is not shown. The M1V mutation is not depicted because residue 1 was not reported in the crystal structure. (**e**) Mutation positions (red) within the TcI_{42} variant.

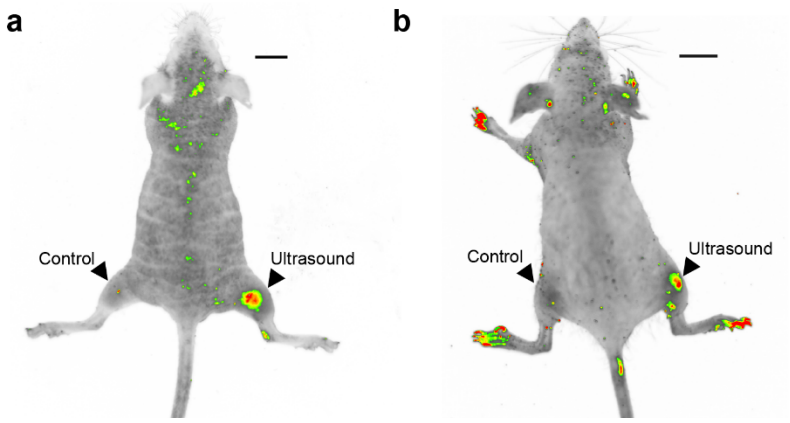

Supplementary Figure 2-S5 – Additional mice with ultrasound-activated gene expression. (**a**) and (**b**) Additional mice that underwent the experiment shown in **Figure 4e**. The images are thresholded fluorescence maps of mice injected subcutaneously in both left and right hindlimbs with *E. coli* expressing GFP under the control of $TlpA_{36}$, following ultrasound activation at only the right hindlimb. Signal at mouse digits is the result of autofluorescence and varies from mouse to mouse; digits were neither injected with bacteria nor exposed to ultrasound.

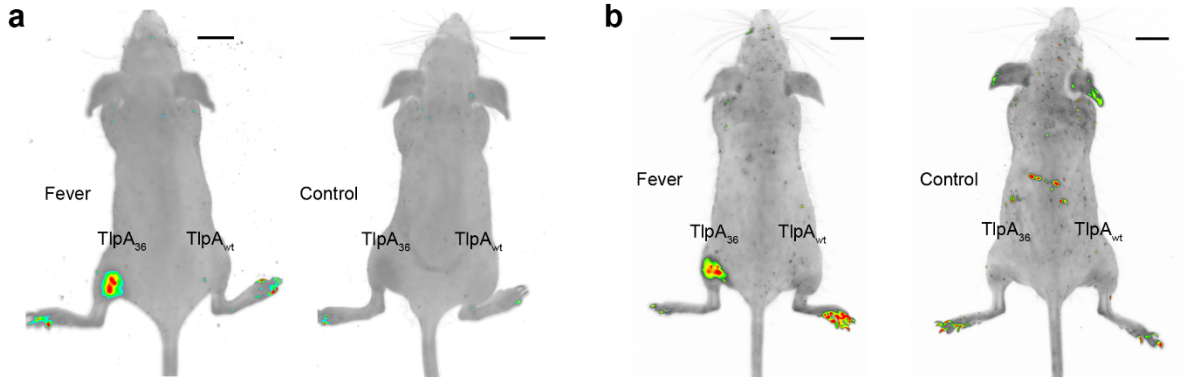

Supplementary Figure 2-S6 – Additional mice with fever-activated gene expression. (**a**) and (**b**) Additional pairs of mice that underwent the experiment shown in **Figure 5, b-c**. Each panel shows thresholded fluorescence maps of one mouse that underwent fever induction after being injected subcutaneously with plasmids expressing $TlpA_{36}$- and TlpA-regulated GFP into the left and right hind limbs, respectively, with a paired mouse that was prepared identically but maintained at room temperature.

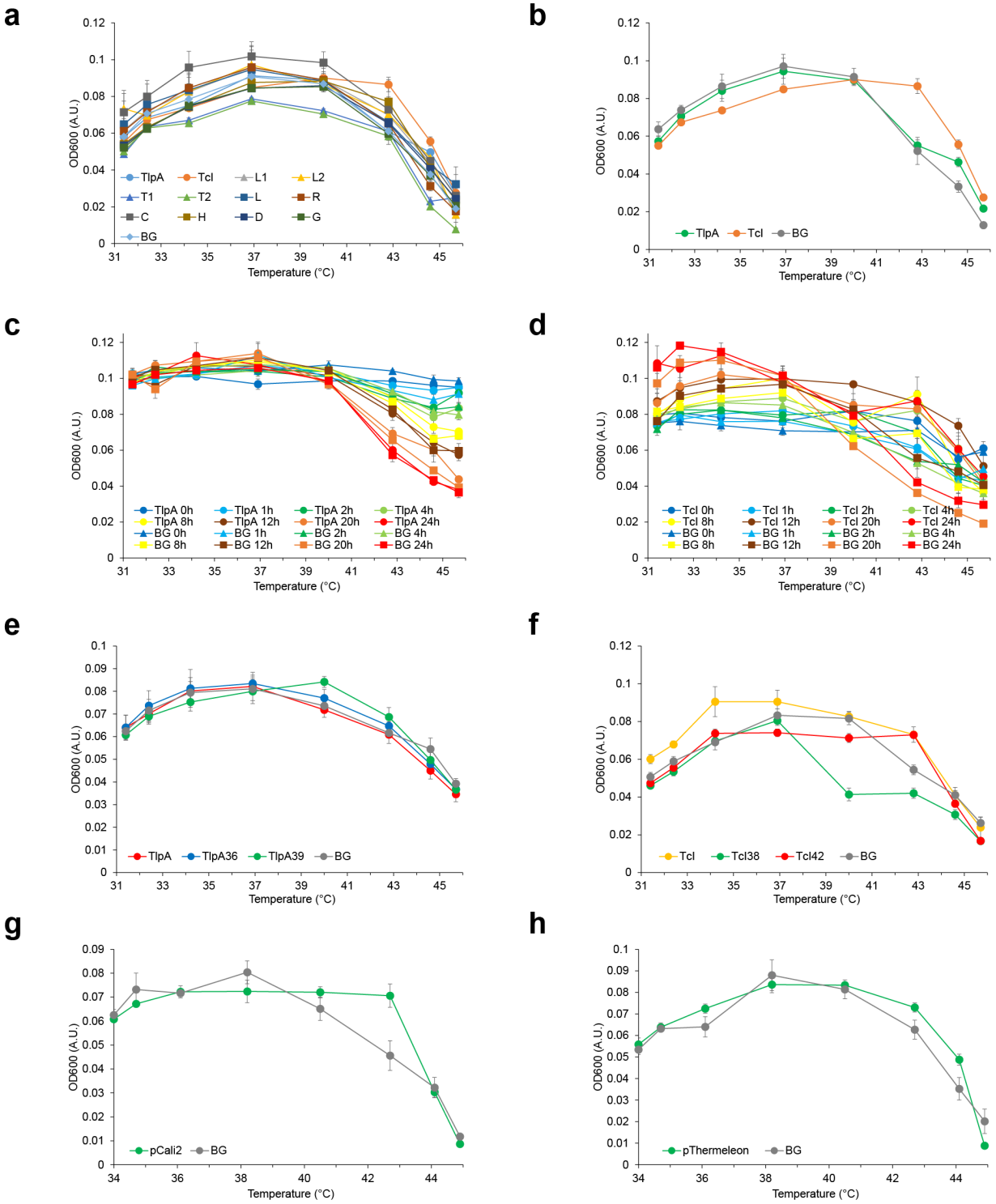
a
b
c
d
e
f
g
h
OD600 (A.U.)
Temperature (°C)
TlpA
Tcl
L1
L2
T1
T2
L
R
C
H
D
G
BG
TlpA 0h
TlpA 1h
TlpA 2h
TlpA 4h
TlpA 8h
TlpA 12h
TlpA 20h
TlpA 24h
BG 0h
BG 1h
BG 2h
BG 4h
BG 8h
BG 12h
BG 20h
BG 24h
Tcl 0h
Tcl 1h
Tcl 2h
Tcl 4h
Tcl 8h
Tcl 12h
Tcl 20h
Tcl 24h
TlpA36
TlpA39
Tcl38
Tcl42
pCali2
pThermeleon

Supplementary Figure 2-S7 – OD_{600} measurements for thermal induction profiles reported in main text. Blank-subtracted measurements of OD_{600} in 90 μL volumes in clear-bottom 96 well plates, corresponding to an optical path length of approximately 1.4 mm. Data corresponds to: (**a**) Fig. 1b; (**b**) Fig. 1c; (**c**) Fig. 1e; (**d**) Fig. 1f; (**e**) Fig. 2d; (**f**) Fig. 2e; (**g**) Fig. 3c; (**h**) Fig. 3g. BG = background.

2.7: Supplementary References

1. Koski, P., Saarilahti, H., Sukupolvi, S., Taira, S., Riikonen, P., Osterlund, K., … Rhen, M. A new alpha-helical coiled coil protein encoded by the Salmonella typhimurium virulence plasmid. *The Journal of Biological Chemistry* **267**, 12258–12265 (1992).
2. Lupas, A., Van Dyke, M., and Stock, J. Predicting Coiled Coils from Protein Sequences. *Science* **252**, 1162-1164 (1991).
3. McDonnel, A.V., Jiang, T., Keating, A.E., Berger B. Paircoil2: Improved prediction of coiled coils from sequence. *Bioinformatics* **22**, 356-358 (2006).
4. Vincent, T.L., Green, P.J., Woolfson, D.N. LOGICOIL—multi-state prediction of coiled-coil oligomeric state. *Bioinformatics* **29**, 69-76 (2013).
5. Grigoryan, G., Keating, A.E. Structural Specificity in Coiled-coil Interactions. *Current Opinion in Structural Biology* **18**, 477-483 (2008).
6. Stayrook. S.E., Jaru-Ampornpan, P., Ni, J., Hochschild, A., Lewis, M. Crystal structure of the lambda repressor and a model for pairwise cooperative operator binding. *Nature* **452**, 1022-1025 (2008).
7. Hurme, R., Berndt, K. D., Namork, E. & Rhen, M. DNA binding exerted by a bacterial gene regulator with an extensive coiled-coil domain. *The Journal of biological chemistry* **271**, 12626-12631 (1996).
8. Marr, M. T. & Roberts, J. W. Promoter Recognition As Measured by Binding of Polymerase to Nontemplate Strand Oligonucleotide. *Science* **276**, 1258-1260 (1997).

Chapter 3

ACOUSTIC REMOTE CONTROL OF MICROBIAL IMMUNOTHERAPY

Abedi, M. H.*, Yao M. S.* et al. (2021). "Acoustic Remote Control of Microbial Immunotherapy". In preparation.

3.1: Introduction

Cell therapies are rapidly emerging as one of the most exciting and effective technologies for cancer treatment[1–3]. Among the cell types being investigated for therapy, immune cells have excelled in the treatment of hematologic malignancies. Unfortunately, these remarkable results have been challenging to reproduce in solid tumors where immune cells are limited in their ability to penetrate into and function within their immunosuppressive environment, especially their immune-privileged hypoxic cores[4–6]. Coincidentally, the absence of immune surveillance within the core of a subset of solid tumors creates an ideal environment for some microbes to thrive[7–9]. By capitalizing on the natural tumor-homing property of certain bacterial strains, microbes can be engineered as effective cellular therapies that can home to otherwise inaccessible areas within tumors. Once deployed, engineered microbes can secrete therapeutic payloads to either directly kill tumor cells or enhance the native immune system's ability to eradicate the tumor by remodeling the tumor microenvironment[10–14]. However, the benefits of microbial therapy are often counterbalanced by safety concerns accompanying the systemic injection of microbes into patients with limited control over their activity[1,15]. This is especially important since microbes also engraft in other healthy tissues, such as the liver, spleen, and certain hypoxic stem cell niches[16–19]. To avoid damaging these tissues, it is crucial that the therapeutic activity of microbes is targeted to tumors.

Systemically administered chemical inducers are commonly used to control the function of microbes in *vivo*[20,21], but are incapable of targeting a particular anatomical site. Optically modulated control elements provide high spatiotemporal control over microbial activity[22–24], but are constrained by the poor penetration of light deep into tissues[25]. Given the limitations of chemical and optical control methods, an alternative technology for spatiotemporal targeting in deep tissues is needed for optimal patient outcomes. Thermally actuated control elements are well suited to fill this technological gap since temperature can be elevated at arbitrary depth and with high spatial precision using noninvasive methods such as focused ultrasound (FUS). In recent work, it has been shown that by combining thermally responsive bioswitches with focused ultrasound hyperthermia, the transcriptional activity of microbes can be spatiotemporally controlled at depth in *vivo*[26]. However, these switches were implemented in cloning strains of bacteria, had non-therapeutic output, and resulted in a transient transcriptional activation that is not suitable for tumor treatment, which typically requires weeks of therapeutic activity[10,11,20].

Here we describe the development of FUS-controlled immunotherapeutic microbes in which a brief thermal stimulus activates sustained release of therapeutic payloads. We first characterized the behavior of several temperature-sensitive repressors in the therapeutically relevant microbe *E. coli* Nissle 1917, then combined the best repressor with the serine integrase Bxb1 to develop a thermally activated state switch[26,27]. To improve the safety and clinical applicability of this switch, we screened random and rationally designed libraries and identified variants with minimal baseline activity and maximal induction upon stimulation. The optimized switch from these screens was adapted to express anti-immunosuppression therapeutic proteins in a temperature-directed fashion. When tested in a murine tumor model, engineered microbes carrying this genetic circuit reliably switched states upon focal activation and successfully suppressed the growth of tumors targeted with focused ultrasound.

3.2: Results

*3.2*a: *Characterizing Thermal Repressors in a Therapeutic Microbe*

To develop a temperature-actuated genetic circuit, we started with high-performance thermally responsive repressors characterized in the context of an *E. coli* cloning strain[26]. However, genetic elements tend to behave differently across cell types due to variations in the host protein expression levels and intracellular environment[28]. Since we are interested in engineering circuits for tumor therapy, we set out to test these repressors in *E. coli* Nissle 1917 (EcN), a strain that is commonly used in microbial tumor therapies[10,29]. We selected three repressor candidates—TlpA39, wild-type TcI, and TcI42 as our starting points due to their desirable activation temperature thresholds of 39 °C, 38 °C, and 42 °C respectively.

To evaluate the performance of these candidates, we designed reporter constructs where the production of GFP is regulated by thermally actuated repressors (**Fig. 3-1a**), transformed them into EcN cells, and measured the corresponding OD600-normalized fluorescence intensity as a function of different temperatures between 33 °C and 42 °C (**Fig. 3-1b**). As we are interested in using these elements in *vivo*, we focused on the fold-change between the mammalian physiological temperature (37 °C) and an elevated temperature at (42 °C) that is sufficient to trigger genetic activation while minimizing thermal damage to local tissues (**Fig. 3-1c**). Results from these experiments indicated that TcI42 is the best candidate for integration into our thermal switch since it exhibits strong induction at 42 °C while maintaining low levels of baseline activity at 37 °C.

With TcI42 being the central effector protein for our circuit, we next sought to determine the minimal heating duration and ideal heating parameters required to achieve strong activation while minimizing damage to cells. To accomplish this, we stimulated cells carrying the same circuit described in **Fig. 3-1a** by elevating the temperature to 42 °C for different durations and measuring the corresponding fluorescence intensity (**Fig. 3-1d**). These results indicated that a minimal heating time of one hour is needed for robust

activation. Since an hour of elevated thermal exposure could be harmful to cells, we quantified the effect of this thermal dose on microbial cell viability and simultaneously tested a pulsatile heating scheme that was previously shown to enhance viability in mammalian cells[30]. For the pulsatile heating scheme, the duty cycle was kept constant at 50% while alternating the temperature between 37 °C and 42 °C resulting in a total of one hour at 42 ºC over a two-hour treatment period (**Fig. 3-1e**). We varied the stimulation duration at each temperature between 1 to 60 minutes. As expected, cell viability decreased as the stimulation duration increased, while induction levels did not significantly vary (**Fig. 3-1f**). Based on these results, we selected a five-minute pulse for subsequent applications, as this heating paradigm enhanced cell viability while being readily achievable with a focused ultrasound setup. Collectively, our experiments identified and characterized TcI42 as a promising thermally responsive repressor to control gene expression in the therapeutically relevant EcN strain.

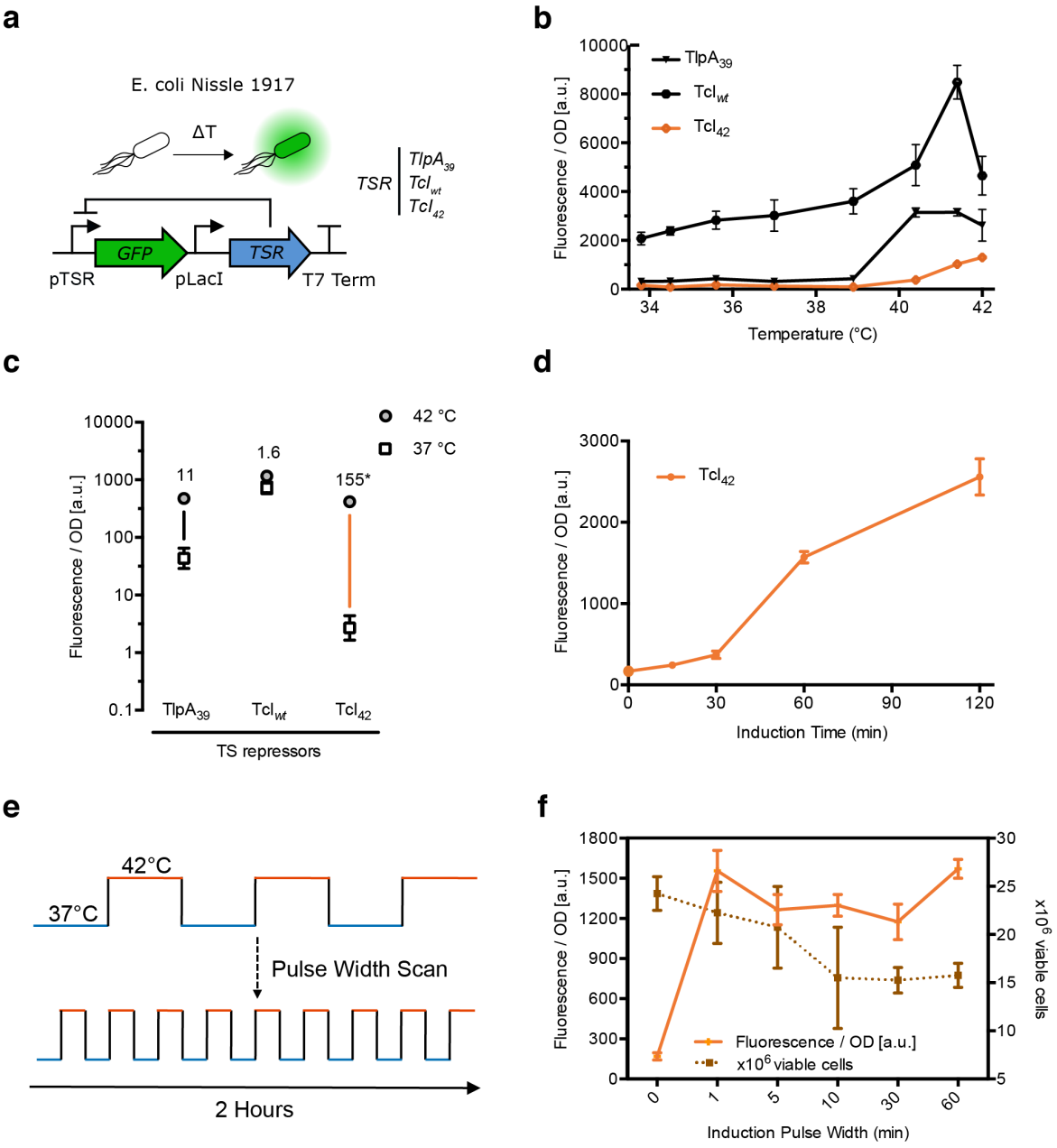

Figure 3-1: Evaluating temperature-sensitive repressors in Nissle 1917. (**a**) Illustration of the genetic circuit used to characterize the behavior of temperature-sensitive repressors in Nissle 1917 *E. coli*. (**b**) Optical density (OD)-normalized fluorescence as a function of induction temperature for a fixed duration of 1 hour. (**c**) OD-normalized fluorescence fold change after 1 hour of thermal

induction for the constructs shown in panel (**a**). (**d**) OD-normalized fluorescence as a function of induction duration. Cells were stimulated at 42 °C. (**e**) Illustration of the pulsatile heating scheme used to optimize thermal induction and cell viability. (**f**) OD-normalized fluorescence as a function of pulse duration. All samples were stimulated for a total of 1 hour at 42 °C and 1 hour at 37 °C. Cell counts at various pulse durations plotted to reflect cell viability. Where not seen, error bars (±SEM) are smaller than the symbol. N=4 biological replicates for each sample.

3.2b: Constructing a Thermally Actuated State Switch

On its own, the TcI42 switch is not sufficient for microbial therapy. This switch is transiently activated for the duration of heating, while tumor therapy requires weeks to effectively suppress tumor growth. Since daily FUS application over this period is infeasible in a clinical setting, a stable circuit is needed that retains its ability to exert a therapeutic response over the course of therapy following a single activation.

To enable stable thermal switching we placed the expression of Bxb1, a serine integrase, under the control of a thermally inducible promoter regulated by TcI42 (**Fig. 3-2a**). Our design combines the temperature sensitivity of TcI42 with the permanent irreversible effector function of the Bxb1 integrase. At physiological temperatures of approximately 37 °C, constitutively expressed TcI42 represses the expression of Bxb1. Upon thermal stimulation, inactivation of TcI42 repression results in a burst of Bxb1 expression. Thermally expressed Bxb1 catalyzes the inversion and activation of a P7 promoter that is responsible for driving the expression of a fluorescent reporter to monitor the state of the circuit and a tetracycline resistance cassette serving as a placeholder for a therapeutic protein (**Fig. 2a**). Because the DNA inversion event that activates P7 is permanent, this promoter will continue to drive the expression of the fluorescent reporter and any payload even when the temperature stimulus is terminated. To avoid unregulated expression of Bxb1 we insulated the activity of the temperature-activated promoter by inserting two strong terminators upstream to block activity from other regions within the plasmid[31].

An ideal design of the circuit described above should maintain low baseline activity at physiological temperature, while providing strong and rapid induction once thermally stimulated. Since Bxb1 expression is the most critical component in our switch determining fold-change, we identified three key tunable sequence elements to modify Bxb1 transcription, translation, and stability (**Fig. 3-2b**). The Bxb1 ribosomal binding sequence (RBS), start codon, and ssrA degradation tag. To efficiently find the best versions of these elements we performed a library screen that consisted of randomized 6-bp sequences within the Bxb1 RBS, two Bxb1 start codon choices, and randomized terminal tripeptides in the Bxb1 ssrA degradation tag[32]. Two start codons were tested because the non-canonical start codon GUG can down-regulate ribosomal efficiency, and the last three amino acids of the ssrA degradation tag were randomized because they strongly modulate the degradation rate of ssrA-tagged proteins[33]. In this screen, we assessed a landscape of approximately 10^7 unique variants using a high-throughput plate-replication assay (**Fig. 3-2b**). To screen these variants, library plates were first replicated and then one plate was incubated at 37 °C to assess baseline expression, while the other plate was stimulated at 42 °C for an hour and returned 37 °C for the rest of the growth period (**Fig. 3-2c**). We selected a subset of variants with low leak and high activation to quantify their fluorescence intensity with a larger number of replicates (**Fig. 3-2d**). Out of these candidates, we selected candidate #5 for further optimization since it yielded the largest fluorescence intensity upon activation, a metric that is important to ensure strong therapeutic activity in *vivo*, while still retaining a reasonable temperature-dependent fold change (**Fig. 3-2d**).

To further reduce the baseline leakage of candidate #5, we modified two additional circuit components (**Fig. 3-2e**). The first modification changed the origin of replication from the low-copy origin pSC101 to the medium-copy origin p15A. The second modification explored the effect of inserting a temperature-sensitive terminator upstream of the Bxb1 coding sequence. This terminator introduces a temperature-sensitive secondary structure in the mRNA transcript that helps terminate protein expression at low temperatures, mitigating

leaky Bxb1 protein production at physiological temperature[34]. At 42 °C, this terminator loses its secondary structure and Bxb1 expression is unimpeded. We assessed the performance of four constructs with either one or two of these modifications (**Fig. 3-2f**). Increasing the copy number of the plasmid and inserting the terminator reduced baseline expression independently. When combined together, these modifications resulted in significantly reduced leakage while maintaining a large fold-change upon induction. This variant, constructed through a combination of randomized and rational engineering, displayed a more than 100-fold change in activity between 37 °C and 42 °C.

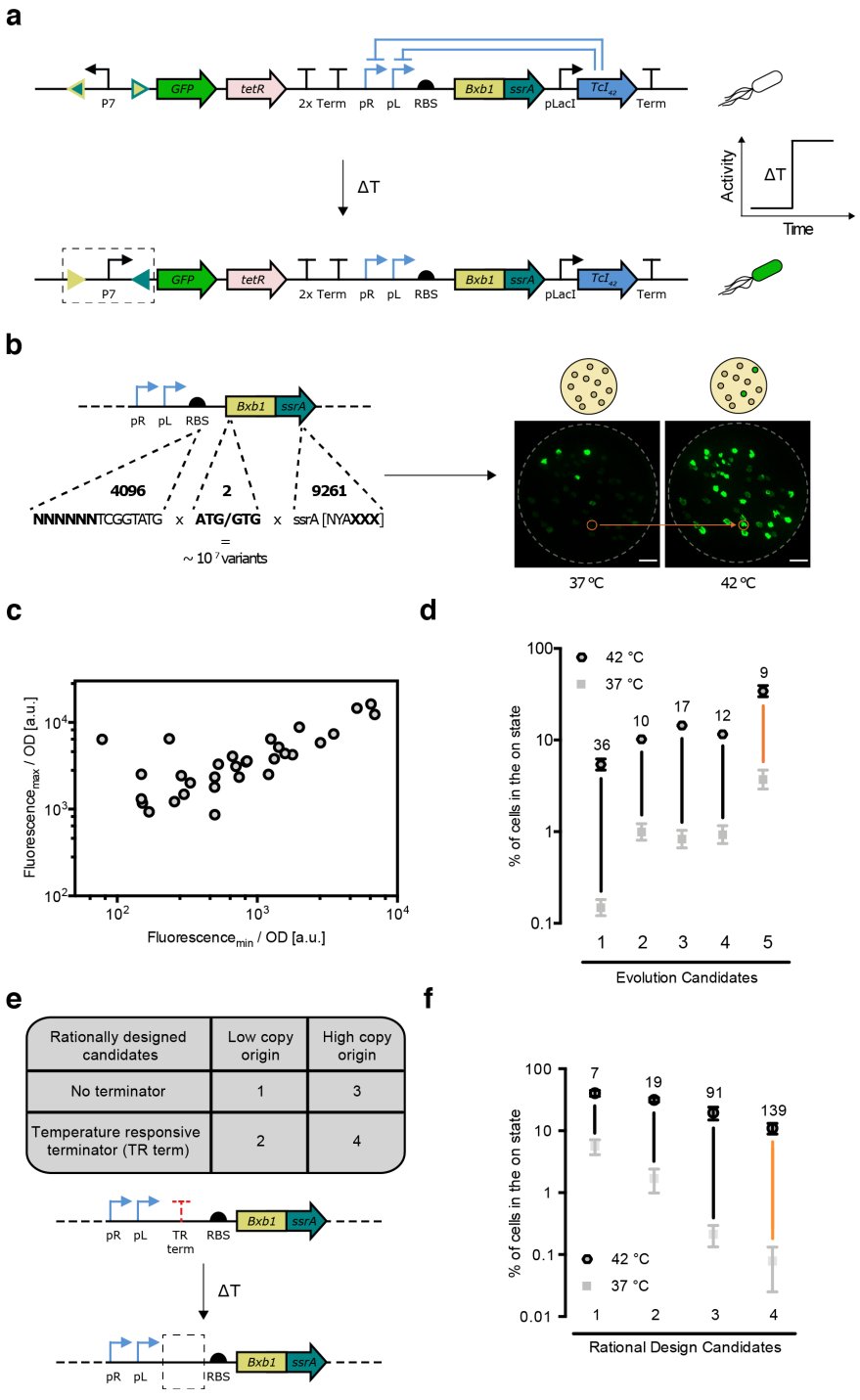

Figure 3-2: Construction and optimization of a temperature-responsive state switch. (**a**) Illustration of the genetic circuit constructed to establish a temperature-responsive state switch. TetR

is tetracycline resistance cassette. (**b**) Illustration of the sites targeted in a high throughput screen to optimize circuit switching. A representative fluorescence image of a replica plate used to screen for circuit variants. Plates were incubated at the indicated temperature for one hour and further incubated at 37 ºC until colonies grew big enough for analysis. The orange circle indicates one colony selected for further assay. (**c**) Circuit variants from the screen in panel (**b).** characterized for their minimal fluorescence in the off state at 37 ºC and maximal fluorescence in the on state at 42 ºC. (**d**) Plot shows percent induction after 1 hour of thermal stimulation at 42ºC compared to baseline at 37 ºC for five of the circuit variants from (**b, c**). (**e**) Summary of rational modifications made to reduce leaking in the circuit at 37 ºC. (**f**) Plot shows percent induction after 1 hour of thermal induction at 42ºC compared to baseline incubation at 37 ºC for four circuit variants described in panel (**e).** Error bars represent ± SEM. N=4 biological replicates for each sample.

3.2c: Modifying the Thermal State Switch for in vivo Activity

To demonstrate that our circuit can function in a clinically relevant scenario, we modified it to express a therapeutic payload and equipped it with a stability cassette to help retain the engineered circuit in *vivo* **(Fig. 3-3a)**. Microbes inhabiting tumors rapidly lose exogenously introduced plasmids without the application of an antibiotic selection, driven by the metabolic burden of exogenous gene expression. To prevent the loss of our plasmid, we introduced an Axe-Txe toxin-antitoxin stability domain that ensures retention of the plasmid within engineered microbial population by eliminating cells that lose the plasmid[35,36].

To test whether the stabilized version of our switch is capable of performing microbial therapy we modified the cells to express a therapeutic protein in place of the tetracycline resistance cassette. We chose to test αCTLA-4 and αPD-L1 nanobodies as they have been shown to achieve therapeutic effects in *vivo*[10]. These nanobodies block signaling through the CTLA-4 and PD-L1 receptor pathways which are heavily implicated in T cell silencing within immunosuppressive tumors. Both proteins were fused to a PelB secretion tag to enhance cell secretion upon activation. Although these checkpoint inhibitors have shown remarkable clinical efficacy and transformed cancer immunotherapy, their therapeutic

efficacy is commonly accompanied with the risk of unintentionally activating autoimmunity in bystander tissues when administered systemically[37,38]. By combining the ability of ultrasound to target cells deep within tissues with the thermal switch developed above, we could target the activity of these checkpoint inhibitors to tumors and mitigate the risk of systemic toxicities. To test this, we transformed EcN cells with the αCTLA-4 circuit and evaluated their switching behavior. Our therapeutic circuit closely resembled the non-therapeutic version tested earlier. It maintained a tight off-state at 37 °C while exhibiting robust fold-changes upon induction at 42 °C and 43 °C **(Fig. 3-3b)**.

To assess the secretion of αCTLA-4 nanobodies upon activation we expanded the cells at 37 °C for a day after stimulation for an hour at 37 °C, 42 °C, and 43 °C, collected the media, and performed a Western Blot to evaluate the levels of αCTLA-4 nanobodies released. This experiment demonstrated that αCTLA-4 nanobodies are reliably secreted into the media upon stimulation at 42 °C and 43 °C **(Fig. 3-3c)**. We could not detect any secretion when the cells were incubated at 37 °C. To assess the therapeutic potential of this circuit, we employed a previously established in *vivo* model[3] and demonstrated that our pre-activated circuits are capable of exerting a therapeutic effect **(Fig. 3-S1).** Altogether, we have developed a thermally actuated state switch that is maintained in vivo, reliably expresses and secretes checkpoint inhibitors upon thermal stimulation, and exerts a therapeutic effect.

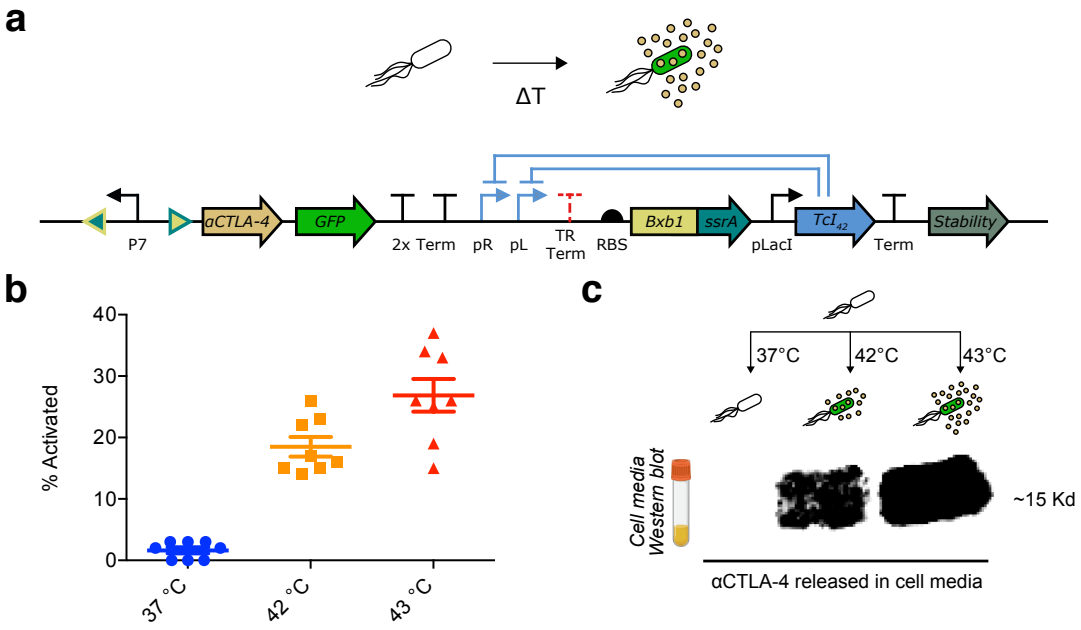

Figure 3-3: A genetic circuit for targeted and sustained release of a therapeutic payload. (**a**) The temperature responsive state switch modified to enable controlled therapeutic delivery of αCTLA-4 nanobodies in *vivo*. The circuit was also equipped with an Axe-Txe stability cassette to retain the plasmid in *vivo* without antibiotic selection. A therapeutic payload replaced the TetR Cassette. (**b**) Plot shows percent induction after 1 hour of thermal induction at 37ºC, 42ºC, and 43ºC for the circuit described in panel (**a**). (**c**) Cells were induced for 1 hour at 37ºC, 42ºC, and 43ºC and then expanded in 5 ml of media for 24 hours at 37ºC before collecting the media and assaying for the release of αCTLA-4 nanobodies into the media.

3.2d: Acoustic Activation of Microbes Elicits Tumor Therapy

To enable thermal control of therapeutic microbes containing our engineered circuit, we built a focused ultrasound stimulation setup that is capable of locally delivering an activation signal to microbes within tumors. An ideal setup should be able to elevate the local temperature within a tumor in a living animal to a predetermined level and autonomously cycle between that temperature and 37 °C every five minutes to enact the pulsatile heating scheme optimized in *vitro*.

To construct this autonomous heating setup, we implemented a mouse version of the clinically established FUS hyperthermia method commonly used to locally heat tissues **(Fig. 3-4a)**. In this version, a holder secures an anesthetized tumor-bearing mouse vertically in a degassed water chamber. The chamber also holds a submerged autonomously controlled ultrasound transducer that acquires the temperature of the tumor and accordingly adjusts its acoustic-output intensity in real-time to achieve the target temperature. We demonstrated that this system is capable of oscillating between 43 °C and 37 °C every five minutes in the tumor of a living animal **(Fig. 3-4a)**. We chose 43 °C to ensure that we get reliable activation within the context of a mouse. While we expect that there will be some thermal damage at this temperature, we reasoned that thermal damage within the tumor is acceptable and could help enhance the microbial therapy.

We used this hyperthermia setup to investigate whether heating microbes engrafted within a tumor with this setup would recapitulate the same activation behavior observed in *vitro*. To test this, we seeded $5x10^6$ A20 murine tumor cells in the right flanks of BALB/c mice **(Fig. 3-4b)**. Once the tumors grew to approximately 100 mm^3 we intravenously injected engineered EcN carrying our therapeutic circuit. The microbes were given two days to engraft in tumors before they were stimulated with FUS to activate the embedded genetic circuit. To assess the percentage of cells activated we collected the tumors two weeks post activation, chemically homogenized them, and plated the suspension. By counting the percentage of activated microbes on these plates, we demonstrated that our thermal switch is reliably activated in tumors targeted with ultrasound while staying off otherwise **(Fig. 3-4c)**. These results also demonstrate that our circuit remains in the on state for at least two weeks. Overall, these results validated that our circuit can be used to activate microbial therapies in the context of a living animal.

Next, we used the same approach to locally activate a therapeutic program as shown in **Figure 3-4b**. Briefly, mice were injected with $5x10^6$ A20 murine tumor cells in their right flank. Tumors were allowed to expand until they reached a mass of around 100 mm^3. At that point, we injected EcN carrying a 1:1 combination of the αCTLA-4 and αPD-L1 circuits, or wild-type EcN. The injected bacteria were allowed to engraft in the tumors for two days before thermally stimulating them. After FUS bacterial activation, tumor growth was monitored to assess therapeutic efficacy. As expected, we observed retardation in tumor growth only in stimulated tumors that were colonized by the therapeutic circuits. These results indicate that our circuit can localize the activity of microbes and allow for safer and more effective therapies **(Fig. 3-4d)**.

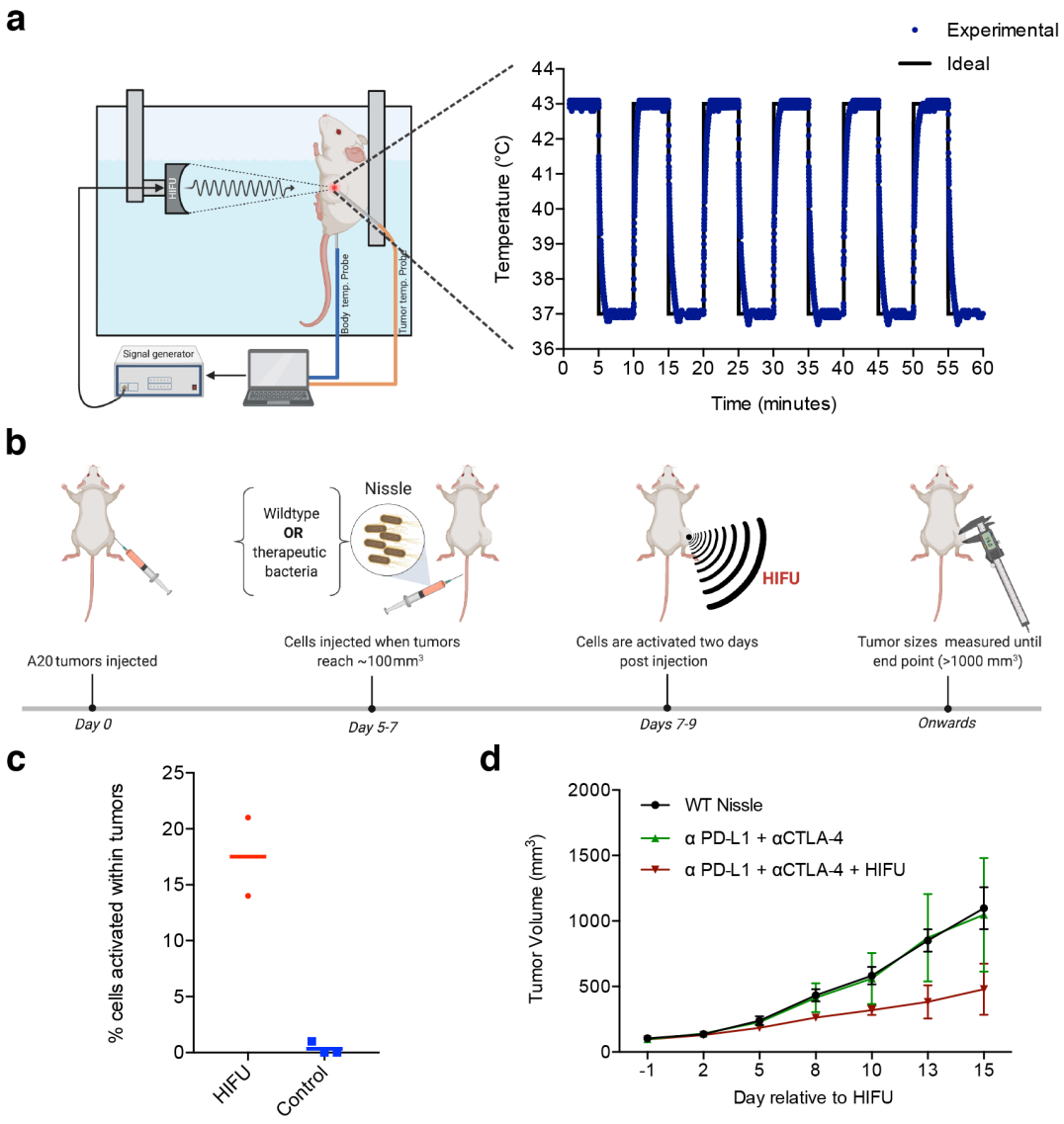

Figure 3-4: Temperature activation of microbes *in vivo*. (**a**) Illustration of the automated setup used to deliver focused ultrasound hyperthermia inside tumors (left). Demonstration of the setup reading the tumor temperature from a mouse and adjusting the ultrasound power to reliably oscillate between two predefined temperatures (Right). (**b**) Diagram illustrating the experiment performed to assess our ability to selectively activate microbial therapies in *vivo* (**c**) Plot shows percent induction within microbes isolated from tumors more than two weeks post focused ultrasound activation in *vivo*. Microbes within tumors were stimulated for 1 hour at 43ºC. (**d**) Tumor sizes were measured

over a period of 15 days in untreated tumors, tumors treated with focused ultrasound, tumors injected with inactivated therapeutic microbes, and tumors with ultrasound activated therapeutic microbes.

3.3: Discussion

Our results establish a thermal state switch with low baseline activity and rapid induction when stimulated that enables targeted and sustained activity of microbial therapy. We constructed and enhanced this bioswitch to meet these desired characteristics by systematically incorporating rationally selected genetic components and tuning them via high-throughput screens. To assess the utility of our switch, we linked its activation to the release of therapeutic payloads and demonstrated that they can be activated at depth with spatial precision when combined with ultrasound hyperthermia. We further showed that our circuit maintains its induced protein expression state within a mammalian host for at least two weeks. Most importantly, our thermally inducible bioswitch demonstrated a promising potential to help enhance the safety and efficacy of tumor homing microbes by localizing their therapeutic activity and subsequently allowing for a more effective therapy.

Given the local temperature modulation capabilities of focused ultrasound, a technique already being used in clinical practice, we expect this bioswitch technology to enhance the safety of microbial immunotherapy by selectively releasing therapeutic payloads at a desired anatomical site while sparing bystander tissues. Our current circuit successfully activated in approximately 20% of the microbial population within tumors. To further enhance the number of activated cells, a thermally inducible antibiotic cassette can be added to the current circuit. By applying antibiotic selective pressure post stimulation, non-stimulated cells within tumors and other organs will be eliminated, allowing the antibiotic resistant (ultrasound activated) population to expand in tumors and achieve full colonization. A chemically inducible kill switch can also be integrated for further safety measures, allowing users to terminate the activity of engineered cells post therapy or in the event of an adverse reaction.

To better enhance therapeutic output, our technology can be further combined with other cellular immunotherapies such as engineered T cells. Engineering microbes within tumors to secrete cytokines can help remodel the environment within solid tumors to be less suppressive and more accessible for engineered T cells. While we have provided evidence for the construction of a permanent, temperature-induced state switch, the overarching framework and optimization process is translatable to a wide array of biomedical applications. In particular, irreversible memory circuits would be helpful in controlling transcription activation of gut microbes, and also in large-scale biofuel production[22,39].

Our circuit successfully accomplished the goals it was designed to address, yet further optimization is needed before it is safe for use in humans. One of the main shortcomings in our current design is that these circuits still exhibit some undesirable activation without stimulation. We believe that this leaky behavior can be attributed to fluctuations in cellular state and metabolism. Any leaky expression of the recombinase will result in unintended permanent activation. To overcome this limitation, we envision that similar circuits can be built with threshold-based activation, such as a bi-stable circuit[40]. In a threshold-activated circuit, leaky expression of a few activator molecules would not be enough to switch the state of the circuit. A sustained cumulative presence of an activator molecule would be needed to alter the state of the switch. While threshold-based circuit designs can address leaky expression, they might also result in slower switching kinetics.

In the process of developing this circuit, we observed that identical genetic elements exhibit drastically different behaviors between different cellular chassis and chemical environments. Specifically, the behavior of our temperature-sensitive repressors varied significantly as they were transferred across different microbial strains or in *vitro* growth media. This variability is an important factor that should be considered when developing tumor targeted microbial therapies since metabolite availability, oxygen levels, and growth densities in tumors are drastically different from the in *vitro* growth conditions used to construct and optimize

genetic circuits. For these reasons, it would be of great importance to further develop and utilize in *vitro* models that can faithfully mimic the tumor environment for future engineering[41].

3.4: Methods

Plasmid Construction and Molecular Biology

All plasmids were designed using SnapGene (GSL Biotech) and assembled via reagents from New England Biolabs for KLD mutagenesis (E0554S) or Gibson Assembly (E2621L). After assembly, constructs were transformed into NEB Turbo (C2984I) and NEB Stable (C3040I) *E. coli* for growth and plasmid preparation. The Bxb1 recombinase-encoding gene was a kind gift from the Laboratory of Richard Murray (Caltech). Integrated DNA Technologies synthesized other genes and all PCR primers.

Preparation of cell lines for in vitro and in vivo experiments

Plasmids containing engineered genetic circuits were transformed into Nissle 1917 *E. coli* (Mutaflor®). Nissle cells were cultured in LB broth (Sigma) and grown on LB agar plates (Sigma) containing appropriate antibiotics. Singular colonies were picked into LB broth, and grown overnight in a shaking incubator (30 °C, 250 rpm). The next day, optical density measurements (OD_{600}) were taken, and the saturated cultures were diluted to 0.1 OD_{600}. Diluted cultures were then allowed to grow to exponential phase until they reached 0.6 OD_{600} before starting assays. Optical density measurements were taken using a Nanodrop 2000c (Thermo Scientific) in cuvette mode.

Western Blot

Five milliliters of cell media were collected for each sample and concentrated with an Amicon® Ultra-15 Centrifugal Filter Unit. Concentrated cell media was then mixed with Laemmli loading buffer and BME before loading into a pre-cast polyacrylamide gels SDS-PAGE gel (Bio Rad) and run at 75 V for 140 minutes. Western blotting was performed using

the Transblot Turbo apparatus and nitrocellulose membrane kit (Bio Rad). Transfer was performed at 25 V for 7 minutes. Membranes were blocked with 5% w/v Blotto milk (Santa Cruz Biotechnology) in 0.05% TBS-Tween for 1 hour at room temperature. Primary staining was performed using the mouse anti-His sc-8036 antibody (Santa Cruz Biotech) overnight at 4 °C. Blots were then washed three times for 15 minutes at 4 °C with 0.05% TBS-Tween and stained for 4 hours with mouse IgG kappa binding protein (m-IgGκ BP) conjugated to Horseradish Peroxidase (HRP) (Santa Cruz Biotech, sc-516102) at room temperature. After three 15-minute washes, HRP visualization was performed using Super signal west Pico PLUS reagent (Thermo Fisher Scientific). Imaging was performed in a Bio-Rad ChemiDoc MP gel imager. A subsequent epi white light image of the blot under the same magnification was acquired to visualize the stained molecular weight standards.

Thermal regulation assay

Once bacterial cell cultures reached approximately 0.6 OD_{600}, 50 μL aliquots of each sample were transferred into individual Bio-Rad PCR strips with optically transparent caps and subsequently heated in conditions specific to the experiment using a Bio-Rad C100 Touch thermocycler with the lid set to 50 °C. Following heating, cells continued to incubate overnight undisturbed at either 30 °C (**Figure 1**) or 37 °C (**Figure 2-4**). The PCR strips were then removed, vortexed, and spun down, and the green fluorescence of each of the samples was measured using the Strategene MX3005p qPCR (Agilent) and an unamplified FAM filter. To measure cell density, the samples were diluted 1:4 with fresh LB media (without antibiotic) and then transferred into individual wells of a 96-well plate (Costar black/clear bottom). Optical density measurements were taken using the SpectraMax M5 plate reader (Molecular Devices). In order to quantify the temperature-dependent gene expression (E) using background-subtracted, OD-normalized fluorescence (**Figure 1b-d, 1f, 2c**), Equation (1) was used:

$$E = \frac{F_{sample} - F_{blank}}{OD_{sample} - OD_{blank}}$$

In this equation, we define F as the raw fluorescence measurement and OD is the OD_{600} measurement of the sample. The value of the blank fluorescence and blank optical density was determined as the average of $N = 4$ samples of untransformed Nissle cells, as opposed to engineered Nissle cells, in LB.

Screens to optimize circuit behavior

To improve Bxb1 thermal regulation, a sequence randomized library of the RBS, start codon, and ssrA degradation tag was ordered from Integrated DNA Technologies. PCR products that included the Bxb1 coding region and immediately surrounding sequences were amplified using custom primers and were inserted into the backbone of the rest of the parent plasmid using Gibson Assembly (Fig. 2b-d). This library was transformed into EcN and plated on LB Agar plates with antibiotic resistance at a low colony density of approximately 30 colonies per petri dish. Following overnight incubation at 30 °C to allow the colonies to become visible, these plates were then replicated into two daughter petri dishes using a replica-plating tool (VWR 25395-380). The parent petri dish was incubated at 4 °C until the conclusion of the experiment. One daughter plate was grown overnight at the baseline temperature of 37 °C, and the other was incubated at 42 °C for 2 hours and then moved to 37 °C overnight. After colonies became visible, the plates were imaged using a 530/28 nm emission filter to determine colonies that were fluorescent at the on temperature but opaque at the off temperature (Bio-Rad ChemiDoc MP imager). Approximately 800 colonies were screened per library. Promising library variants were then picked from the corresponding parent petri dish at 4 °C and analyzed against the parent plasmid of the library using the liquid culture fluorescence-based assay described above.

Percent switching assay

The rapidness and validity of the high-throughput plate-based screening assay deployed during the plasmid library testing motivated the development of a similar assay for subsequent testing of genetic circuits, moving away from liquid culture fluorescence

measurements described above. Strips of liquid bacteria samples were still prepared and incubated in the Bio-Rad Touch thermocycler. After the prescribed thermal stimulus and incubation at 37 °C, PCR strips were removed, vortexed, and spun down on a tabletop centrifuge. Five 1:10 serial dilutions in liquid LB were then performed, transferring 10 μL of sample into 90 μL of LB media sequentially. After thorough mixing, 50 μL of the most diluted samples were plated onto an LB plate and allowed to incubate at 30 °C overnight. Upon the appearance of visible colonies, plates were imaged using the same Bio-Rad ChemiDoc MP imager with both blue epifluorescence illumination and the 530/28 nm emission filters. The percentage of colonies in the on state (P) was determined according to Equation (2):

$$P = \frac{\text{number of green colonies counted on a plate}}{\text{total number of colonies counted on a plate}}$$

This percentage served as an estimate of the gene expression as a function of temperature.

Animal procedures

All animal procedures were performed under a protocol approved by the California Institute of Technology Institutional Animal Care and Use Committee (IACUC). Nine-week-old BALB/c female mice were purchased from Jackson Laboratory (JAX). To establish A20 tumor models in mice, five million A20 cells were collected and suspended in 100 μL of PBS prior to subcutaneous injection into the flank of each mouse. When tumor volumes reached about 100 mm^3, engineered EcN cells prepared according to the procedure outlined in the section above were then collected by centrifugation (3000 g for 5 min), washed with phosphate buffer saline (PBS) 3 times, and diluted in PBS to 0.625 OD. 100 μL of the resulting solution of bacterial cells was injected into each of the A20 tumor bearing mice via the tail vein. For thermal actuation using ultrasound, mice were anesthetized using a 2% isoflurane-air mixture and placed on a dedicated animal bed. Anesthesia was maintained over the course of the ultrasound procedure using 1-1.5% isoflurane, adjusted in real-time to maintain the respiration rate at 20-30 breaths per minute. Body temperature was continuously

monitored using a fiber optic rectal thermometer (Neoptix). When appropriate, the target flank was thermally activated using the automated HIFU setup described below, cycling between the temperatures of 43 °C and 37 °C every 5 minutes for 1 hour of total heating. Following ultrasound treatment, the mice were returned to their cages, and the size of their tumors was measured with a caliper to track the therapeutic efficacy. When the tumors reached ~1000 mm^3 mice were culled and the tumors were collected for analysis. Mice that did not have microbial cells colonizing their tumors were excluded from the study.

Tumor analysis

Tumors were collected and homogenized in ten milliliters of PBS containing 2 mg/ml collagenase and 0.1 mg/ml DNAse for one hour at 37 °C. Homogenized tumors were serially diluted and plated onto LB plates to quantify the number of cells colonizing the tumors. The percentage of cells activated within tumors was determined by counting the number of GFP^{+ve} cells.

Automated high intensity focused ultrasound

We developed an autonomous closed loop thermal control setup to maintain a specified predetermined temperature within the tumor of a mouse by modulating the intensity of the focused ultrasound. This setup includes a water bath filled with pure distilled water that is being actively cleaned and degassed with an AQUAS-10 water conditioner (ONDA) and maintained at 33 °C with a sous vide immersion cooker (InstantPot Accu Slim). A tumor-bearing mouse that has been anesthetized as described above is fastened nose up vertically to an acrylic arm that is connected to a manual 3D positioning system (Thorlabs) to enable 3D motion of the mouse within the water bath. A Velmex BiSlide motorized positioning system is used to submerge and position the 0.67 MHz HIFU transducer (Precision Acoustics PA717) such that the focal point of the transducer lies within the tumor of the mouse. A signal generator (B&K #4054B) generates the thermal ultrasound signal which is then amplified (AR #100A250B) and sent to drive the FUS transducer. The water in this chamber

acts as a coupling medium to transfer the ultrasound wave from the transducer to the tumor. To measure the internal tumor temperature during a heating session, we implant a fiber optic temperature probe from the Neoptix system into the tumors. This temperature readout is also used to align the focus of the transducer with the tumor by emitting a constant test thermal ultrasound signal. Once the system is aligned, we deactivate the test signal and run a Matlab closed loop thermal control script that controls the signal generator output. Feedback for the controller is provided by the temperature measurements taken using the Neoptix fiber optic thermometry system with a sampling rate of 4 Hz. The actuator for the controller is the voltage amplitude of the continuous sinusoidal signal of 0.67 MHz used to drive the HIFU transducer, where the signal generator is adjusted also at 4 Hz. The system uses a PID controller with anti-windup control that modifies the amplitude of the thermal ultrasound waveform to achieve a desired temperature in the targeted tissues. The Kp, Ki, Kd, and Kt parameters for the PID and anti-windup needed to be tuned starting with Ziegler-Nichols method and subsequent trial-and-error tuning to achieve thermal control for each mouse. The scripts are available at the following link:
https://github.com/drmittelstein/thermal_control

Statistics and replicates

Data is plotted and reported in the text as the mean ± S.E.M. Sample size is $N = 4$ biological replicates in all in vitro experiments unless otherwise stated. This sample size was chosen based on preliminary experiments indicating that it would be sufficient to detect significant differences in mean values. *P* values were calculated using a two-tailed unpaired *t*-test.

Data and code availability

Plasmids will be made available through Addgene upon publication. All other materials and data are available from the corresponding author upon reasonable request.

3.5: Supplementary figures

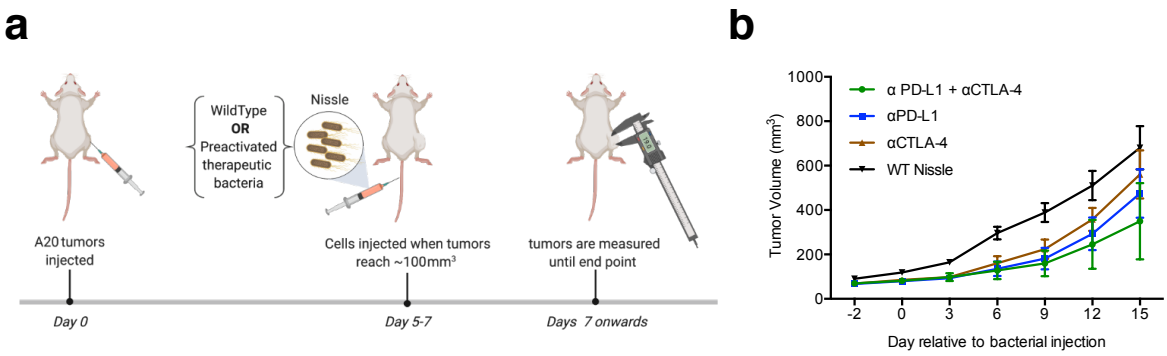

Figure 3-S1: In *vivo* model experiment to verify therapeutic functionality of pre-activated microbes. (**a**) Diagram describing the experiment performed to assess the ability of thermally activated microbes to induce a therapeutic effect in *vivo*. (**b**) Plot shows tumor growth in mice injected with WT Nissle 1917 *E. coli* or preactivated microbes secreting αCTLA-4 nanobodies, αPD-L1 nanobodies, or αCTLA-4 and αPD-L1 nanobodies.

3.6: References

(1) Zhou, S., Gravekamp, C., Bermudes, D., and Liu, K. (2018) Tumour-targeting bacteria engineered to fight cancer. *Nature Reviews Cancer 18*, 727–743.
(2) Weber, E. W., Maus, M. V., and Mackall, C. L. (2020) The Emerging Landscape of Immune Cell Therapies. *Cell 181*, 46–62.
(3) Yu, J. X., Upadhaya, S., Tatake, R., Barkalow, F., and Hubbard-Lucey, V. M. (2020) Cancer cell therapies: the clinical trial landscape. *Nature Reviews Drug Discovery 19*, 583–584.
(4) Fucà, G., Reppel, L., Landoni, E., Savoldo, B., and Dotti, G. (2020) Enhancing Chimeric Antigen Receptor T-Cell Efficacy in Solid Tumors. *Clinical Cancer Research 26*, 2444–2451.
(5) Anderson, K. G., Stromnes, I. M., and Greenberg, P. D. (2017) Obstacles posed by the tumor microenvironment to T cell activity: a case for synergistic therapies. *Cancer Cell 31*, 311–325.
(6) Mirzaei, H. R., Rodriguez, A., Shepphird, J., Brown, C. E., and Badie, B. (2017) Chimeric Antigen Receptors T Cell Therapy in Solid Tumor: Challenges and Clinical Applications. *Front. Immunol. 8*.
(7) Dang, L. H., Bettegowda, C., Huso, D. L., Kinzler, K. W., and Vogelstein, B. (2001) Combination bacteriolytic therapy for the treatment of experimental tumors. *Proc Natl Acad Sci U S A 98*, 15155–15160.
(8) Leschner, S., Westphal, K., Dietrich, N., Viegas, N., Jablonska, J., Lyszkiewicz, M., Lienenklaus, S., Falk, W., Gekara, N., Loessner, H., and Weiss, S. (2009) Tumor Invasion of Salmonella enterica Serovar Typhimurium Is Accompanied by Strong Hemorrhage Promoted by TNF-α. *PLoS One 4*.
(9) Kang, S.-R., Jo, E. J., Nguyen, V. H., Zhang, Y., Yoon, H. S., Pyo, A., Kim, D.-Y., Hong, Y., Bom, H.-S., and Min, J.-J. (2020) Imaging of tumor colonization by Escherichia coli using 18F-FDS PET. *Theranostics 10*, 4958–4966.
(10) Gurbatri, C. R., Lia, I., Vincent, R., Coker, C., Castro, S., Treuting, P. M., Hinchliffe, T. E., Arpaia, N., and Danino, T. (2020) Engineered probiotics for local tumor delivery of checkpoint blockade nanobodies. *Science Translational Medicine 12*.
(11) Jiang, S.-N., Phan, T. X., Nam, T.-K., Nguyen, V. H., Kim, H.-S., Bom, H.-S., Choy, H. E., Hong, Y., and Min, J.-J. (2010) Inhibition of Tumor Growth and Metastasis by a Combination of Escherichia coli–mediated Cytolytic Therapy and Radiotherapy. *Molecular Therapy 18*, 635–642.
(12) Ryan, R. M., Green, J., Williams, P. J., Tazzyman, S., Hunt, S., Harmey, J. H., Kehoe, S. C., and Lewis, C. E. (2009) Bacterial delivery of a novel cytolysin to hypoxic areas of solid tumors. *Gene Therapy 16*, 329–339.
(13) Groot, A. J., Mengesha, A., Wall, E. van der, Diest, P. J. van, Theys, J., and Vooijs, M. (2007) Functional antibodies produced by oncolytic clostridia. *Biochemical and Biophysical Research Communications 364*, 985–989.
(14) Duong, M. T.-Q., Qin, Y., You, S.-H., and Min, J.-J. (2019) Bacteria-cancer interactions: bacteria-based cancer therapy. *Experimental & Molecular Medicine 51*, 1–15.
(15) Felgner, S., Pawar, V., Kocijancic, D., Erhardt, M., and Weiss, S. (2017) Tumour-targeting bacteria-based cancer therapies for increased specificity and improved outcome. *Microbial Biotechnology 10*, 1074–1078.
(16) Clairmont, C., Lee, K. C., Pike, J., Ittensohn, M., Low, K. B., Pawelek, J., Bermudes, D., Brecher, S. M., Margitich, D., Turnier, J., Li, Z., Luo, X., King, I., and Zheng, L. M. (2000) Biodistribution and Genetic Stability of the Novel Antitumor Agent VNP20009, a Genetically Modified Strain of Salmonella typhimuvium. *The Journal of Infectious Diseases 181*, 1996–2002.

(17) Park, S.-H., Zheng, J. H., Nguyen, V. H., Jiang, S.-N., Kim, D.-Y., Szardenings, M., Min, J. H., Hong, Y., Choy, H. E., and Min, J.-J. (2016) RGD Peptide Cell-Surface Display Enhances the Targeting and Therapeutic Efficacy of Attenuated Salmonella-mediated Cancer Therapy. *Theranostics 6*, 1672–1682.
(18) Stritzker, J., Weibel, S., Hill, P. J., Oelschlaeger, T. A., Goebel, W., and Szalay, A. A. (2007) Tumor-specific colonization, tissue distribution, and gene induction by probiotic Escherichia coli Nissle 1917 in live mice. *International Journal of Medical Microbiology 297*, 151–162.
(19) Massa, P. E., Paniccia, A., Monegal, A., de Marco, A., and Rescigno, M. (2013) Salmonella engineered to express CD20-targeting antibodies and a drug-converting enzyme can eradicate human lymphomas. *Blood 122*, 705–714.
(20) Zheng, J. H., Nguyen, V. H., Jiang, S.-N., Park, S.-H., Tan, W., Hong, S. H., Shin, M. G., Chung, I.-J., Hong, Y., Bom, H.-S., Choy, H. E., Lee, S. E., Rhee, J. H., and Min, J.-J. (2017) Two-step enhanced cancer immunotherapy with engineered Salmonella typhimurium secreting heterologous flagellin. *Science Translational Medicine 9*.
(21) Dai, Y., Toley, B. J., Swofford, C. A., and Forbes, N. S. (2013) Construction of an inducible cell-communication system that amplifies Salmonella gene expression in tumor tissue. *Biotechnology and Bioengineering 110*, 1769–1781.
(22) Hartsough, L. A., Park, M., Kotlajich, M. V., Lazar, J. T., Han, B., Lin, C.-C. J., Musteata, E., Gambill, L., Wang, M. C., and Tabor, J. J. (2020) Optogenetic control of gut bacterial metabolism to promote longevity. *eLife* (Gruber, J., Tyler, J. K., and Mair, W., Eds.) *9*, e56849.
(23) Lalwani, M. A., Ip, S. S., Carrasco-López, C., Day, C., Zhao, E. M., Kawabe, H., and Avalos, J. L. (2021) Optogenetic control of the lac operon for bacterial chemical and protein production. *Nature Chemical Biology 17*, 71–79.
(24) Liu, Z., Zhang, J., Jin, J., Geng, Z., Qi, Q., and Liang, Q. (2018) Programming Bacteria With Light—Sensors and Applications in Synthetic Biology. *Front Microbiol 9*.
(25) Ash, C., Dubec, M., Donne, K., and Bashford, T. (2017) Effect of wavelength and beam width on penetration in light-tissue interaction using computational methods. *Lasers Med Sci 32*, 1909–1918.
(26) Piraner, D. I., Abedi, M. H., Moser, B. A., Lee-Gosselin, A., and Shapiro, M. G. (2017) Tunable thermal bioswitches for in vivo control of microbial therapeutics. *Nature Chemical Biology 13*, 75–80.
(27) Hsiao, V., Hori, Y., Rothemund, P. W., and Murray, R. M. (2016) A population-based temporal logic gate for timing and recording chemical events. *Molecular Systems Biology 12*, 869.
(28) Meysman, P., Sánchez-Rodríguez, A., Fu, Q., Marchal, K., and Engelen, K. (2013) Expression Divergence between Escherichia coli and Salmonella enterica serovar Typhimurium Reflects Their Lifestyles. *Molecular Biology and Evolution 30*, 1302–1314.
(29) Leventhal, D. S., Sokolovska, A., Li, N., Plescia, C., Kolodziej, S. A., Gallant, C. W., Christmas, R., Gao, J.-R., James, M. J., Abin-Fuentes, A., Momin, M., Bergeron, C., Fisher, A., Miller, P. F., West, K. A., and Lora, J. M. (2020) Immunotherapy with engineered bacteria by targeting the STING pathway for anti-tumor immunity. *Nature Communications 11*, 2739.
(30) Abedi, M. H., Lee, J., Piraner, D. I., and Shapiro, M. G. (2020) Thermal Control of Engineered T-cells. *ACS Synth. Biol. 9*, 1941–1950.

(31) Chen, Y.-J., Liu, P., Nielsen, A. A. K., Brophy, J. A. N., Clancy, K., Peterson, T., and Voigt, C. A. (2013) Characterization of 582 natural and synthetic terminators and quantification of their design constraints. *Nature Methods 10*, 659–664.
(32) Courbet, A., Endy, D., Renard, E., Molina, F., and Bonnet, J. (2015) Detection of pathological biomarkers in human clinical samples via amplifying genetic switches and logic gates. *Science Translational Medicine 7*, 289ra83-289ra83.
(33) Flynn, J. M., Levchenko, I., Seidel, M., Wickner, S. H., Sauer, R. T., and Baker, T. A. (2001) Overlapping recognition determinants within the ssrA degradation tag allow modulation of proteolysis. *PNAS 98*, 10584–10589.
(34) Roßmanith, J., Weskamp, M., and Narberhaus, F. (2018) Design of a Temperature-Responsive Transcription Terminator. *ACS Synth. Biol. 7*, 613–621.
(35) Grady, R., and Hayes, F. (2003) Axe-Txe, a broad-spectrum proteic toxin-antitoxin system specified by a multidrug-resistant, clinical isolate of Enterococcus faecium. *Mol Microbiol 47*, 1419–1432.
(36) Fedorec, A. J. H., Ozdemir, T., Doshi, A., Ho, Y.-K., Rosa, L., Rutter, J., Velazquez, O., Pinheiro, V. B., Danino, T., and Barnes, C. P. (2019) Two New Plasmid Post-segregational Killing Mechanisms for the Implementation of Synthetic Gene Networks in Escherichia coli. *iScience 14*, 323–334.
(37) Martins, F., Sofiya, L., Sykiotis, G. P., Lamine, F., Maillard, M., Fraga, M., Shabafrouz, K., Ribi, C., Cairoli, A., Guex-Crosier, Y., Kuntzer, T., Michielin, O., Peters, S., Coukos, G., Spertini, F., Thompson, J. A., and Obeid, M. (2019) Adverse effects of immune-checkpoint inhibitors: epidemiology, management and surveillance. *Nature Reviews Clinical Oncology 16*, 563–580.
(38) Bertrand, A., Kostine, M., Barnetche, T., Truchetet, M.-E., and Schaeverbeke, T. (2015) Immune related adverse events associated with anti-CTLA-4 antibodies: systematic review and meta-analysis. *BMC Medicine 13*, 211.
(39) Lee, S. J., Lee, S.-J., and Lee, D.-W. (2013) Design and development of synthetic microbial platform cells for bioenergy. *Front. Microbiol. 4*.
(40) Gardner, T. S., Cantor, C. R., and Collins, J. J. (2000) Construction of a genetic toggle switch in Escherichia coli. *Nature 403*, 339–342.
(41) Harimoto, T., Singer, Z. S., Velazquez, O. S., Zhang, J., Castro, S., Hinchliffe, T. E., Mather, W., and Danino, T. (2019) Rapid screening of engineered microbial therapies in a 3D multicellular model. *PNAS 116*, 9002–9007.

C h a p t e r 4

THERMAL CONTROL OF ENGINEERED T CELLS

Abedi, M. H., Lee, J., Piraner, D. I., & Shapiro, M. G. (2020). Thermal Control of Engineered T-cells. *ACS Synthetic Biology*, *9*(8), 1941–1950. https://doi.org/10.1021/acssynbio.0c00238

4.1: Introduction

Unlike small molecule and biologic therapies, cells have a natural ability to navigate, persist, and proliferate within the body, providing the potential for more targeted and sustained disease treatment. This potential is enhanced by the capacity of cells to probe, process, and respond to their environment and carry out a wide range of sophisticated behaviors, which can be engineered using the tools of synthetic biology[1]. Among the cell types being developed for therapy, T-cells are one of the most promising due to their central role in cancer, infectious disease, and autoimmune disorders, along with their relative ease of isolation, genetic modification, and re-engraftment. For example, this potential has been realized in T-cells engineered to express modularly targeted chimeric antigen receptors (CARs), allowing them to specifically eradicate cancers such as lymphomas bearing the CD19 antigen[2,3,4,5]. Unfortunately, it has been challenging to translate these successful results into solid tumors, where CAR T-cells encounter a more immunosuppressive environment[6] and the risk of sometimes fatal on-target off-tumor toxicity due to the presence of tumor-overexpressed epitopes in healthy tissues[7,8]. Likewise, emerging approaches in which T-cells are used to treat autoimmune disease through local immunosuppression carry the risk of reducing important immune system activity outside the target tissues[9]. Existing strategies seeking to reduce off-target toxicity use additional target recognition elements[10,11] or chemically triggered kill switches[12,13,14]. However, it can be difficult to ensure perfect

recognition solely through molecular markers, and premature termination of T-cell therapy using kill-switches turns off their beneficial therapeutic action.

Here we describe a cellular engineering approach to regulate the activity of therapeutic T-cells with greater specificity through a combination of molecular and physical actuation. This approach is designed to take advantage of the ability of technologies such as focused ultrasound (FUS) and magnetic hyperthermia to non-invasively deposit heat at precise locations in deep tissue[15–18]. By engineering thermal bioswitches that allow T-cells to sense small changes in temperature and use them as inputs for the actuation of genetic circuits, we enable these penetrant forms of energy to spatially control T-cell activity. Our approach is based on heat shock promoters (pHSP), which have been shown to drive gene expression in response to FUS-delivered heating[19–21], but have not been tested in primary human T-cells. This is important because the behavior of pHSPs varies greatly between cell types and cellular states. In this study, we screen a library of pHSPs in primary T-cells and engineer gene circuits providing transient and sustained activation of gene expression in response to brief thermal stimuli within the well-tolerated temperature range of 37–42ºC[22–24]. Our circuits incorporate feed-forward amplification, positive feedback, and recombinase-based state switches. We demonstrate the use of these circuits to control the secretion of a therapeutic cytokine, expression of a CAR, and killing of target tumor cells.

4.2: Results

4.2a: Evaluating Candidate pHSPs in Primary T cells

To enable thermal control of T-cell activity, we required a pHSP with robust switching behavior in primary human T-cells. Given the variability in pHSP responses between cell types[25], we decided to systematically evaluate the activity of 13 different pHSPs in response to a 1-hour incubation at 42ºC. This thermal stimulus was chosen based on its tolerability by most tissues[24], and the convenience of relatively short treatment durations in potential clinical scenarios. Our panel of pHSPs included nine human, three mouse, and one *C. elegans*

promoter. The human promoters included four naturally occurring sequences (HSPB, HSPB'2, HSP A/A, HSP A/B), two modifications of HSPB'2 generated by varying the 5' UTR (HSPB'1, HSPB'3), and three rational modifications of HSPB'2 (SynHSPB'1, SynHSPB'2, SynHSPB'3) inspired by a previously developed sensor of cellular stress[26]. Truncating HSPB'2 and leaving 192 base pairs resulted in SynHSPB'1. To lower potential baseline activity, the AP-1 binding site in SynHSPB'1 was mutated leading to SynHSPB'2. Duplicating SynHSPB'2 four times to increase the number of heat shock elements (HSE) resulted in SynHSPB'3. The three mouse-derived pHSPs were naturally occurring promoters. HSP16, derived from *C. elegans*, was first described in 1986 and is rationally modified to form a minimal bidirectional promoter encompassing four HSE binding sites[27]. HSP16 excludes other transcription factor binding sites that typically exist in human promoters. We incorporated each pHSP into a standardized lentiviral construct in which the pHSP drives the expression of a green fluorescent protein (GFP), with a constitutively expressed blue fluorescent protein (BFP) serving as a marker of transduction (**Figure 4-1a**).

Once stimulated, all of the promoters displayed a uniform level of activation across the cell population allowing us to use mean fluorescence as a metric of fold induction (**Fig. 4-S1**). Of our 13 promoters, HSPB had the lowest baseline expression at 37ºC (**Fig. 4-1b**), an important property for minimizing activity in the absence of the thermal trigger. HSPB'1 showed the largest fold-change in gene expression, reflecting a combination of relatively low baseline expression and strong promoter activity when stimulated. Among the rationally engineered HSPB'2 variants, SYNHSPB'3 had a lower baseline than the natural promoter, albeit with lower maximum expression on activation. The rest of the human and mouse-derived promoters exhibited high baseline activity, resulting in their elimination from further experiments. Finally, the *C. elegans* minimal promoter exhibited acceptable performance and was included in further testing to investigate whether its minimal composition would be advantageous for specific activation in response to temperature. Based on these factors, we

chose HSPB, HSPB'1, SynHSPB'3, and HSP16 as our starting points for further circuit engineering.

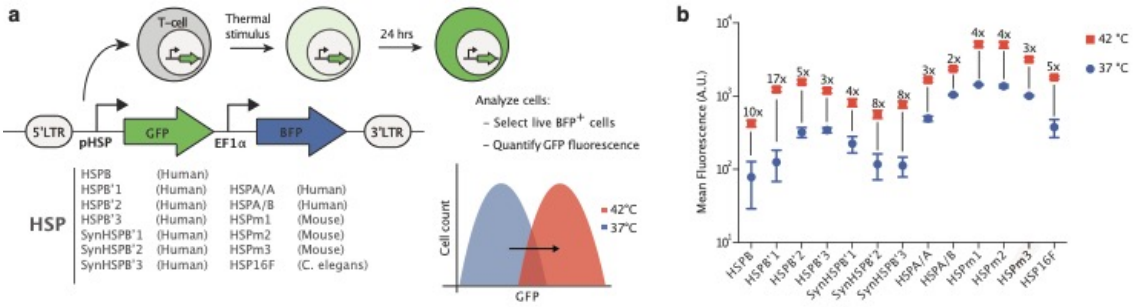

Figure 4-1: Evaluating candidate pHSPs in primary T-cells. (**a**) Illustration of the screening strategy used to characterize the behaviour of pHSPs. The viral construct used to assay pHSPs is shown, along with the promoters tested. LTR, long terminal repeat. (**b**) Mean fluorescence intensity 24 hours after a 1-hour incubation at 37°C or 42ºC, as measured via flow cytometry. The fold change between 37°C and 42°C is listed above each sample. Where not seen, error bars (±SEM) are smaller than the symbol. N=3 biological replicates for each sample.

4.2b: Thermal Parameters for pHSP Activation

After identifying four candidate pHSPs, we tested their response to a range of induction parameters. To search for temperatures that provide rapid induction with minimal thermal burden to the cells, we incubated pHSP-transduced T-cells at temperatures ranging from 37ºC to 44ºC for 1 hour. All four promoters exhibited a significant increase in activity starting at 42ºC (**Fig. 4-2a**). Increasing the induction temperature beyond this point resulted in a significant enhancement of transcriptional activity, but compromised cell viability (**Fig. 4-2b**). To optimize induction with minimal cell damage, we chose 42ºC for further experiments. We note that unlike the gradual increase in gene expression observed with the mammalian promoters above 42ºC, HSP16 exhibited a large jump between this temperature and 43ºC, which may make it useful in future circuit engineering applications.

To reduce the effect of thermal exposure on cell viability, we tested a pulsatile heating scheme with a 50% duty cycle[28]. In this scheme, cells underwent repeated cycles of heating to 42ºC for a fixed duration and an equal amount of time at 37ºC, adding up to a total of one hour at 42ºC over a two-hour treatment period. We varied the stimulation period between one minute and continuous heating for 60 min. This experiment revealed a trade-off between promoter activity (**Fig. 4-2c**) and cell viability (**Fig. 4-2d**), with shorter pulses reducing the former while increasing the latter. For the purposes of T-cell therapy, in which cells can expand after activation, we decided that a 40% decrease in cell viability was a suitable trade-off for improved activation, therefore selected a continuous heating paradigm. This paradigm also simplifies the application of heating during therapy. We also investigated continuous stimulation durations ranging from 15 to 120 minutes. Shorter induction enhanced viability (**Fig. 4-2e**) at the expense of lower gene expression (**Fig. 4-2f**), with a one-hour stimulation providing a reasonable balance. While the optimal stimulation scheme would heavily depend on the promoter used, circuit design, targeted tissue, and therapeutic dose required, we chose a one-hour continuous stimulus at 42ºC as our heating paradigm for our subsequent experiments to maximize our chances of getting a meaningful response despite some damage to the cells.

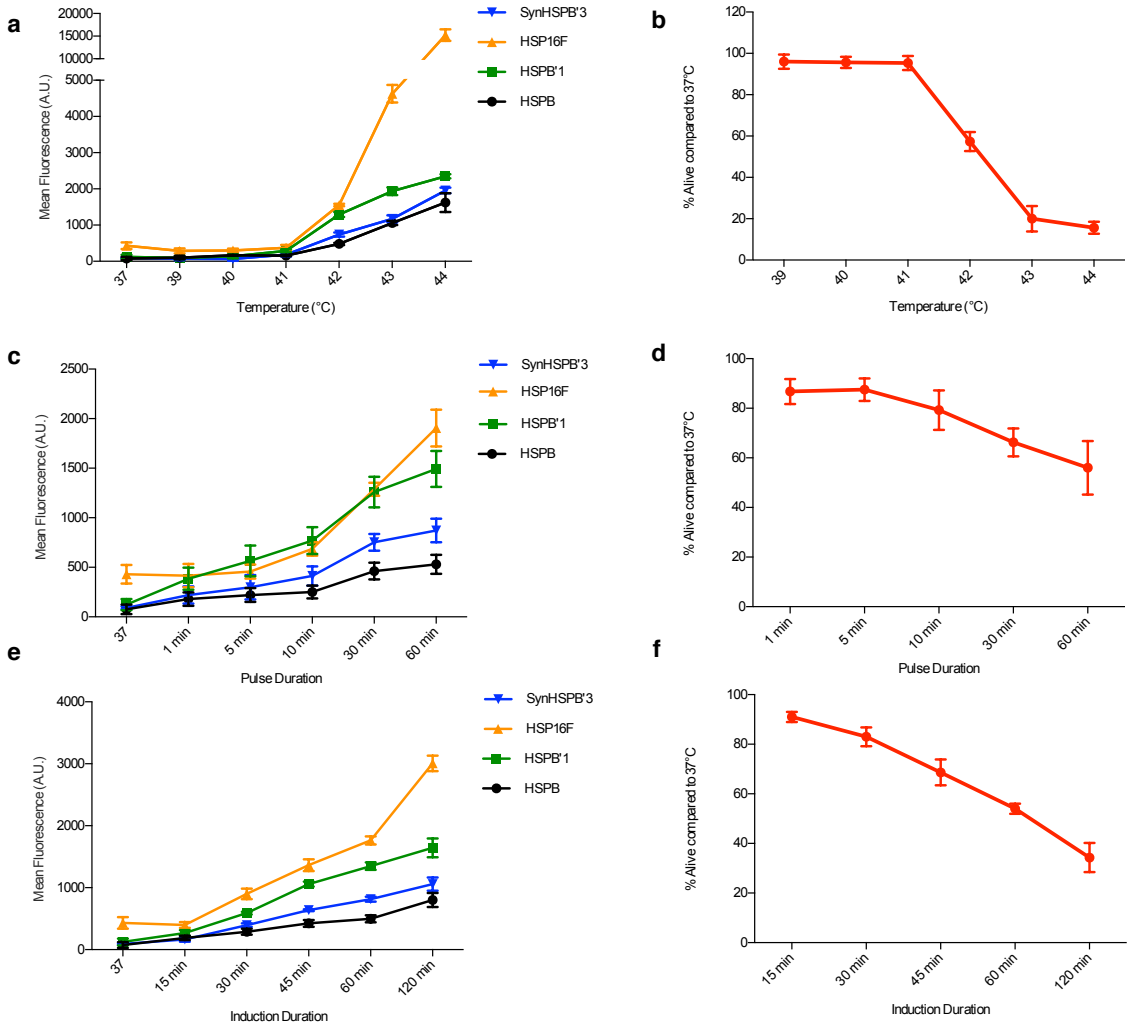

Figure 4-2: Thermal parameters for pHSP activation in primary human T-cells. GFP expression from constructs driven by the HSPB, HSPB'1, SynHSPB'3, and HSP16F promoters **(a, c, e)** and T-cell viability **(b, d, f)** as a function of **(a,b)** induction temperature for a continuous 1 hour stimulus, **(c,d)** pulse duration of stimuli delivered with a 50% duty cycle alternating between 37ºC and 42ºC for a fixed thermal exposure of 1 hour, and **(e,f)** induction duration for continuous heating at 42ºC. Where not seen, error bars (±SEM) are smaller than the symbol. N=3 biological replicates for each sample.

4.2c: Genetic Circuits for Amplified and Sustained Thermal Activation

On their own, pHSPs drove a relatively small amount of transient protein expression upon induction. To enable the use of pHSPs in T-cell therapy applications, it is useful to amplify the output of pHSP-driven circuits. This would enable cells to, for example, release a relatively large therapeutic bolus after a single thermal stimulus. To achieve this goal, we implemented a feed-forward amplification circuit in which the pHSP drives an rtTA transactivator, which produces stronger transcriptional activation tunable with doxycycline. In addition, LNGFR was constitutively expressed to identify virally transfected cells (**Fig. 4-3a**). Amplification circuits incorporating HSPB, HSPB'1, SynHSPB'3, and HSP16 all exhibited a substantial increase in their fold-induction, while only modestly elevating baseline expression. HSPB showed the best performance, suggesting that in the context of feed-forward amplification driving the maximum expression level, a promoter with lower leakage (**Fig. 4-1b**) is preferable. The expression of a constitutive transduction marker was similar across constructs (e.g. **Fig. 4-S2**), indicating that infection levels did not affect their relative performance. To further tune the performance of the HSPB amplifier circuit, we designed constructs with reduced translation of the GFP by varying the Kozak sequence or inserting a micro open reading frame upstream[29] (**Fig. 4-3b**). These modifications enabled the tuning of both the baseline expression and the maximal activation level.

In some therapeutic scenarios, it is critical to prolong the therapeutic action of T-cells following a thermal induction treatment. This would eliminate the need to apply repeated stimuli to maintain treatment efficacy. To develop this capability, we established a positive feedback amplifier circuit by rearranging the elements of our feed-forward amplifier such that rtTA could drive its own expression in the presence of doxycycline (**Fig. 4-3c**). A similar design was previously tested in human cervical cancer HeLa cells[30]. The HSPB feedback circuit maintained its thermal induction level, and we were able to reduce baseline activity by tuning the Kozak sequence upstream of rtTA. In the current design, the output of the positive feedback circuit is lower than that of the feed-forward amplifier, as expected from

the GFP payload being placed after an IRES element. While we envision that such "low but steady" activity is desirable in many applications, a "high and steady" mode could in principle be achieved by exchanging the IRES for a 2A element. The dynamic expression profiles of our direct, feed-forward, and feedback HSPB circuits are compared in **Fig. 4-3d**, demonstrating prolonged expression with positive feedback.

While the positive feedback circuit sustained expression for several days, this circuit can eventually turn off amid dilution or fluctuating expression of the transactivator. To establish a permanent thermal switch, we tested gene circuits in which we placed the expression of CRE recombinase under the control of candidate pHSPs (**Fig. 4-3e**). In these circuits, the pHSP-driven expression of CRE permanently toggles the circuit from expressing RFP to expressing anti-CD19 CAR by recombining the target vector. When tested in a Jurkat T-cell line, these circuits demonstrated robust activation and minimal leakage (**Fig. 4-3f**). However, when tested in primary T-cells, we observed significantly higher levels of background activation (**Fig. 4-3f**). This may arise from the fact that immune stimulation is used to maintain primary T-cells in culture and our finding, discussed below, that pHSPs show significant background activity in stimulated primary T-cells. Taken together, these results suggest that in primary T-cells, feed-forward and feed-back amplification provide robust methods for thermal control of gene expression, while pHSP-controlled CRE recombination may produce an unacceptable level of irreversibly accumulating background activation.

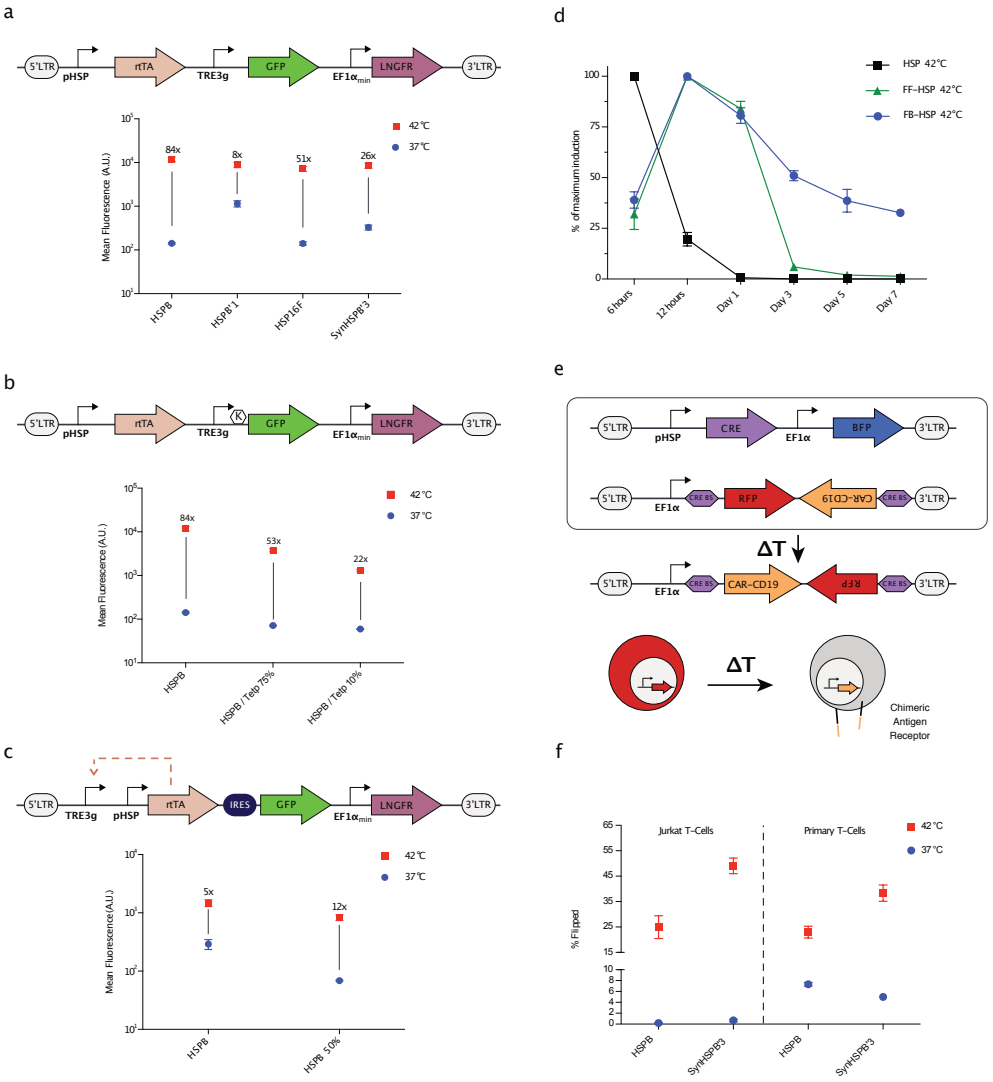

Figure 4-3: Genetic circuits for amplified and sustained thermal activation. (**a**) Diagram illustrating the thermally trigged feed-forward circuit (top). Fluorescence analyzed 24 hours post a 1-hour induction at 37º or 42ºC for cells supplemented with doxycycline (bottom). (**b**) Diagram illustrating a feed-forward circuit driven by HSPB, <K> indicates varying kozak strength (top). Fluorescence analysed 24 hours post a 1-hour induction at 37º or 42ºC for cells supplemented with doxycycline (bottom). The HSPB data is the same as in panel (**a**), and is re-shown here to facilitate comparisons. (**c**) Diagram illustrating the thermally trigged positive feedback circuit (top). Fluorescence analysed 24 hours post a 1-hour induction at 37º or 42ºC for cells supplemented with

doxycycline (bottom). (**d**) Normalized expression monitored over seven days after a 1-hour induction at 42ºC for direct HSPB-driven, feed-forward HSPB, and positive-feedback HSPB circuits. Circuits have been modified to replace GFP with a destabilised version of the protein. (**e**) Illustration of the CRE-based thermally triggered permanently stable switch designed to express CAR-CD19 upon induction. (**f**) Cells were either incubated at 37ºC or thermally stimulated for 1 hour at 42ºC and analyzed 24 hours later to determine the number of activated cells. Where not seen, error bars (±SEM) are smaller than the symbol. N=3 biological replicates for each sample.

4.2d: Temperature-activated Cytokine Release

To demonstrate the ability of our positive feedback circuit to sustain a therapeutically relevant function after thermal induction, we connected its output to the production of a cytokine. The local delivery of cytokines from engineered T-cells would be useful in cancer immunotherapy by allowing T-cells to secrete immune-stimulatory factors to remodel the tumor microenvironment and reduce immunosuppression. It would also be useful in treatments of autoimmune disease by allowing T-cells to secrete factors locally down-regulating the activity of endogenous immune cells. As a model cytokine, we selected IL-21, which has potential utility in cancer immunotherapy due to its ability to stimulate NK cells and $CD8^+$ T-cells[31,32]. We incorporated human IL-21 in place of GFP in our positive feedback circuit (**Fig. 4-4a**). Without thermal induction, primary T-cells transduced with this circuit produced minimal IL-21. Once stimulated, the cells rapidly secreted IL-21, reaching a near-maximal level by 12 hours, and sustained activity for at least 5 days (**Fig. 4-4a**). The dependence of continued circuit function on doxycycline provides an additional layer of control, allowing the termination of therapy production at a desired time by removing doxycycline. To demonstrate this capability, we removed doxycycline 24 hours after cell induction, resulting in the abrogation of cytokine production by day five. The ability to chemically terminate the activity of our circuit enhances its safety profile in potential therapeutic applications.

In some scenarios, it would be useful for cytokine release to be triggered from a T-cell constitutively expressing a CAR, allowing the cytokine to locally boost immune activation

during CAR-directed killing. To test this possibility, we co-transduced primary T-cells with our positive IL-21 circuit and a constitutively expressed anti-CD19 CAR (**Fig. 4-4b**). In the absence of target Raji bait cells expressing CD19, IL-21 release was well-controlled by thermal induction (**Fig. 4-4b**). However, co-incubation with bait cells resulted in the activation of IL-21 release after 3 days in co-culture even in the absence of a thermal treatment (**Fig. 4-4b**). These results suggested that HSP activity may be driven by T-cell stimulation, as evidenced by IL-21 release. However, since certain subsets of T-cells have been shown to release endogenous IL-21 when stimulated[33], we set out to directly test the induction of pHSP upon T-cell stimulation using a non-cytokine output, as discussed below.

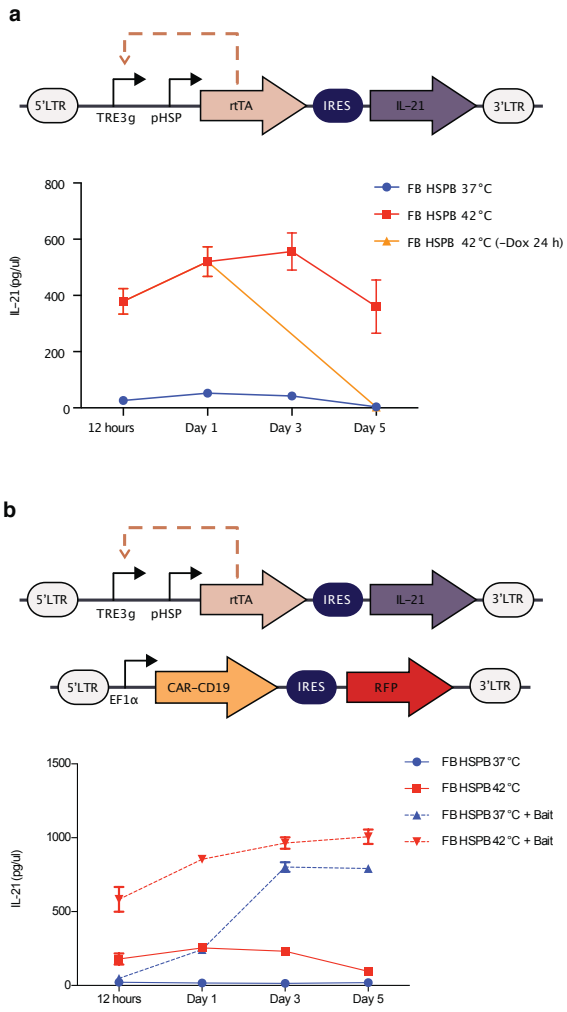

Figure 4-4: Temperature-activated cytokine release. (**a**) Diagram illustrating the positive feedback circuit used to express IL-21 (top). Cumulative IL-21 release from 1-hour induction at 37º or 42ºC. In one sample, doxycycline was removed after 24 hours (bottom). (**b**) Illustration of the constructs used to assay the ability of CAR activity to trigger expression of IL-21 in the feedback pHSP circuit (top). Cells were either incubated at 37 ºC or thermally stimulated for 1 hour at 42ºC with and without bait cells (bottom). Media was collected and frozen at each time point and all samples were analyzed simultaneously at the end of collection. Cumulative IL-21 expression was quantified by using an IL-21 ELISA. Where not seen, error bars (±SEM) are smaller than the symbol. N=3 biological replicates for each sample.

4.2e: Dependence of pHSP-driven Circuits on T cell Activation

To directly examine the possibility that pHSPs are turned on in response to CAR-driven T-cell activation, we tested the expression of pHSP-driven GFP in constitutively CAR-expressing T-cells (**Fig. 4-5a**) upon exposure to a thermal stimulus or bait cells. We found that both thermal stimulation and CAR engagement led to pHSP-driven gene expression (**Fig. 4-5b**). This response occurred in cells expressing circuits based on HSPB, SynHSPB'3, and HSPmin promoters. Because SynHSPB'3 lacks the AP-1 site present in wild-type pHSPs such as HSPB, and HSPmin is composed of only HSE binding sites driving a minimal promoter, these results suggest that pHSP induction takes place via an HSF1-mediated mechanism. This unexpected finding suggests that activated T-cells experience cellular stress--for example due to rapid proliferation--potentially resulting in an increased number of mis-folded proteins, leading to HSP upregulation. This provides an important insight for the design of thermally inducible immunotherapies.

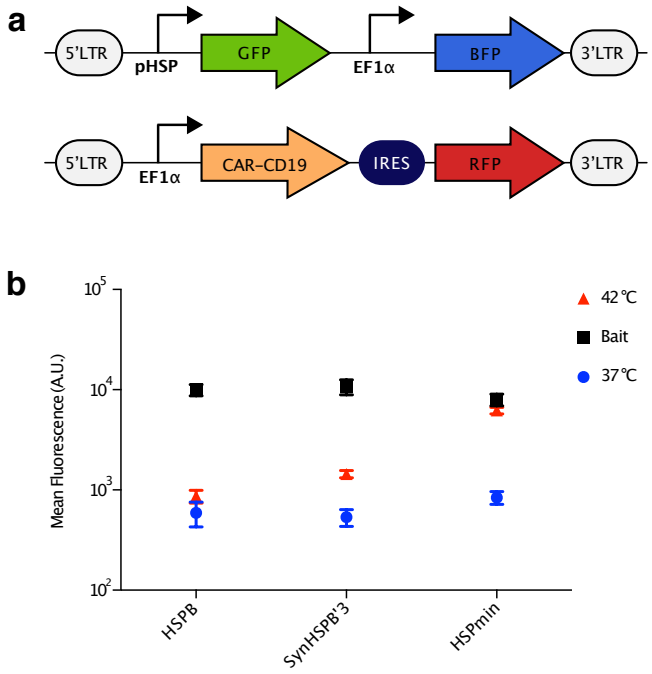

Figure 4-5: Dependence of pHSP-driven circuits on T-cell activation. (**a**) Illustration of the constructs used to assay the ability of CAR activity to trigger pHSP. (**b**) Cells were either incubated at 37ºC, thermally stimulated for 1 hour at 42ºC, or incubated with $CD19^+$ bait cells. pHSP triggered activity was determined by quantifying GFP expression 24 hours after induction. Where not seen, error bars (±SEM) are smaller than the symbol. N=3 biological replicates for each sample.

4.2f: Auto-Sustained Thermally Induced Tumor Killing

Our finding that CAR engagement drives pHSP activity suggested that a simple, auto-sustained gene circuit could drive CAR-mediated killing in response to the combination of a thermal stimulus and the presence of target cells. In particular, we hypothesized that placing CAR expression under the control of a pHSP (**Fig. 4-6a**) would result in T-cells with no initial CAR expression or activity, even in the presence of target cells. Upon thermal induction, CAR would become transiently expressed. If the CAR target is present in the vicinity of T-cells, these cells would become activated, driving sustained expression of additional CAR from the pHSP and target cell killing.

As predicted, this pHSP-CAR circuit showed no baseline CAR expression in primary T-cells, but began to express CAR when thermally stimulated (**Fig. 4-6a**). CAR expression was greatly reduced after 24 hours in the absence of target engagement (**Fig. 4-6b**). When cultured with $CD19^+$ bait cells (**Fig. 4-6c**), thermally activated pHSP-CAR T-cells eliminated the bait cells after 9 days in co-culture (**Fig. 4-6d, Fig. 4-S3**). This killing was as complete as with positive control T-cells carrying a constitutively expressed CAR driven by the EF1α promoter, albeit over a longer time span. This difference may be due to the maximum level of pHSP-driven CAR expression being lower than the level observed with a constitutive EF1α promoter (**Fig. 4-S4)**. When pHSP-CAR T-cells and bait cells were co-incubated without thermal stimulation, no apparent killing took place. While the initial thermal stimulus results in some cell death, T-cells maintain their proliferative capacity and rapidly make up for the initial loss in T-cells (**Fig. 4-S5**). These results suggest that a thermal stimulus can kick-start a positive feedback loop of activation-driven expression of CAR from pHSP, leading to effective bait cell elimination. This activation paradigm could help with mitigating off-target toxicity since CAR expression will be abrogated once T-cells leave the tumor site.

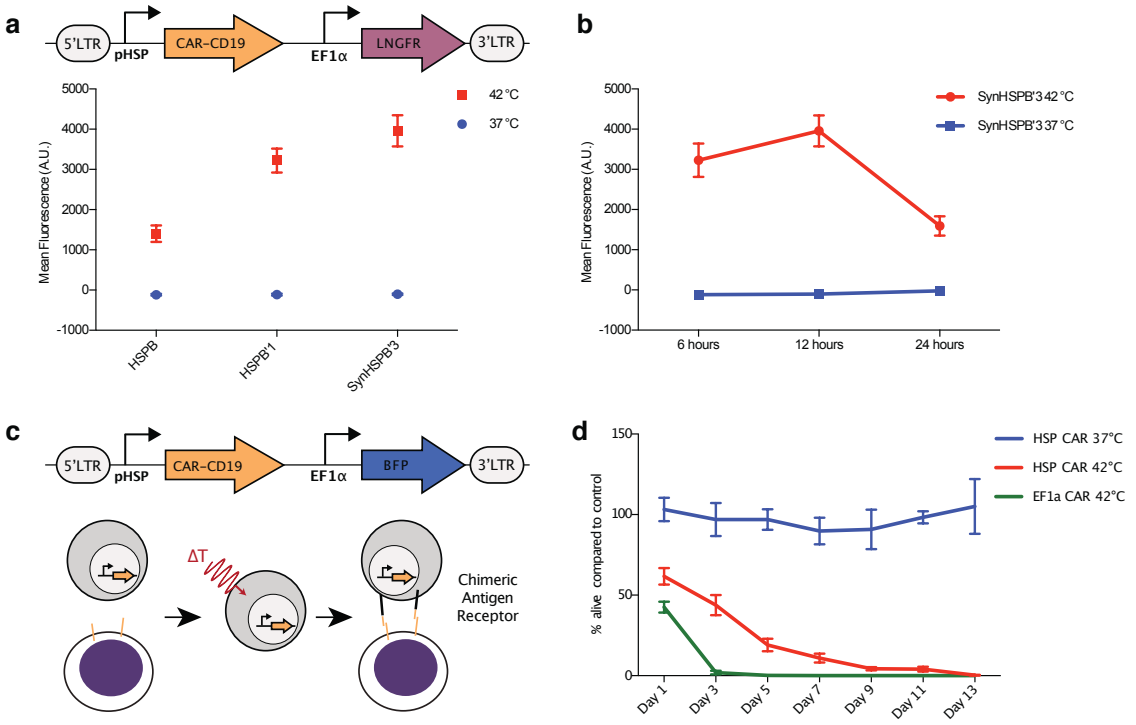

Figure 4-6: Auto-sustained thermally induced CAR expression and tumor cell killing. (**a**) Illustration of the viral construct used to assay pHSP (SynHSPB'3)-driven expression of CAR-CD19. Cells were either incubated at 37ºC or thermally stimulated for 1 hour at 42ºC, and pHSP-triggered CAR-CD19 expression was quantified by surface staining of an HA tag appended to the CAR 12 hours after induction. N=3 biological replicates. (**b**) CAR-CD19 expression 6, 12, and 24 hours after 1-hour induction with 37ºC or 42ºC. N=3 biological replicates. Negative values in 37ºC samples result from subtraction of signal acquired from wild-type T-cells. Raw data is provided in **(Fig. S6)**. (**c**) Illustration of the viral construct and assay used to test the ability of pHSP-inducible CAR expression to conditionally kill bait cells. Cells were either incubated at 37ºC or thermally stimulated for 1 hour at 42ºC before being incubated with $CD19^{+}$ bait cells. (**d**) Unmodified T-cells and T-cells constitutively expressing CAR-CD19 were used as a negative and positive control respectively. pHSP (SynHSPB'3)-triggered killing activity was quantified by counting the % of bait cells alive compared to the negative control for a duration of 13 days. N= 3 biological replicates for two T-cell collections from different patients, total N=6. Where not seen, error bars (±SEM) are smaller than the symbol.

4.3: Discussion

Our results demonstrate that engineered bioswitch circuits using pHSP can provide control of T-cell therapy with mild hyperthermia. While it has been previously shown that light-switchable proteins could also confer spatiotemporal control over T-cell activity[34], light has poor penetration into tissues, limiting the utility of such tools. On the other hand, temperature can be elevated at arbitrary depth and with high spatial precision using non-invasive methods such as FUS or magnetic hyperthermia[15–18].

Our study showed that temperatures in the well-tolerated range of 37-42ºC[35,36] can provide control over T-cell function, including the synthesis and release of a cytokine and the CAR-mediated killing of cancer cells *in vitro*, with minimal baseline activity. In future studies, this performance must be characterized and optimized in the *in vivo* setting. In particular, it will be useful to optimize the thermal requirements of ultrasound activation. While thermal tissue damage is not a major concern in tumor therapy (where it can be synergistic), damage to healthy tissues in non-tumor applications could be detrimental[35,36]. It would also be desirable to shorten the FUS treatment duration to substantially less than the 1 hour heat pulse used in this study. Further promoter engineering, protein engineering, and thermal pulse optimization could broaden the range of applications for this technology.

Despite their name, pHSPs can respond to a variety of stimuli such as heat, hypoxia, heavy metals, cytokines, and cell division[37,38]. Therefore, the context in which these promoters are being used must be carefully considered. In this work, we capitalized on non-thermal pHSP induction by the T-cell receptor pathway to generate sustained killing circuits. In other contexts where the promiscuous responsiveness of pHSPs presents an un-exploitable hindrance, it may be desirable to develop thermal response mechanisms based on orthogonal molecular bioswitches[22,23].

4.4: Methods

Plasmid Construction and Molecular Biology

All plasmids were designed using SnapGene (GSL Biotech) and assembled via reagents from New England Biolabs for KLD mutagenesis (E0554S) or Gibson Assembly (E2621L). After assembly, constructs were transformed into NEB Turbo (C2984I) and NEB Stable (C3040I) *E. coli* for growth and plasmid preparation. The CAR-CD19 gene containing the CD28 and CD3z signaling domain was a kind gift from the Laboratory of David Baltimore (Caltech). Integrated DNA Technologies synthesized other genes, the pHSP, and all PCR primers. Kozak used in **Figure 3B**: CGG-ATG for 75% and ACCATGGGTTGAGCC-ATG for 10%. The original Kozak was ACC-ATG.

Cell Lines

Raji cells (CCL-86) were obtained from ATCC and cultured in RPMI 1640 media (Thermo Fisher Scientific) with 1x Penicillin/Streptomycin (Corning). 1000 ng/ml of doxycycline was used for induction of the Tet promoter. GFP^+ Raji cells were constructed via viral infection of a GFP driven by the EF1a promoter. Lentivirus was prepared using a third-generation viral vector and helper plasmids (gifts of D. Baltimore). Virus was packaged in HEK293T cells grown in 10 cm dishes. After 3 days of transfection, viral particles were concentrated via ultracentrifugation. Infection was performed by following the "RetroNectin" (T100B Takara Bio) reagent protocol. Experiments were performed at least two weeks after infection.

Primary T-cells

T-cells were isolated with the EasySep Human T-cell isolation Kit (STEMCELL Technologies 17951) from frozen human peripheral blood mononuclear cells obtained from healthy donors. T-cells were stimulated with CD3/CD28 Dynabeads (Thermo Fisher Scientific 11132D) at 1:1 cell:bead ratio for 1 day before viral transduction. Dynabeads were removed on day seven and the cells were allowed to rest until day fourteen before proceeding with experiments. This delay was designed to avoid any activation interference with HSP

activity. T-cells were cultured in RPMI supplemented with 50 U/ml IL-2 (Miltenyi Biotech 130-097-744) and 1 ng/ml IL-15 (Miltenyi Biotech 130-095-762) every other day. T-cells were enriched by LNGFR magnetic bead based sorting (Miltenyi Biotech 130-091-330) when appropriate.

Thermal Regulation Assay

Thermal stimulation of T-cells was performed in a Bio-Rad C1000 thermocycler. T-cells at 1-2 million/ml were supplemented with doxycycline, if needed, and mixed well before transferring 50 µl into a sterile PCR tube. The temperature and duration of stimulation was varied based on the experimental procedure. Upon completion of thermal stimulation, cells were moved back into a mammalian incubator and supplemented 1:1 with fresh media containing cytokines and in some cases doxycycline. Cells were typically incubated for 24 hours unless stated otherwise before assaying with a flow cytometer (MACSQuant VYB). Dead cells were typically excluded via FSC/SSC gating for routine assays. In **Figure 2**, a LIVE/DEAD viability/cytotoxicity kit (Thermo Fisher L3224) was used for a more accurate quantification of cell state. Live cells were further gated via a transfection marker to isolate virally infected cells for further analysis. The change in mean fluorescence of the cell population was used to characterize the fold change of pHSP constructs. To account for cellular auto-fluorescence, the mean fluorescence signal from non-transduced T-cells was collected in each experiment and subtracted from the mean fluorescence of experimental T-cells. Anti-HA antibodies (Miltenyi Biotech 130-120-722) were used to stain for CAR expression, and V450 Mouse Anti-human CD271 was used to stain LNGFR (BD biosciences 562123). IL-21 expression was measured using a human IL-21 DuoSet ELISA (R&D systems DY8879-05).

T-cell Bait Assay

Raji and GFP^+ Raji cells were used as bait cells for CAR-CD19 T-cells. Bait assays were initiated by mixing T-cells with bait cells at a 3:1 ratio. This ratio was established to avoid

excessive bait cell growth before T-cell engagement. To assess T-cell killing of bait cells, GFP^+ Raji were used and the count of GFP^+ cells was tracked over time.

Data and Code Availability

Plasmids will be made available through Addgene upon publication. All other materials and data are available from the corresponding author upon reasonable request.

4.5: References

(1) P Teixeira, A., and Fussenegger, M. (2019) Engineering mammalian cells for disease diagnosis and treatment. *Curr. Opin. Biotechnol. 55*, 87–94.
(2) Brentjens, R. J., Davila, M. L., Riviere, I., Park, J., Wang, X., Cowell, L. G., Bartido, S., Stefanski, J., Taylor, C., Olszewska, M., Borquez-Ojeda, O., Qu, J., Wasielewska, T., He, Q., Bernal, Y., Rijo, I. V., Hedvat, C., Kobos, R., Curran, K., Steinherz, P., Jurcic, J., Rosenblat, T., Maslak, P., Frattini, M., and Sadelain, M. (2013) CD19-Targeted T Cells Rapidly Induce Molecular Remissions in Adults with Chemotherapy-Refractory Acute Lymphoblastic Leukemia. *Sci. Transl. Med. 5*, 177ra38-177ra38.
(3) Turtle, C. J., Hanafi, L.-A., Berger, C., Gooley, T. A., Cherian, S., Hudecek, M., Sommermeyer, D., Melville, K., Pender, B., Budiarto, T. M., Robinson, E., Steevens, N. N., Chaney, C., Soma, L., Chen, X., Yeung, C., Wood, B., Li, D., Cao, J., Heimfeld, S., Jensen, M. C., Riddell, S. R., and Maloney, D. G. (2016) CD19 CAR-T cells of defined CD4+:CD8+ composition in adult B cell ALL patients. *J. Clin. Invest. 126*, 2123–2138.
(4) Brentjens, R. J., Rivière, I., Park, J. H., Davila, M. L., Wang, X., Stefanski, J., Taylor, C., Yeh, R., Bartido, S., Borquez-Ojeda, O., Olszewska, M., Bernal, Y., Pegram, H., Przybylowski, M., Hollyman, D., Usachenko, Y., Pirraglia, D., Hosey, J., Santos, E., Halton, E., Maslak, P., Scheinberg, D., Jurcic, J., Heaney, M., Heller, G., Frattini, M., and Sadelain, M. (2011) Safety and persistence of adoptively transferred autologous CD19-targeted T cells in patients with relapsed or chemotherapy refractory B-cell leukemias. *Blood 118*, 4817–4828.
(5) Kochenderfer, J. N., Wilson, W. H., Janik, J. E., Dudley, M. E., Stetler-Stevenson, M., Feldman, S. A., Maric, I., Raffeld, M., Nathan, D.-A. N., Lanier, B. J., Morgan, R. A., and Rosenberg, S. A. (2010) Eradication of B-lineage cells and regression of lymphoma in a patient treated with autologous T cells genetically engineered to recognize CD19. *Blood 116*, 4099–4102.
(6) Zhang, Y., and Ertl, H. C. J. (2016) Starved and Asphyxiated: How Can CD8(+) T Cells within a Tumor Microenvironment Prevent Tumor Progression. *Front. Immunol. 7*, 32.
(7) Morgan, R. A., Chinnasamy, N., Abate-Daga, D., Gros, A., Robbins, P. F., Zheng, Z., Dudley, M. E., Feldman, S. A., Yang, J. C., Sherry, R. M., Phan, G. Q., Hughes, M. S., Kammula, U. S., Miller, A. D., Hessman, C. J., Stewart, A. A., Restifo, N. P., Quezado, M. M., Alimchandani, M., Rosenberg, A. Z., Nath, A., Wang, T., Bielekova, B., Wuest, S. C., Akula, N., McMahon, F. J., Wilde, S., Mosetter, B., Schendel, D. J., Laurencot, C. M., and Rosenberg, S. A. (2013) Cancer regression and neurological toxicity following anti-MAGE-A3 TCR gene therapy. *J. Immunother. 36*, 133–151.
(8) Morgan, R. A., Yang, J. C., Kitano, M., Dudley, M. E., Laurencot, C. M., and Rosenberg, S. A. (2010) Case Report of a Serious Adverse Event Following the Administration of T Cells Transduced With a Chimeric Antigen Receptor Recognizing ERBB2. *Mol. Ther. 18*, 843–851.
(9) Ellebrecht, C. T., Bhoj, V. G., Nace, A., Choi, E. J., Mao, X., Cho, M. J., Zenzo, G. D., Lanzavecchia, A., Seykora, J. T., Cotsarelis, G., Milone, M. C., and Payne, A. S. (2016) Reengineering chimeric antigen receptor T cells for targeted therapy of autoimmune disease. *Science 353*, 179–184.
(10) Zah, E., Lin, M.-Y., Silva-Benedict, A., Jensen, M. C., and Chen, Y. Y. (2016) T Cells Expressing CD19/CD20 Bispecific Chimeric Antigen Receptors Prevent Antigen Escape by Malignant B Cells. *Cancer Immunol. Res. 4*, 498–508.

(11) Roybal, K. T., Rupp, L. J., Morsut, L., Walker, W. J., McNally, K. A., Park, J. S., and Lim, W. A. (2016) Precision Tumor Recognition by T Cells With Combinatorial Antigen-Sensing Circuits. *Cell 164*, 770–779.
(12) Traversari, C., Marktel, S., Magnani, Z., Mangia, P., Russo, V., Ciceri, F., Bonini, C., and Bordignon, C. (2007) The potential immunogenicity of the TK suicide gene does not prevent full clinical benefit associated with the use of TK-transduced donor lymphocytes in HSCT for hematologic malignancies. *Blood 109*, 4708–4715.
(13) Di Stasi, A., Tey, S.-K., Dotti, G., Fujita, Y., Kennedy-Nasser, A., Martinez, C., Straathof, K., Liu, E., Durett, A. G., Grilley, B., Liu, H., Cruz, C. R., Savoldo, B., Gee, A. P., Schindler, J., Krance, R. A., Heslop, H. E., Spencer, D. M., Rooney, C. M., and Brenner, M. K. (2011) Inducible apoptosis as a safety switch for adoptive cell therapy. *N. Engl. J. Med. 365*, 1673–1683.
(14) Tey, S.-K., Dotti, G., Rooney, C. M., Heslop, H. E., and Brenner, M. K. (2007) Inducible caspase 9 suicide gene to improve the safety of allodepleted T cells after haploidentical stem cell transplantation. *Biol. Blood Marrow Transplant. 13*, 913–924.
(15) Thiesen, B., and Jordan, A. (2008) Clinical applications of magnetic nanoparticles for hyperthermia. *Int. J. Hyperthermia 24*, 467–474.
(16) Huang, X., El-Sayed, I. H., Qian, W., and El-Sayed, M. A. (2006) Cancer Cell Imaging and Photothermal Therapy in the Near-Infrared Region by Using Gold Nanorods. *J. Am. Chem. Soc. 128*, 2115–2120.
(17) Piraner, D. I., Farhadi, A., Davis, H. C., Wu, D., Maresca, D., Szablowski, J. O., and Shapiro, M. G. (2017) Going Deeper: Biomolecular Tools for Acoustic and Magnetic Imaging and Control of Cellular Function. *Biochemistry 56*, 5202–5209.
(18) Haar, G., and Coussios, C. (2007) High intensity focused ultrasound: Physical principles and devices. *Int. J. Hyperthermia 23*, 89–104.
(19) Guilhon, E., Voisin, P., Zwart, J. A. de, Quesson, B., Salomir, R., Maurange, C., Bouchaud, V., Smirnov, P., Verneuil, H. de, Vekris, A., Canioni, P., and Moonen, C. T. W. (2003) Spatial and temporal control of transgene expression in vivo using a heat-sensitive promoter and MRI-guided focused ultrasound. *J. Gene Med. 5*, 333–342.
(20) Deckers, R., Quesson, B., Arsaut, J., Eimer, S., Couillaud, F., and Moonen, C. T. W. (2009) Image-guided, noninvasive, spatiotemporal control of gene expression. *Proc. Natl. Acad. Sci. U. S. A. 106*, 1175–1180.
(21) Kruse, D. E., Mackanos, M. A., O\textquotesingleConnell-Rodwell, C. E., Contag, C. H., and Ferrara, K. W. (2008) Short-duration-focused ultrasound stimulation of Hsp70 expressionin vivo. *Phys. Med. Biol. 53*, 3641–3660.
(22) Piraner, D. I., Abedi, M. H., Moser, B. A., Lee-Gosselin, A., and Shapiro, M. G. (2017) Tunable thermal bioswitches for *in vivo* control of microbial therapeutics. *Nat. Chem. Bio. 13*, 75–80.
(23) Piraner, D. I., Wu, Y., and Shapiro, M. G. (2019) Modular Thermal Control of Protein Dimerization. *ACS Synth. Biol. 8*, 2256–2262.
(24) Hildebrandt, B., Wust, P., Ahlers, O., Dieing, A., Sreenivasa, G., Kerner, T., Felix, R., and Riess, H. (2002) The cellular and molecular basis of hyperthermia. *Crit. Rev. Oncol. Hemat. 43*, 33–56.
(25) Rome, C., Couillaud, F., and Moonen, C. T. W. (2005) Spatial and temporal control of expression of therapeutic genes using heat shock protein promoters. *Methods 35*, 188–198.
(26) Wada, K.-I., Taniguchi, A., and Okano, T. (2007) Highly sensitive detection of cytotoxicity using a modified HSP70B′ promoter. *Biotechnol. Bioeng. 97*, 871–876.

(27) Kay, R. J., Boissy, R. J., Russnak, R. H., and Candido, E. P. (1986) Efficient transcription of a Caenorhabditis elegans heat shock gene pair in mouse fibroblasts is dependent on multiple promoter elements which can function bidirectionally. *Mol. Cell. Biol. 6*, 3134–3143.
(28) Miller, I. C., Gamboa Castro, M., Maenza, J., Weis, J. P., and Kwong, G. A. (2018) Remote Control of Mammalian Cells with Heat-Triggered Gene Switches and Photothermal Pulse Trains. *ACS Synth. Biol. 7*, 1167–1173.
(29) Ferreira, J. P., Overton, K. W., and Wang, C. L. (2013) Tuning gene expression with synthetic upstream open reading frames. *Proc. Natl. Acad. Sci. U. S. A. 110*, 11284–11289.
(30) Yamaguchi, M., Ito, A., Okamoto, N., Kawabe, Y., and Kamihira, M. (2012) Heat-inducible transgene expression system incorporating a positive feedback loop of transcriptional amplification for hyperthermia-induced gene therapy. *J. Biosci. Bioeng. 114*, 460–465.
(31) Søndergaard, H., and Skak, K. (2009) IL-21: roles in immunopathology and cancer therapy. *Tissue Antigens 74*, 467–479.
(32) Singh, H., Figliola, M. J., Dawson, M. J., Huls, H., Olivares, S., Switzer, K., Mi, T., Maiti, S., Kebriaei, P., Lee, D. A., Champlin, R. E., and Cooper, L. J. N. (2011) Reprogramming CD19-Specific T Cells with IL-21 Signaling Can Improve Adoptive Immunotherapy of B-Lineage Malignancies. *Cancer Res. 71*, 3516–3527.
(33) Parrish-Novak, J., Dillon, S. R., Nelson, A., Hammond, A., Sprecher, C., Gross, J. A., Johnston, J., Madden, K., Xu, W., West, J., Schrader, S., Burkhead, S., Heipel, M., Brandt, C., Kuijper, J. L., Kramer, J., Conklin, D., Presnell, S. R., Berry, J., Shiota, F., Bort, S., Hambly, K., Mudri, S., Clegg, C., Moore, M., Grant, F. J., Lofton-Day, C., Gilbert, T., Raymond, F., Ching, A., Yao, L., Smith, D., Webster, P., Whitmore, T., Maurer, M., Kaushansky, K., Holly, R. D., and Foster, D. (2000) Interleukin 21 and its receptor are involved in NK cell expansion and regulation of lymphocyte function. *Nature 408*, 57–63.
(34) Xu, Y., Hyun, Y.-M., Lim, K., Lee, H., Cummings, R. J., Gerber, S. A., Bae, S., Cho, T. Y., Lord, E. M., and Kim, M. (2014) Optogenetic control of chemokine receptor signal and T-cell migration. *Proc. Natl. Acad. Sci. U.S.A. 111*, 6371–6376.
(35) McDannold, N. J., King, R. L., Jolesz, F. A., and Hynynen, K. H. (2000) Usefulness of MR Imaging-Derived Thermometry and Dosimetry in Determining the Threshold for Tissue Damage Induced by Thermal Surgery in Rabbits. *Radiology 216*, 517–523.
(36) McDannold, N., Vykhodtseva, N., Jolesz, F. A., & Hynynen, K. (2004) MRI investigation of the threshold for thermally induced blood-brain barrier disruption and brain tissue damage in the rabbit brain. *Magn. Reson. Med. 51*, 913–923.
(37) Kregel, K. C. (2002) Invited Review: Heat shock proteins: modifying factors in physiological stress responses and acquired thermotolerance. *J. Appl. Physiol. 92*, 2177–2186.
(38) Morimoto, R. I. (1998) Regulation of the heat shock transcriptional response: cross talk between a family of heat shock factors, molecular chaperones, and negative regulators. *Genes Dev. 12*, 3788–3796.

4.6: Supplementary Figures

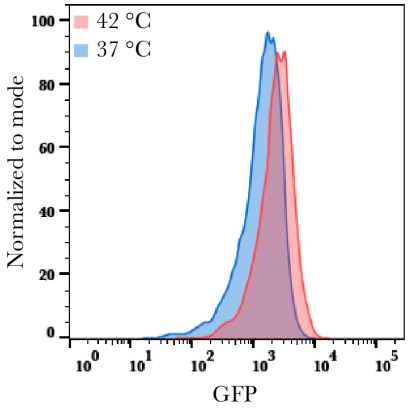

Figure 4-S1 | Thermally induced shift in gene expression. T-cells were transfected with the HSPB'1 promoter viral vector from **Figure 1**. The histogram represents the green fluorescence intensity of infected cells 24 hours after a 1-hour incubation at 37°C or 42ºC, as measured via flow cytometry. Thermal induction led to a uniform increase in gene expression across the cell population.

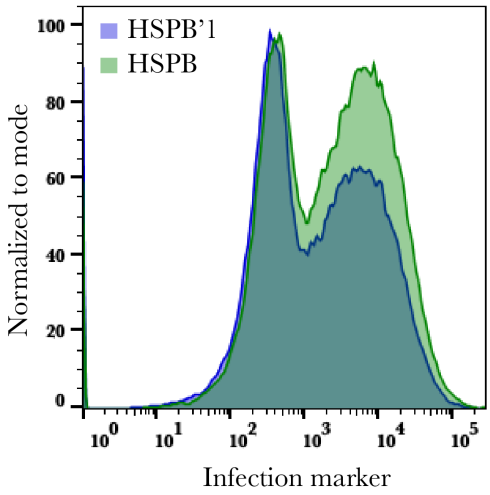

Figure 4-S2 | Expression of a transduction marker to control for variability in infection. Constructs in our experiments carried an infection marker that was used to assess any differences in viral integration efficiency. In this example, T-cells were infected with the HSPB and HSPB'1 feed-forward circuits from **Figure 3A**. Both constructs had similar expression levels of the infection marker and comparable transduction efficiency HSPB (63%) and HSPB'1 (54%).

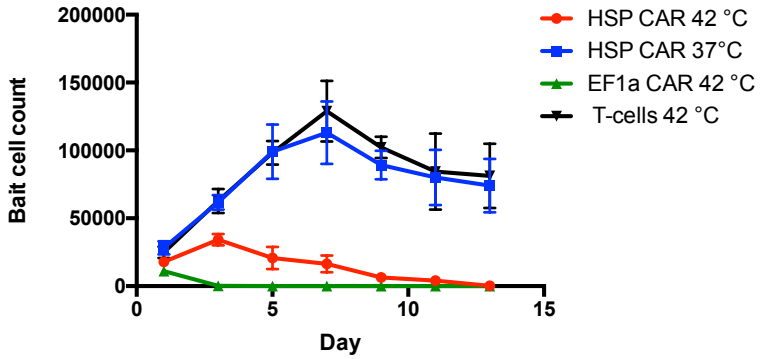

Figure 4-S3 | Bait cell count for the HSP CAR killing experiment. Primary T-cells were either incubated at 37ºC or thermally stimulated for 1 hour at 42ºC before being incubated with $CD19^+$ bait cells. Unmodified T-cells and T-cells constitutively expressing CAR-CD19 were used as a negative and positive control, respectively. HSP (SynHSPB'3) triggered killing activity was quantified by counting the number of bait cells alive over 13 days. N= 3 biological replicates. Where not seen, error bars (±SEM) are smaller than the symbol.

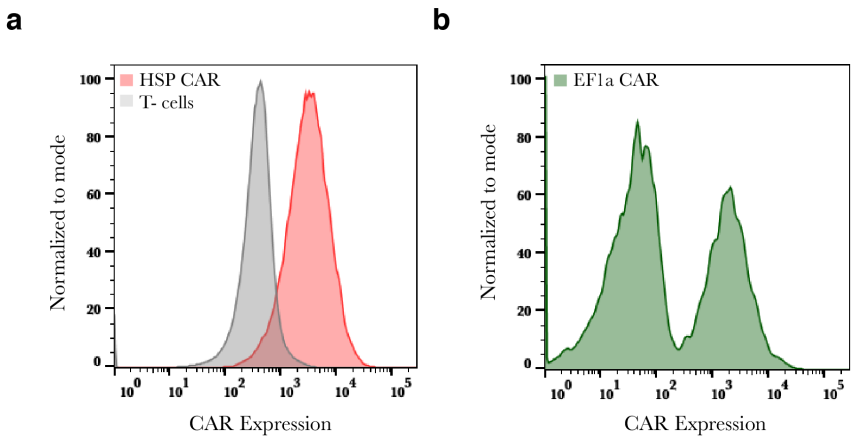

Figure 4-S4 | CAR expression from constitutive and induced constructs. (**a**) Primary T-cells infected with SynHSPB'3 were thermally stimulated for 1 hour at 42ºC. CAR expression was assessed 12 hours post stimulation by using an Anti-HA antibody. Cells were gated based on a transfection marker before CAR expression analysis. (**b**) Primary T-cells constitutively expressing CAR-CD19 were used as a positive control. Cells in panel (**b**) were not gated with a transfection marker. The left peak represents uninfected cells.

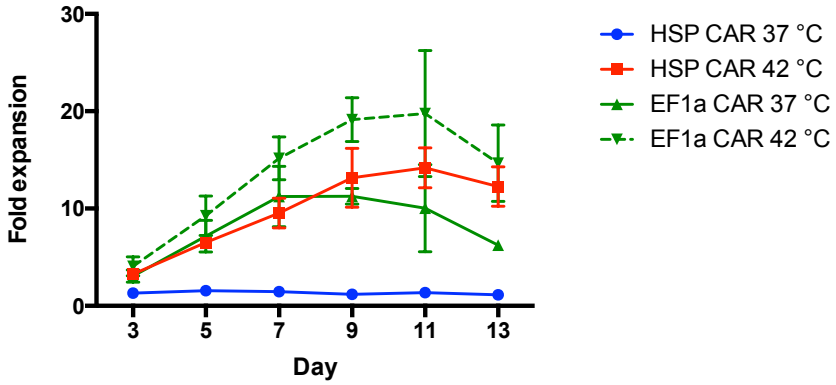

Figure 4-S5 | Assessing the proliferative capacity of stimulated T-cells. T-cells constitutively expressing CAR-CD19 were used as a control, and SynHSPB'3 was used for HSP T-cells. Cells were either incubated at 37ºC or thermally stimulated for 1 hour at 42ºC before being incubated with $CD19^{+}$ bait cells. T-cell proliferation was quantified by counting the number of T-cells alive and comparing it to day 1 to establish fold change. N= 3 biological replicates. Where not seen, error bars (±SEM) are smaller than the symbol.

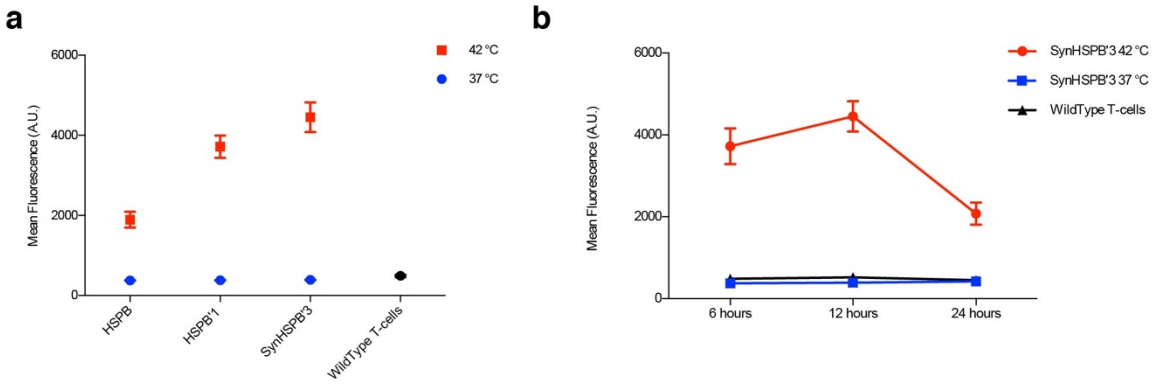

Figure 4-S6 | Thermally induced CAR expression. Raw measurements underlying the data shown in **Figure 6 (a, b)**, including the fluorescence of wild-type T-cells. This background value was subtracted from the experimental cell measurements to generate the plots in **Figure 6 (a, b)**. (**a**) Cells were either incubated at 37ºC or thermally stimulated for 1 hour at 42ºC and pHSP-triggered CAR-CD19 expression was quantified by surface staining of an HA tag appended to the CAR 12 hours after induction. N=3 biological replicates. (**b**) CAR-CD19 expression 6, 12, and 24 hours after 1-hour induction with 37ºC or 42ºC. Where not seen, error bars (±SEM) are smaller than the symbol.